XXXV INTERNATIONAL SCIENTIFIC SYMPOSIUM

METROLOGY AND METROLOGY ASSURANCE 2025

PROCEEDINGS

September 7-11, 2025, Sozopol, Bulgaria

https://metrology-bg.org/

TECHNICAL UNIVERSITY OF SOFIA

8 Blvd Kl. Ohridski, 1797, Sofia, Bulgaria

MFACULTY OF MECHANICAL ENGINEERING
Department of
PRECISION ENGINEERING AND MEASURING INSTRUMENTS

Prof. Dimitar Diakov, PhD
Phone: (+359) 2 965 3056
Mobile: (+359) 889 531 258
E-mail: diakov@tu-sofia.bg
metrology@tu-sofia.bg

FACULTY OF AUTOMATICS
Department of
ELECTRICAL MEASUREMENTS

assoc. prof. Ivan Kodjabashev
Phone: (+359) 2 965 2896
Mobile: (+359) 887 516 765
E-mail: kodjabashev@tu-sofia.bg

assoc. prof. Georgi Milushev
Phone: (+359) 2 965 2380
Mobile: (+359) 888 501 235
E-mail: gm@tu-sofia.bg
metrology@tu-sofia.bg

Technical University of Sofia

Bulgarian Institute of Metrology

Union of Metrologists in Bulgaria

Bulgarian Academical Association of Metrology

Kozloduy Nuclear Power Plant

35TH INTERNATIONAL SCIENTIFIC SYMPOSIUM

METROLOGY AND METROLOGY ASSURANCE 2025

PROCEEDINGS

7-11 September 2025

Sozopol, Bulgaria

ORGANISED BY

Technical University of Sofia

- ***Department of Information and Measurement Technology***
- ***Department of Precision Engineering and Measuring Instruments***

Institute of Electrical and Electronics Engineers, Bulgaria Section

WITH THE ATTENDANCE OF

Bulgarian Institute of Metrology

Union of Metrologists in Bulgaria

Kozloduy Nuclear Power Plant

WITH THE SUPPORT OF

RESEARCH AND DEVELOPMENT SECTOR BY THE TU-SOFIA

SOFTTRADE **NIK 47 Ltd** **R&DL "CMME"**

NATIONAL ORGANIZING COMMITTEE

Co-Chairmen

Assoc. Prof. Ivan Kodjabashev, PhD	*TU-Sofia*
Prof. Dimitar Diakov, DSc	*TU-Sofia*

Vice Chairmen

Paun Ilchev, MEng	*BIM*
Vessela Konstantinova, PhD	*UMB*
Dariush Novak, MEng	*Kozloduy NPP*
Prof. Branko Sotirov, PhD	*BAAM*

Scientific Secretary

Prof. Georgi Djukendjiev, PhD	*TU-Sofia*

Members

Kiril Banev, MEng	*Kozloduy NPP*
Assoc. Prof. Vassil Bogev, PhD	*TU-Sofia*
Milko Djambazov, PhD	*TU-Sofia*
Assist. Prof. Bozhidar Dzhudzhev, PhD	*TU-Sofia*
Assist. Prof. Krasimir Galabov, PhD	*TU-Sofia*
Assoc. Prof. Ivanka Kalimanova, PhD	*TU-Sofia*
Assist. Prof. Dobri Komarski, PhD	*TU-Sofia*
Assoc. Prof. Valentina Markova, PhD	*IEEE Bulgarian Section*
Assoc. Prof. Hristiana Nikolova, PhD	*TU-Sofia*
Nikola Panchev, MEng	*NIK 47*
Assoc. Prof. Nikolay Stoyanov, PhD	*TU-Sofia*
Prof. Plamen Tzvetkov, PhD	*NBU*
Assoc. Prof. Velizar Vassilev, PhD	*TU-Sofia*
Antoaneta Yovcheva, PhD	*BIM NCM*

Secretariat

Assist. Prof. Ivailo Blagov, PhD	*TU-Sofia*
Assoc. Prof. Radoslav Deliyski,PhD	*TU-Sofia*
Assist. Prof. Nikolay Gurov, MEng	*NBU*
Sen. Res. Fel. Momchil Hardalov, PhD	*TU-Sofia*
Assoc. Prof. Rositza Miteva, PhD	*TU-Sofia*
Assist. Prof. Antonia Pandelova, PhD	*TU-Sofia*

INTERNATIONAL PROGRAMME COMMITTEE

Chairman

Assoc. Prof. George Milushev, PhD	*TU-Sofia*

Members

Assoc. Prof. Kiril Aleksiev, PhD	*BAS, IEEE, Bulgaria*
Prof. Konstantionos Athanasiadis	*EMI, Greece*
Anna Chunovkina, DSc	*VNIIM, Russia*
Prof. Dimitar Dichev, DSc	*TU-Gabrovo, Bulgaria*
Prof. Vladimir Dmitriev, DSc	*TsAGI, Russia*
Dr. Manus Henry	*University of Oxford, England*
Prof. Dietrich Hofmann, PhD	*ICC Spectronet, Germany*
Assoc. Prof. Kiril Kirov, PhD	*TU-Varna, Bulgaria*
Assoc. Prof. Ivan Kodjabashev, PhD	*TU-Sofia, Bulgaria*
Prof. Ivan Kralov, DSc	*TU-Sofia, Bulgaria*
Prof. Peter Lauda, DSc	*TU-Liberec, Czech Republic*
Prof. Ignacio Lira, DSc	*PUCC, Chile*
Prof. Valeri Mladenov, DSc	*TU-Sofia, Bulgaria*
Prof. Zvezditza Nenova, PhD	*TU-Gabrovo, Bulgaria*
Assoc. Prof. Elmo Pettai, PhD	*TUT, Estonia*
Prof. Georgii Rannev, DSc	*IIT, Russia*
Acad. Chavdar Rumenin, DSc	*BAS, Bulgaria*
Prof. Alexandru Salceanu, DSc	*TU Gheorghe Asachi, Romania*
Assoc. Prof. Nikolay Serov, PhD	*NRU MPEI, Russia*
Prof. Alexandr Shestakov, DSc	*SUSU NRU, Russia*
Prof. Branko Sotirov, PhD	*RU Angel Kanchev, Bulgaria*
Jiri Šurán	*CMI, Czech Republic*
Roald Taymanov, DSc	*VNIIM, Russia*
Assoc. Prof. Danko Tonev, PhD	*RU Angel Kanchev, Bulgaria*
Assoc. Prof. Stanimir Valchev, PhD	*NOVA, Portugal*
Prof. Wiesław Winiecki, DSc	*WUT, Poland*
Prof. Ighor Zaharov, DSc	*NURE, Ukraine*
Prof. Ilia Zhelezarov, PhD	*TU-Gabrovo, Bulgaria*

All papers published in the Proceedings of the 35th International Scientific Symposium "Metrology and Metrology Assurance 2025" are reviewed by the International Programme Committee.

METROLOGY AND METROLOGY ASSURANCE 2025

7-11 September 2025

Sozopol, Bulgaria

PROCEEDINGS

Technical University of Sofia

Technical University of Sofia Publishing House

ISSN 2603-3194

CONTENT

PLENARY SESSION

P.1. *Nikolay Alexandrov*
DIGITALIZATION OF THE PHYSICAL QUANTITIES IN THE NEW MATRIX REPRESENTATION OF THE INTERNATIONAL SYSTEM OF UNITS (SI). REPRESENTATION OF THE PHYSICAL EQUATIONS IN THE MATRIX STRUCTURE ..... *IEEE Xplore*

Section I GENERAL ASPECTS OF METROLOGY. MEASUREMENT METHODS. UNITY AND ACCURACY OF MEASUREMENTS

I.1. *Iryna Morozova, Olga Ivanets, Rimvidas Khrashchevskyi, Pavlo Kulakov, Rynat Salimov and Anton Plugovyi*
INCREASING THE RELIABILITY OF DIAGNOSIS AND CONTROL IN THE UNCERTAINTY OF PRIMARY INFORMATION ..... *IEEE Xplore*

I.2. *Nikolay Koshevoy, Tatiana Rozhnova, Olena Kostenko, Maksym Tsekhovskyi, Oleksii Potylchak and Andrii Andriushko*
METHODOLOGY FOR DEVELOPING MEASURING TRANSDUCERS OF PHYSICAL QUANTITIES ..... *IEEE Xplore*

I.3. *Rumyana Komarska*
MECHANICAL NEURAL NETWORKS *1*

I.4. *Dobri Komarski, Dimitar Diakov, Velizar Vassilev and Hristiana Nikolova*
STUDY OF TRIPOD ELASTIC PARALLEL MECHANISM FOR MECHANICAL NEURAL NETWORK ..... *IEEE Xplore*

I.5. *Radoslav Marinov*
COMPARISON OF GUM AND MONTE CARLO METHODS FOR EVALUATION THE MEASUREMENTS UNCERTAINTY OF DC VOLTAGE, DC MAGNETIC FLUX DENSITY AND DC RESISTANCE ..... *IEEE Xplore*

I.6. *Igor Zakharov, Kiril Banev, Elena Nicolova, Dimitar Diakov, Olesia Botsiura and Oleg Novoselov*
PROCEDURE FOR REVISING THE INTERCALIBRATION INTERVAL OF MEASURING INSTRUMENTS ..... *IEEE Xplore*

I.7. *Igor Zakharov and Olesia Botsiura*
MEASURING THE OBJECTS COORDINATES IN THREE-DIMENSIONAL SPACE USING THE RANGEFINDER METHOD ..... *IEEE Xplore*

I.8. *Roald Taymanov and Kseniia Sapozhnikova*
WHAT KIND OF ROBOT DO YOU NEED: A FRIEND OR A SERVANT? ..... *IEEE Xplore*

Section II SENSORS, TRANSDUCERS AND DEVICES FOR MEASUREMENT OF PHYSICAL QUANTITIES

II.1. *Nikolay Koshevoy, Tatiana Rozhnova, Olena Kostenko, Oleksandr Zabolotnyi, Vitalii Siroklyn and Andriushko Andrii*
NEW FIBER-OPTIC TRANSDUCERS OF PHYSICAL QUANTITIES.....*IEEE Xplore*

II.2. *Oleksandr Zabolotnyi, Andrii Khodieiev, Roman Trishch and Vitalii Zabolotnyi*
INFRARED TURBIDITY SENSORS APPLICATION FOR THE WATER IN DIESEL EMULSION STABILITY CONTROL .....*IEEE Xplore*

II.3. *Artem Yakovenko and Alexander Shestakov*
SELF-DIAGNOSING MULTI-POINT THERMOCOUPLE MEASUREMENT CIRCUIT WITH DECISION TREE-BASED ERROR CORRECTION.....*7*

II.4. *Denys Onishchuk, Kyrylo Titov and Vitalii Svitlychnyi*
DEVELOPMENT OF A DIGITAL COLOR MEASUREMENT SENSOR .....*IEEE Xplore*

II.5. *Luboslav Hristov, Momchil Lazarov and Ivan Ivanov*
AUTOMATED METROLOGY VERIFICATION AND DIAGNOSTICS OF PRESSURE TRANSDUCERS *12*

Section III MEASUREMENT AND INFORMATION SYSTEMS AND TECHNOLOGIES

III.1. *Teodor Popov, Bozhidar Dzhudzhev, Antonia Pandelova and Nikolay Stoyanov*
DEVELOPMENT OF AIR PURIFICATION DRONE.....*16*

III.2. *Teodor Popov, Bozhidar Dzhudzhev, Antonia Pandelova and Nikolay Stoyanov*
RESEARCH ON AIR PURIFICATION DRONE..... *IEEE Xplore*

III.3. *Maryna Miroshnyk, Olga Zaichenko, Anatolii Miroshnyk and Nataliia Hapon*
MULTIPLE-FREQUENCY ANALYSIS METHOD FOR NON-DESTRUCTIVE TESTING OF 3D FILAMENT PARAMETERS ..... *IEEE Xplore*

III.4. *Marina Miroshnyk, Boris Sytnik, Volodymyr Bryksin, Anatolii Miroshnyk, Yurii Pakhomov and Andrei Shafranskyi*
SYSTEM OF INDEX IDENTIFICATION OF PARAMETERS OF THE EQUIVALENT MODEL OF SUBSTITUTION OF OBJECTS WITH DISTRIBUTED PARAMETERS.....*21*

III.5. *Boris Velev, Bozhidar Dzhudzhev, Vladimir Kamenov and Vladimir Dimitrov*
DEVICE FOR RAPID TESTING OF LITHIUM-ION BATTERIES.....*25*

III.6. *Aleksey Erpalov, Vladimir Sinitsin, Olga Ibryaeva and Aleksander Shestakov*
DECOMPOSITION-BASED AUGMENTATION OF MULTIVARIATE TIME-SERIES MEASUREMENT DATA ..... *IEEE Xplore*

III.7. *Krasimir Bosilkov, Snezhana Spasova and Elena Nikolova*
AUTOMATED WORKPLACE FOR METROLOGICAL VERIFICATION OF RESISTANCE THERMOMETERS *29*

III.8. *Filip Filipov and Stoyan Doynov*
AUTOMATED SYSTEM FOR SILICA MEASURING – "AMI SILICA" TYPE *32*

III.9. *Dimitar Dichev, Iliya Zhelezarov, Tsanko Karadzhov, Borislav Georgiev, Oleksandr Kupriyanov, Ralitza Dicheva and Krasimir Drumev*
IMPROVING ACCURACY IN DYNAMIC SYSTEMS THROUGH ADAPTIVE IDENTIFICATION OF MODEL ERRORS WITHIN THE KALMAN FILTER STRUCTURE ..... *IEEE Xplore*

Section IV MEASUREMENTS IN THE INDUSTRY

IV.1. *Radoslav Keremidchiev*
ENHANCING DEEP NEURAL NETWORK CLASSIFICATION IN FINANCIAL APPLICATIONS: A HYBRID RULE-BASED ALERT SYSTEM FOR ERROR DIAGNOSIS ..... *IEEE Xplore*

IV.2. *Abdullahi Abdulkadir, Alexander Ichtev, Saheed Salahudeen Abdullahi, Alexander Gegov, Olumiyiwa Mathew and Aliyu Umar*
OIL WELL PERFORMANCE MODELING UNDER MEASUREMENT UNCERTAINTY USING FUZZY LOGIC ..... *IEEE Xplore*

IV.3. *Teodor Grakov, Valentin Mateev, Iliana Marinova, Georgi Kotlarski, Stefan Valkov and Maria Ormanova*
TEMPERATURE MODELING OF SOFT METAL FDM 3D PRINTING PROCESS ..... *IEEE Xplore*

IV.4. *Tsanko Karadzhov, Dimitar Dichev, Iliya Zhelezarov, Borislav Georgiev, Dimcho Pulov, Krasimir Drumev and Hristiana Nikolova*
IMPROVING THE ACCURACY OF TEMPERATURE MEASUREMENT WITH THERMORESISTIVE SENSORS ..... *IEEE Xplore*

IV.5. *Dimitar Dichev, Iliya Zhelezarov, Borislav Georgiev, Tsanko Karadzhov, Oleksandr Kupriyanov and Ralitza Dicheva*
AN ADAPTIVE APPROACH TO DETERMINING THE NOISE AND MEASUREMENT ERROR VARIANCES IN SYSTEMS USING THE KALMAN FILTER ..... *IEEE Xplore*

Section VI MEASUREMENTS IN THE ELECTRICAL POWER ENGINEERING

VI.1. *Anton Pavlovich, Artem Orlov, Gennady Antipov, Elizaveta Koniushenko, Nikolay Serov and Andrey Serov*
COMPARATIVE ANALYSIS OF THE EFFICIENCY OF WINDOW FUNCTIONS FOR THE FREQUENCY MEASUREMENT METHOD BASED ON THE AMPLITUDE SPECTRUM ANALYSIS ..... *IEEE Xplore*

VI.2. *Mykola Kundenko, Ivaylo Blagov, Antonina Rybalka, Vitalii Mardziavko and Andrii Rudenko*
METHODOLOGY FOR ASSESSING THE INFLUENCE OF GEOMETRIC PARAMETERS OF OPEN RESONATORS ON THE METROLOGICAL CHARACTERISTICS OF ENERGY LOSSES ..... *IEEE Xplore*

VI.3. *Elizaveta Budkina, Alsu Nurtdinova, Ekaterina Dolgacheva, Alexander A. Shatokhin, Nikolay Serov and Andrey Serov*
APPLICATION OF THE VERNIER METHOD TO REDUCE THE EFFECT OF AMPLITUDE SPECTRUM LEAKAGE ..... *IEEE Xplore*

VI.4. *Iliyana Bogdanova, George Milushev and Krasimir Galabov*
INCOMING INSPECTION OF VACUUM CIRCUIT BREAKERS ..... *IEEE Xplore*

VI.5. *George Milushev*
ELECTRICAL POWER - THE MISSING ELEMENT IN ELECTRICAL POWER QUALITY ASSESSMENT AND STANDARTISATION ..... *IEEE Xplore*

Section VII MEASUREMENTS IN THE ECOLOGY, BIOTECHNOLOGY, MEDICINE, AND SPORT

VII.1. *Ihor Hryhorenko, Iurii Khoroshailo, Svitlana Hryhorenko and Pavlo Biletskyy*
METROLOGICAL ANALYSIS OF COLORIMETRIC CONTROL TOOLS FOR BIOLOGICAL OBJECTS ..... *IEEE Xplore*

VII.2. *Olga Ivanets, Rimvidas Khrashchevskyi, Maryna Arkhyrei, Vladyslav Shlykov, Oleksii Horskyi and Nataliia Bilak*
FEATURES OF USING NONLINEAR DYNAMICS METHODS FOR ANALYZING THE STABILITY OF AN OBJECT'S FUNCTIONING ..... *IEEE Xplore*

VII.3. *Iurii Y. Khoroshailo, Yuriy P. Gnidenko, Maksym V. Korbetskyi, Oleksandr B. Galat and Oleksandr Degtiarov*
RESEARCH OF APPLICABILITY OF THE ELECTRONIC COLORIMETRY METHOD IN MEDICAL DIAGNOSTICS *35*

VII.4. *Lidiia Solodovnikova, Volodymyr Semynozhenko, Ilias Shcherbakov, Nadiia Markina, Serhii Chumachenko and Antonina Korotenko*
ASSESSMENT OF MILITARY OPERATIONS IMPACT ON POLLUTION OF WATER RESOURCES AND SOIL IN KHARKIV CITY AND KHARKIV REGION ..... *IEEE Xplore*

VII.5. *Mykola Kundenko, Antonina Rybalka, Ivaylo Blagov, Larisa Vakhonina, Vitalii Mardziavko and Andrii Rudenko*
DEVELOPMENT OF A SYSTEM FOR MEASURING THE DIELECTRIC PERMEABILITY OF THE AIR ENVIRONMENT TO IMPROVE THE STORAGE OF POUME FRUITS ..... *IEEE Xplore*

VII.6. *Stamen Sarchev, Antonia Pandelova, Bozhidar Dzhudzhev and Nikolay Stoyanov*
MONITORING OF PARTICULATE MATTER POLLUTION FOR THE REGION OF THE CITY OF KARDZHALI ..... *IEEE Xplore*

VII.7. *Dimitar Diakov and Hristiana Nikolova*
SIMULATION STUDY OF FEMORAL-ACETABULAR IMPLANTS FATIGUE ..... *IEEE Xplore*

VII.8. *Dimitar Diakov, Hristiana Nikolova and Alexander Gerchev*
FATIGUE TESTING OF JOINT IMPLANTS ..... *IEEE Xplore*

Section VIII METROLOGY PRACTICE

VIII.1. *Miryana Masheva, Tzvetelin Gueorguiev and Hristiana Nikolova*
METHODOLOGY FOR VERIFICATION OF EXHAUST GAS ANALYSERS IN TECHNICAL INSPECTION POINTS ..... *IEEE Xplore*

VIII.2. *Ivaylo Stoyanov*
VERIFICATION PROCEDURE FOR LOW SPEED AUTOMATIC INSTRUMENTS FOR WEIGHING ROAD VEHICLES IN MOTION AND MEASURING AXLE LOADS *39*

VIII.3. *Petko Sinapov*
METHODOLOGY FOR THE VERIFICATION OF ROLLER BRAKE TESTERS FOR ROAD VEHICLES *43*

VIII.4. *Valerii Semenikhin, Dmytro Taran and Inna Moshchenko*
SPECIAL REQUIREMENTS FOR CALIBRATION OF CLIMATE CHAMBERS *47*

VIII.5. *Borislav Georgiev, Dimitar Dichev, Iliya Zhelezarov, Tsanko Karadzhov and Krasimir Drumev*
COMPARATIVE ANALYSIS OF CLASSICAL AND HYBRID SIGNAL PROCESSING IN AN ELECTRO-HYDRAULIC SYSTEM ..... *IEEE Xplore*

VIII.6. *Zlatka Chavdarova, Desislava Koleva and Hristiana Nikolova*
VERIFICATION OF THE METHODOLOGY FOR VERIFICATION OF PRESSURE GAUGES USED IN PRESSURE EQUIPMENT AND RAILWAY TRANSPORT *IEEE Xplore*
VIII.7. *Dimitar Diakov, Desislava Dimitrova and Hristiana Nikolova*
INDUSTRIAL CMM CLASIFICATION ..... *IEEE Xplore*
VIII.8. *Radoslav Deliyski, Radoslav Vasilev and Veselin Petrov*
APPLICATION OF INERTIAL MEASUREMENT UNIT GY-521 IN LENGTH MEASUREMENT AND STEPS COUNTING..... *IEEE Xplore*

Section X QUALITY MANAGEMENT AND CONTROL, STANDARDIZATION, CERTIFICATION, ACCREDITATION

X.1. *Velizar Vassilev and Dobri Komarski*
STUDY OF THE CAPABILITIES OF A RETROFITTED ROUNDNESS MEASURING INSTRUMENT..... *IEEE Xplore*
X.2. *Tzvetelin Gueorguiev, Iliya Zhelezarov and Miroslav Kokalarov*
APPLICATION OF QUALITY TOOLS IN THE AUTOMOTIVE INDUSTRY.... *IEEE Xplore*
X.3. *Ivan Ivanchev*
EXPERIMENTAL DETERMINATION OF CURVATURE OF RC ELEMENTS SUBJECTED TO BENDING..... *IEEE Xplore*
X.4. *Ivan Ivanchev*
COMPARISON OF EXPERIMENTALLY DETERMINED DEFLECTIONS OF RC BEAMS WITH THOSE CALCULATED ACCORDING EC2 AND ACI 318 USING THE REAL CURVATURE..... *IEEE Xplore*
X.5. *Martin Ralchev, Valentin Mateev, Iliana Marinova, Georgi Kotlarski, Stefan Valkov and Maria Ormanova*
CONTACT FORCE CONTROL FOR SURFACE ELECTRIC IMPEDANCE MEASUREMENTS ..... *IEEE Xplore*
X.6 *Roald Taymanov and Kseniia Sapozhnikova*
MEASURING THE QUALITY OF PRODUCTS AND SERVICES USING ARTIFICIAL INTELLIGENCE SYSTEMS..... *IEEE Xplore*
X.7 *Dimcho Pulov and Krasimir Drumev*
A SYSTEM OF CRITERIA FOR EVALUATING THE QUALITY OF OPTICAL SYSTEMS ..... *IEEE Xplore*
X.8 *Boryana Ilieva-Mihaylova*
THE ROLE OF STANDARDS IN PROMOTING CIRCULAR CONSTRUCTION AND SUSTAINABLE BUILDING PRACTICES ..... *IEEE Xplore*

Section XI IONIZING RADIATION MEASUREMENTS

XI.1. *Aleks Manchev and Dimitar Dimitrov*
INTERLABORATORY COMPARISON OF RESULTS OBTAINED BY METHODS FOR ANALYSIS OF LIQUID RADIOACTIVE SAMPLES ..... *IEEE Xplore*
XI.2. *Vladislav Todorov, Strahil Georgiev, Petya Kovacheva and Krasimir Mitev*
USE OF TDCR SYSTEMS AT SOFIA UNIVERSITY FOR CONTROL OF CERTIFIED RADIOACTIVE SOLUTIONS..... *IEEE Xplore*

XI.3. *Temenuzhka Stoyanova, Neli Ivanova and Alexander Mladenov*
METROLOGYCAL ASSURANCE IN IONIZING RADIATION MEASUREMENTS AT KOZLODUY NPP EAD - ACCEPTANCE AND DEVELOPMENT.....*53*
XI.4. *Bozhidar Krastev, Strahil Georgiev, Vladislav Todorov, Ivelina Dimitrova and Krasimir Mitev*
STUDIES ON THE FEASIBILITY OF RAPID TESTING METHODS FOR ELECTRONIC RADON DETECTORS..... *IEEE Xplore*

SECTION I
GENERAL ASPECTS OF METROLOGY. MEASUREMENT METHODS. UNITY AND ACCURACY OF MEASUREMENTS

Mechanical neural networks

Rumyana Komarska
Precision Engineering and Measurement Instruments
Technical University of Sofia
Sofia, Bulgaria
rumy_ar@abv.bg

***Abstract* – Neural networks are powerful tool in modern artificial intelligence and machine learning, enabling breakthroughs in various fields. This concept is inspired by the structure and function of the human brain. A neural network is a computational model composed of interconnected nodes (called neurons or units) organized in layers. These networks are designed to recognize patterns, learn from data, and make predictions or decisions. Most commonly artificial neural networks are linked to the computer science but there are networks that are bridging the gap between mechanical/physical systems and artificial intelligence. These mechanical/physical neural networks are focus of this paper.**

Keywords – neural network, artificial intelligence, mechanical, layers, nodes

I. INTRODUCTION

Artificial neural networks are computational models composed of interconnected nodes (called neurons or units) organized in layers. These networks are designed to recognize patterns, learn from data, and make predictions or decisions. Neural networks are divided in multiple types of neural networks such as Recurrent neural networks (RNNs), Long short-term memory (LSTM), Convolutional neural network (CNN), Generative Adversarial Networks (GAN)s and more are introduced every day. Mechanical Neural Networks (MNNs) are an emerging concept that draws inspiration from biological and artificial neural networks but applies the principles to mechanical systems. MNN are physical systems designed to mimic the behavior of artificial neural networks (ANNs) using mechanical components. These systems leverage the properties of materials and structures to process information, adapt to external stimuli, and perform tasks such as pattern recognition, optimization, or control. Mechanical Neural Networks (MNNs) have exciting potential for shape-shifting structures—systems that can dynamically change their shape, stiffness, or configuration in response to external stimuli or environmental conditions [1].

Common types of artificial neural network:

- Feedforward Neural Networks (FNNs)
- Convolutional Neural Networks (CNNs)
- Recurrent Neural Networks (RNNs)
- Long Short-Term Memory Networks (LSTMs)
- Gated Recurrent Units (GRUs)
- Generative Adversarial Networks (GANs)
- Autoencoders
- Radial Basis Function Networks (RBFNs)
- Self-Organizing Maps (SOMs)
- Graph Neural Networks (GNNs)
- Modular Neural Networks
- Memory-Augmented Neural Networks (MANNs)
- Physics-Informed Neural Networks (PINNs)
- Extreme Learning Machines (ELMs)
- Neural Architecture Search (NAS)
- Hybrid Neural Networks
- Quantum Neural Networks (QNNs)
- Mechanical Neural Networks (MNNs)
- Optical Neural Networks
- Neuromorphic Networks

The types and applications of neural networks are growing every day but there are several challenges and limitations that still need to be overcome. These systems require a large amount of labeled data for training and computational resources for deep learning that make them expensive. Sometimes the used neural model works well on training data but poorly on unseen data.

II. MECHANICAL (PHYSICAL) NEURAL NETWORKS

Mechanical Neural Networks (MNNs) are a fascinating area of research that bridges mechanics, materials science, and artificial intelligence. MNNs have exciting potential for shape-shifting structures—systems that can dynamically change their shape, stiffness, or configuration in response to external stimuli or environmental conditions. These structures are inspired by biological systems (e.g., muscles, plants) and can be used in applications like adaptive architecture, soft robotics, and aerospace engineering. These kinds of networks belong to a unique and emerging category of neural networks that are not part of the traditional groups like feedforward, recurrent, or convolutional networks. Instead, MNNs fall under the broader category of physical or embodied neural networks, which use mechanical components (e.g., springs, masses, dampers) to mimic the behavior of artificial neural networks (ANNs) in a physical, rather than digital, form. Focus of this paper is indeed mechanical structures and their development in the last years. Mechanical neural networks are commonly used to create shape-shifting structures that can morph e.g. change their geometry or configuration, adapt e.g. adjust their properties (e.g., stiffness, damping) to suit different conditions and respond or react to external stimuli like temperature, pressure, or force. As MNNs mimic the behavior of artificial neural networks (ANNs) but use mechanical elements instead of software a common working flow is as follows:

Key Components of the Neural Networks Structure

Neurons (Nodes) – Basic units of computation in a neural network. Each neuron receives input, processes it using an activation function and produces an output.

Input Layers – Receive the initial data. External stimuli (e.g., force, temperature) are applied to the structure

Hidden Layers – Intermediate layers where computation, feature extraction occurs, or reaction is accumulated/transferred. Mechanical elements (e.g., springs, beams, or actuators) process the input and propagate the response.

Output Layers – Produces the final result (e.g., classification, prediction). The structure changes its shape or configuration based on the processed input.

Weights and Biases – Weights determine the strength of connections between neurons. Biases allow the model to adjust the output independently of the input.

Activation Function – Calculates the output of the node based on its individual inputs and decides whether a neuron should be activated or not. This means that it decides whether the neuron's input to the network is important or not.

Loss Function – Measures the difference between the predicted output and the actual target.

Optimization Algorithm – Adjusts weights and biases to minimize the loss function.

Backpropagation - The error (loss) is calculated and propagated backward through the network. Gradients are computed to update weights and biases.

Training - The process of iteratively adjusting weights and biases to minimize the loss function.

The key idea is that the mechanical connections (e.g., springs, hinges) act as the "weights" of the network, and the non-linear behavior of the system (e.g., buckling, snapping) acts as the "activation function." [1]

Often the MNNs behavior in the application rely on elastic properties of materials (e.g., springs, beams, or flexible structures) to achieve adaptive, learning-like behavior, so mostly MNNs are Elastic Mechanical Neural Networks as a subset of MNNs. These systems use elasticity to store and process mechanical energy, enabling them to perform computations or adapt to external stimuli. Key characteristics of the elastic MNNs are their non-linearity - elastic elements can exhibit non-linear behavior (e.g., buckling, snapping), which is essential for complex computation. Their adaptability is also valuable feature - the stiffness or geometry of elastic elements can be adjusted to change the system's behavior. Elastic systems are also having good energy efficiency as elastic systems can store and release energy, making them efficient for certain applications. Common types of MNNs, categorized based on their design and functionality are Spring-Mass Networks, Beam-Based Networks, Lattice Structures, Tensegrity Networks, Origami-Based Networks, Acoustic Elastic Networks, Hybrid Elastic (Mechanical) Networks.

A. *Spring-Mass Networks*

These are the simplest and most common types of elastic MNNs. They consist of masses connected by elastic springs, where the springs act as the "weights" and the masses act as the "neurons." In these networks, input forces or displacements are applied to the masses. Then the springs transmit forces between masses, and the system's response is determined by the stiffness of the springs. The output is the displacement or force at specific masses. They can be used for pattern recognition, signal filtering, vibration control, etc.

Example of such MNNs are lattices consisting of beams with adjustable axial stiffness. The adjustable beams shown in Fig. 1a) are electromechanical compliant mechanisms that use voice coil actuators, flexure bearings, and strain gauge sensors to adjust their axial stiffness via closed-loop control. The beams are assembled within a regular triangular lattice and join together at nodes, which are composed of rotary flexures (Fig. 1a). These flexures allow the lattice to accommodate deformations as they extend and contract along their axes. To load the MNN, pairs of voice coil actuators connected to a set of decoupling flexures (Fig. 1b) are placed on each of the lattice's input nodes (Fig. 1c), which allow the actuators to independently apply forces to the input nodes. The blue lines drawn on top of each tunable beam. Two shape-morphing behaviors that the simulated MNN achieved by finding a working combination of axial stiffness values using a learning algorithm (Fig. 1d). [2], [7]

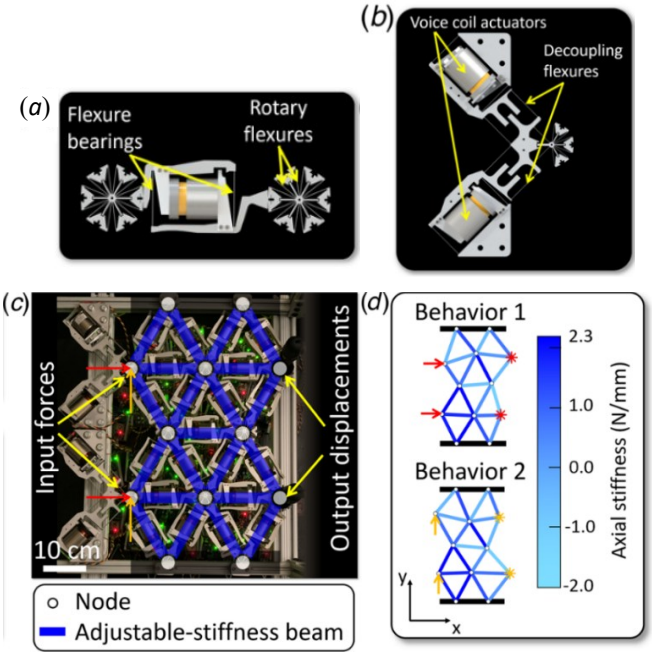

Fig. 1 Spring-Mass Networks.

B. *Beam-Based Networks*

In these systems, elastic beams (e.g., cantilevers or bridges) are used instead of springs.

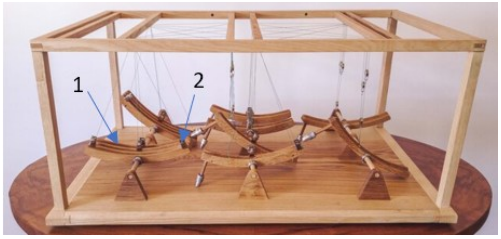

Fig. 2: Beam-Based Networks

The beams can bend, buckle, or vibrate, providing non-linear behavior that mimics activation functions in artificial neural networks. Input forces or displacements are applied to

the beams. The beams deform, and their bending stiffness determines how forces propagate through the network. The output is the displacement or stress at specific points. Their application could be in structural health monitoring, adaptive structures, mechanical computing, etc. The MNN has two input neurons (pos. 1) on the left, four hidden neurons in the middle, and two output neurons on the right. On each neuron, the position of the clamps (pos. 2) set up the weights between the neurons of each layer (fig. 2). [8]

C. *Lattice Structures*

Lattice-based MNNs (fig. 3) are made up of interconnected elastic elements arranged in a periodic or non-periodic pattern. These structures can exhibit complex behaviors due to their geometry and material properties. Forces are applied to specific nodes in the lattice. The elastic elements (e.g., beams, springs) transmit forces, and the lattice's geometry determines the system's response. The output is the deformation or stress distribution across the lattice. Application could be for metamaterials with tunable properties, energy absorption, acoustic wave control, etc.

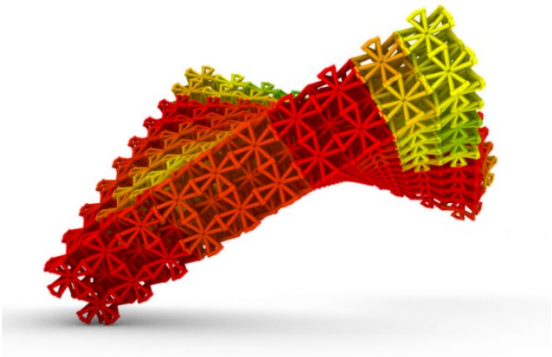

Fig. 3. An example of a metamaterial: the geometry of the lattice determines the emergent material property of the volume

The application to design geometries consisting of volumes filled with lattices (Fig….) that are being modified (pushed, pulled, stretched etc.). In this setting, our model offers real-time structural feedback to the designer. In the examples shown here, green lattice blocks are stiffer than expected (0.5X compression), yellow blocks represent the expected (1.0X) compression, and red blocks are more compressive than average (1.5X). [3]

D. *Tensegrity Networks*

cables to create stable, lightweight systems. These networks can adapt their shape and stiffness in response to external forces. Input forces are applied to the cables or rods.

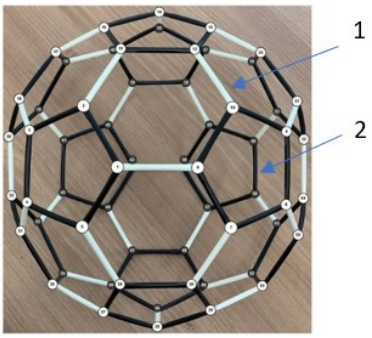

Fig. 4. Tensegrity structures combining rigid rods and elastic flexures

The elastic cables stretch or compress, and the rigid rods maintain the structure's integrity. The output is the overall deformation or stiffness of the structure. Application could be in soft robotics adaptive architecture, biomechanical modeling, etc. Such a structure is shown on fig. 4 where pos. 1 is the flexures and pos. 2 are the rigid rods. The nodal points of the 3D-truncated tetrahedron tensegrity are numbered on the model. [4]

E. *Origami-Based Networks*

Origami-inspired MNNs use folded elastic sheets to create structures that can change shape and stiffness in response to external forces. Input forces are applied to specific folds or panels. The elastic properties of the material determine how the structure deforms. The output is the final shape or stiffness of the structure. Applications could be in deployable structures, soft robotics, adaptive packaging, etc. Metastructure that contains and creates different structures based on origami-inspired systems is shown in fig. 5. [5]

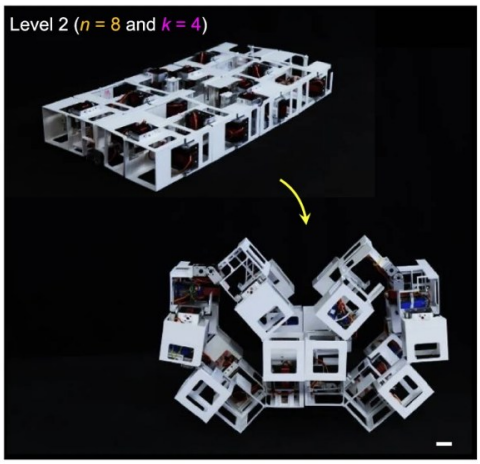

Fig.5. Adaptive hierarchical origami-based metastructures

F. *Acoustic Elastic Networks*

These systems use elastic elements to control and manipulate acoustic waves, mimicking the behavior of neural networks in the acoustic domain. Acoustic waves are applied as input. The elastic elements (e.g., resonators, waveguides) filter or amplify specific frequencies. The output is the modified acoustic signal. Application could be in noise cancellation, acoustic sensors, sound filtering, etc.

Time-of-Flight Convolutional Neural Networks for Noninvasive Acoustic Measurements. Schematic of the symmetric FEM model of the cylindrical container. A wavefield snapshot at an arbitrary time shows the bulk and guided waves (fig.6). [6]

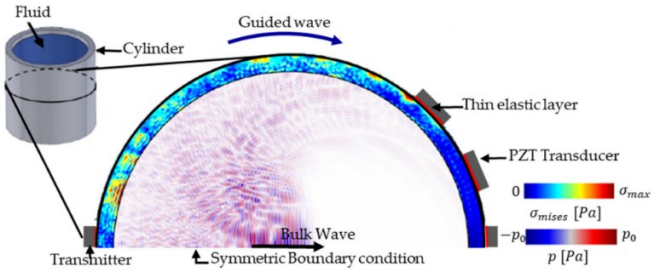

Fig. 6. Acoustic Elastic Networks.

G. Hybrid Elastic (Mechanical) Networks

Hybrid Mechanical Neural Networks (Hybrid MNNs) combine mechanical components (e.g., springs, masses, dampers) with non-mechanical elements (e.g., electronic sensors, actuators, or smart materials) to create adaptive systems that leverage the strengths of both physical and computational systems. These networks leverage the strengths of both physical and computational systems, enabling them to process information, learn, and adapt in ways that purely mechanical or purely electronic systems cannot. Input in these networks are forces or stimuli (e.g., magnetic fields, temperature changes) are applied. The elastic elements interact with the other components (e.g. hidden layers) to produce a response. The output is the combined effect of the elastic and non-elastic components. Application could be for multi-functional materials, advanced robotics, energy harvesting, etc.

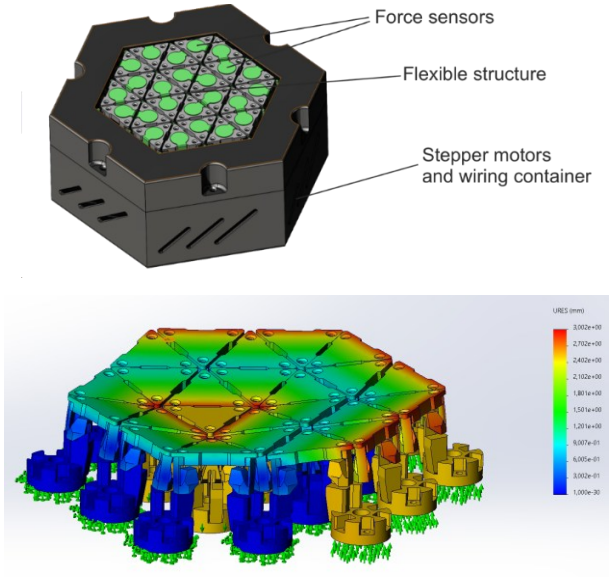

Fig. 7. Surface shaping mechatronic neural network

The mechanical neural network shown on fig. 7 that can be categorized as a Hybrid or Elastic neural network as it contains linear actuators with stepper motors that can change the form of the surface based on the input from the force sensors mounted on the surface. [9]

H. Feedforward structure of Mechanical Neural Networks

There are two main categories of network architectures depending on the type of the connections between the neurons, "feed-forward neural networks" and "recurrent neural networks". If there is no "feedback" from the outputs of the neurons towards the inputs throughout the network, then the network is referred as a "feed-forward neural network".

Otherwise, if there exists such feedback, i.e. a synaptic connection from the outputs towards the inputs (either their own inputs or the inputs of other neurons), then the network is called a "recurrent neural network". Usually, neural networks are arranged in the form of "layer's". Feed-forward neural networks fall into two categories depending on the number of the layers, either "single layer" fig.8 or "multi-layer" fig.9.

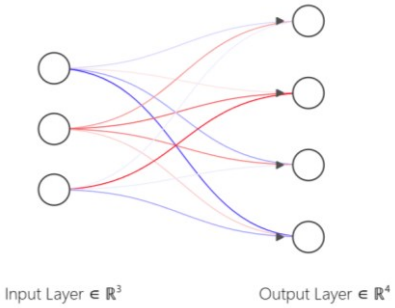

Fig.8. Single layer Feedforward Neural Network

On Fig. 8, a single layer feed-forward neural network (fully connected) is shown. Including the input layer, there are two layers in this structure. Input signals are passed on to the output layer via the weights and the neurons in the output layer compute the output signals.

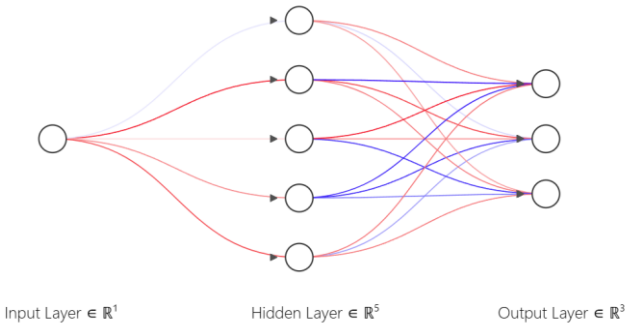

Fig.9. Multi-layer Feedforward Neural Network

On Fig. 9 a multi-layer feed-forward neural network with one "***hidden layer***" is depicted. This is the main difference between single layer and multi-layer FNNs, where the hidden layers could be one or multiple. These layers enable the network to calculate higher order statistics. Both shown FNNs are fully connected because every neuron in each layer is connected to every other neuron in the next forward layer. If some of the synaptic connections were missing, the network would be called as "*partially connected*"

Activation Functions: Introducing Non-Linearity into the Network

A critical component of each neuron in a feedforward neural network, except for the input layer, is the activation function.5 The primary role of the activation function is to introduce non-linearity into the output of a neuron.5 This non-linearity is essential because without it, the entire neural network would essentially behave as a linear regression model, regardless of the number of layers it contains.25 By introducing non-linearity, activation functions enable the network to learn complex patterns and model non-linear relationships that are prevalent in real-world data.3 Several types of activation functions are commonly employed in feedforward neural networks, each with its own mathematical formula and distinct properties.

Common activation functions include:

$$\sigma = \frac{1}{1 + e^{-x}},$$

where x is the input value,

e is Euler's number (≈2.718).

Sigmoid is a mathematical function that maps any real-valued number into a value between 0 and 1. In machine learning, x could be a weighted sum of inputs in a neural network neuron or a raw score in logistic regression. If the output value is close to 1, it indicates high confidence in one class and if the value is close to 0, it indicates high confidence in the other class.

$$\tanh(x) = \frac{e^x - e^{-x}}{e^x + e^{-x}}.$$

Tanh (hyperbolic tangent) is a type of activation function that transforms its input into a value between -1 and 1. As the input becomes more positive, the output approaches 1. As the input becomes more negative, the output approaches -1. At x=0, the output is 0, which is the center of the function. The tanh function has several advantages that make it widely used in neural networks:

Non-linearity: Tanh introduces non-linearity to the model, which allows neural networks to learn complex patterns and relationships in the data. Without non-linear activation functions, a neural network would essentially behave as a linear model, no matter how many layers it has.

Centered Around Zero: The output of the tanh function is centered around 0, unlike the sigmoid function, which outputs values between 0 and 1. This makes the tanh activation function more useful for many types of tasks, as the mean of the output is closer to zero, leading to more efficient training and faster convergence.

Gradient Behavior: Tanh helps mitigate the vanishing gradient problem (to some extent), especially when compared to sigmoid activation. This is because the gradient of the tanh function is generally higher than that of the sigmoid, enabling better weight updates during backpropagation.

Rectified Linear Unit: ReLU(x)=max(0, x),

Where x is the input to the neuron.

The function returns x if x is greater than 0. If x is less than or equal to 0, the function returns 0. Rectified Linear Unit (ReLU) is a popular activation functions used in neural networks, especially in deep learning models. It has become the default choice in many architectures due to its simplicity and efficiency. The ReLU function is a piecewise linear function that outputs the input directly if it is positive; otherwise, it outputs zero. In simpler terms, ReLU allows positive values to pass through unchanged while setting all negative values to zero. This helps the neural network maintain the necessary complexity to learn patterns while avoiding some of the pitfalls associated with other activation functions.

Loss Function Calculation for Feedforward Neural Networks (FNNs)

In Feedforward Neural Networks (FNNs), the loss function (or cost function) measures how well the model's predictions match the true target values. The choice of loss function depends on the task (e.g., regression, classification). Common loss functions for FNNs are shown in the Table 1.

TABLE 1 COMMON LOSS FUNCTIONS FOR FNNS

Task	Loss Function	Formula
Regression	Mean Squared Error (MSE)	$\text{MSE} = \frac{1}{n}\sum_{i=1}^{n}(y_i - \hat{y}_i)^2$
Binary Classification	Binary Cross-Entropy (Log Loss)	$-\frac{1}{n}\sum_{i=1}^{n}[y_i \log(\hat{y}_i) + (1-y_i)\log(1-\hat{y}_i)]$
Multi-class Classification	Categorical Cross-Entropy	$-\frac{1}{n}\sum_{i=1}^{n}\sum_{c=1}^{C} y_{i,c}\log(\hat{y}_{i,c})$

Calculation steps for FNNs

First step is to calculate the forward propagation, where the input passes through the layers and producing prediction $\hat{y}$.

In this case regression function used is:

$$\hat{y} = \sigma(W_2.\,\text{ReLU}(W_1 x + b_1) + b_2,$$

where σ is the output activation, e.g., linear for regression, sigmoid for binary classification.

Next step is to compute loss using functions shown in table 1 to compare predictions $\hat{y}$.

With true labels y. The following example is using MSE regression.

$$L = \frac{1}{n}\sum_{i=1}^{n}(y_i - \hat{y}_i)^2.$$

After that backpropagation (gradient calculation) could be calculated. Compute gradients of loss w.r.t. weights W and biases b. Chain rule trough each layer using MSE gradient for weight W_1 can be applied:

$$\frac{\delta L}{\delta W_1} = \frac{2}{n}\sum_{i=1}^{n}(y_i - \hat{y}_i).\frac{\delta \hat{y}_i}{\delta W_1}.$$

When backpropagation is completed, optimization or update of the parameters can be introduced by adjusting the weights using gradient descent:

$$W_{new} = W_{old} - \eta \frac{\delta L}{\delta W},$$

where η is the learning rate.

III. CONCLUSION

After analysis of all reviewed in this paper mechanical neural networks and type of artificial neural networks (ANNs), the following conclusions can be made:

- Complexity of MNNs is mostly linked to their design (especially compared to ANNs). Creating mechanical systems that mimic the behavior of artificial neural networks or biological neural system is challenging due to the complexity of physical interactions. Once fabricated, mechanical systems are harder to reprogram or adapt compared to software-based ANNs. Manufacturing complex 3D MNN structures with the necessary precision at a micro- or nano-scale presents considerable scalability challenges compared to ANNs and achieving precise control over mechanical components can be more difficult than tuning digital parameters.
- Most common type of neural network used to create MNNs is Feedforward neural network. Even that this is one of the simpler type of networks (compared to the other ANNs reviewed in this paper) combined with the complexity of the mechanical (physical) structures that need to be created, make it one of the preferable choices in this case.
- Mechanical neural networks offer a unique set of advantages. Unlike electronic computers that require continuous power for computation, MNNs can operate based on fundamental physical principles, potentially leading to significantly lower energy consumption. This inherent efficiency could be particularly advantageous in remote or resource-constrained environments. The direct mechanical operation also offers the potential for real-time responsiveness to physical forces, making them suitable for applications requiring immediate adaptation. Furthermore, MNNs have the capability to learn and adapt in situ, without the constant need for external computational resources for every adjustment, allowing for autonomous improvement over time. This ability to develop a form of "muscle memory" could be transformative for creating materials and structures that become increasingly proficient at their tasks with repeated use.

Overall, the field of mechanical neural networks is still in its nascent stages, and many theoretical and practical hurdles remain to be overcome before its full potential can be realized.

ACKNOWLEDGMENT

The authors would like to thank the Research and Development Sector at the Technical University of Sofia for the financial support via Contract № 252ПД0022-06.

REFERENCES

[1] Ryan H. Lee, Pietro Sainaghi, Jonathan B. Hopkins - Comparing Mechanical Neural-Network Learning Algorithms, doi: https://doi.org/10.1115/1.4062313 , 2023

[2] A. Schaffland and J. Schöning, "Mechanical Neural Network: Making AI Comprehensible for Everyone," 2023 IEEE 2nd German Education Conference (GECon), Berlin, Germany, 2023, pp. 1-6, doi: 10.1109/GECon58119.2023.10295144

[3] Dzhudzhev B., Stoyanov N., Pandelova A., Functional Generator, Software Optimization Through Virtual Instruments, 31st International, Scientific Symposium Metrology and Metrology Assurance 2021, DOI:10.1109/MMA52675.2021.9610942Lissa Ross, Using a Graph Neural Network to Learn Mechanical Properties From 3D Lattice Geometry, MESH Consultants, 2020

[4] Lee, S.; Lieu, Q.X.; Vo, T.P.; Lee, J. Deep Neural Networks for Form-Finding of Tensegrity Structures. Mathematics 2022, *10*, 1822. https://doi.org/10.3390/ math10111822

[5] Yanbin Li et al, Adaptive hierarchical origami-based metastructures, *Nature Communications* (2024). DOI: 10.1038/s41467-024-50497-5

[6] Dichev, D., Koev, H., Bakalova, T., Louda, P., "An algorithm for improving the accuracy of systems measuring parameters of moving objects", *Metrology and Measurement Systems*, Vol. 23, issue 4, 2016, pp. 543–554. DOI: 10.1515/mms-2016-0041.

[7] Kupriyanov, O., Trishch, R., Dichev, D., Kupriianova, K., "A general approach for tolerance control in quality assessment for technology quality analysis", In *Grabchenko's International Conference on Advanced Manufacturing Processes*, 2022, pp. 330–339. Cham: Springer International Publishing. DOI: 10.1007/978-3-031-16651-8_31

[8] Dichev, D., Koev, H., Diakov, D., Panchev, N., Miteva, R., Nikolova, H., "Automated system for calibrating instruments measuring parameters of moving objects", In *2017 International Symposium ELMAR*, 2017, pp. 219–224. IEEE. DOI: 10.23919/ELMAR.2017.8124472.

[9] Saini, A.; Greenhall, J.J.; Davis, E.S.; Pantea, C. On the Generalizability of Time-of-Flight Convolutional Neural Networks for Noninvasive Acoustic Measurements. Sensors 2024, 24, 3580. https://doi.org/10.3390/s24113580

[10] Mechanical neural networks: Architected materials that learn behaviors - Ryan H. Lee, Erwin A. B. Mulder, and Jonathan B. Hopkins, Science Robotics,Oct 2022, Vol 7, Issue 7, DOI: 10.1126/scirobotics.abq7278

[11] Schöning, Julius & Wawer, Tim & Griese, Kai-Michael. (2024). AI for non-programmers: Applied AI in the lectures for students without programming skills. 5. 10.48550/arXiv.2403.05547.

[12] Diakov D., Komarski D., Goniometric Compliant Mechanism with Elastic Guides Design and Accuracy Characteristic Analysis, (2024) 34th International Scientific Symposium Metrology and Metrology Assurance 2024, MMA 2024, DOI: 10.1109/MMA62616.2024.10817675

[13] Kupriyanov, O., Trishch, R., Dichev, D., Kupriianova, K., "A general approach for tolerance control in quality assessment for technology quality analysis", In *Grabchenko's International Conference on Advanced Manufacturing Processes*, 2022, pp. 330–339. Cham: Springer International Publishing. DOI: 10.1007/978-3-031-16651-8_31.

[14] Dichev, D., Zhelezarov, I., Madzharov, N., "System for measuring the attitude of moving objects, using a Kalman filter and MEMS sensors", *Comptes rendus de l'Académie bulgare des Sciences*, Vol. 72, issue 11, 2019, pp. 1527–1536. DOI: 10.7546/CRABS.2019.11.10.

[15] Komarski D., Diakov D., Nikolova H., Vassilev V., Analysis of the Impact of the Central Connecting Element Stiffness on the Accuracy Characteristics of Micro-Positioning Elastic Module with 'Butterfly' Flexures, (2023) 33rd International Scientific Symposium Metrology and Metrology Assurance, MMA 2023, DOI: 10.1109/MMA59144.2023.10317907

[16] Komarski D., Vassilev V. Nikolova H., Surface-shaping mechatronic neural network, International Scientific and Technical Conference Automation of Discrete Production Engineering ADP 2025, Sozopol, Bulgaria, 2025, pp. 98-108, https://doi.org/10.53656/adpe-2025.09

SECTION II
SENSORS, TRANSDUCERS AND DEVICES FOR MEASUREMENT OF PHYSICAL QUANTITIES

Self-Diagnosing Multi-Point Thermocouple Measurement Circuit with Decision Tree-Based Error Correction

Artem D. Yakovenko
Self-Validating Sensors, Systems, and Advanced Instrumentation International Laboratory
South Ural State University
Chelyabinsk, Russia
yakovenkoartem00@gmail.com

Alexander L. Shestakov
Self-Validating Sensors, Systems, and Advanced Instrumentation International Laboratory
South Ural State University
Chelyabinsk, Russia
alshestakov@susu.ru

***Abstract* — This article considers a new measurement circuit for a multi-point thermoelectric converter (thermocouple). The proposed circuit consists of four thermoelectrodes forming three measuring junctions. Based on this circuit, a self-diagnostic method for multipoint thermoelectric converters was developed. The method utilizes the algebraic sum of thermoelectric voltages (TEMF) in circuits formed by three thermocouple conductors. Experimental tests were conducted using chromel-copel and chromel-alumel thermocouples. The results showed a temperature measurement deviation of up to 26.7% under varying temperature gradients along the thermoelectrodes. To address this issue, a correction model based on the decision tree method was proposed. By processing additional data from the multi-point thermocouple circuit using decision trees, the temperature measurements were effectively corrected. After correction, the average deviation was reduced to below 3.4%.**

Keywords — multipoint thermoelectric converter, thermocouple, temperature gradient, improvement accuracy of temperature, self-diagnosis of the thermocouple, measurement result correction, thermocouple drift, decision tree

I. Introduction

Multipoint thermoelectric converters measure temperature in multiple zones simultaneously. These devices find application in hydrotreatment reactor monitoring, liquid storage tank temperature gradient assessment, and heat treatment furnace profiling. Three key operational challenges exist:

- thermoelectric characteristic drift occurs during prolonged exposure to temperature cycling;
- measurement deviations appear in individual zones when axial temperature gradients develop;
- field diagnostics prove difficult due to extended service periods or inaccessible installations.

The aim of the article is experimentally evaluating a novel measurement circuit for multipoint thermoelectric converters. The study objectives include:

1. Comparing operational issues between conventional and proposed measurement circuits.
2. Developing a self-diagnostic method using algebraic summation of thermocouple TEMFs.
3. Proposing and experimentally validating an accuracy enhancement method for multizone measurements.

This work was supported by the Ministry of Science and Higher Education of the Russian Federation (project №FENU-2023-0010).

The article comprises seven substantive sections. (Section II) describes the proposed measurement scheme and corresponding equations. (Section III) presents the self-diagnostic method for multipoint thermocouples. (Section IV) analyzes sources of thermocouple measurement errors. (Section V) introduces the correction model using decision tree algorithms for thermocouple signal processing. The experimental portion includes two key sections. (Section VI) demonstrates the effect of temperature profiles on measurement accuracy. (Section VII) presents the correction results.

II. A New Measurement Circuit of the Multipoint Thermocouple

The proposed measurement circuit for a multizone thermoelectric converter (Fig. 1) consists of four thermoelectrodes forming three measurement junctions: one for temperature zone 1 (T1) and two for zone 2 (T2). The study examined a converter with thermoelectrodes 1 and 3 made of chromel, and 2 and 4 made of copel or alumel, forming type K (chromel-alumel) and type L (chromel-copel) thermocouples.

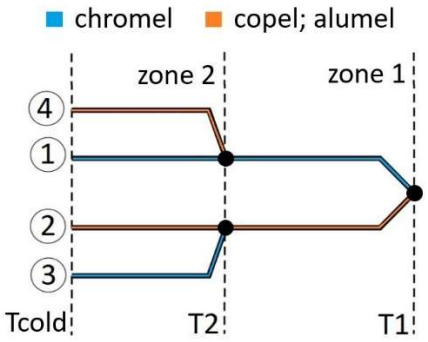

Fig. 1. Measuring circuit of the multipoint thermocouple

This circuit measures the following thermoelectromotive forces:

1. E_{12} (T_1, T_{cold}) – TEMF corresponding to temperature T1. Thermocouple conductors 1 and 2 (Fig. 1).
2. E_{14}, E_{23} (T_2, T_{cold}) – TEMFs corresponding to temperature T2. All conductors of the thermocouple are used (Fig. 1).
3. E_{13}, E_{34}, E_{24} – auxiliary TEMFs for diagnostic purposes. All conductors of the thermocouple are used (Fig. 1).

Thermodynamic analysis of thermoelectric effects shows that the thermoelectromotive force in electrode pair 1-2 (Fig. 1) represents the algebraic summation of individual TEMFs across each conductor branch. For homogeneous thermoelectrodes, this is expressed by Equation 1:

$$E_{12}(T_1,T_{cold}) = \int_{T_1}^{T_{cold}} S_{12}(T)dT = \int_{T_1}^{T_{cold}} S_1 dT - \int_{T_1}^{T_{cold}} S_2 dT\,, \quad (1)$$

where T_{cold} is the cold junction temperature.

Parameters S_1 and S_2 denote the absolute (differential) TEMF of materials 1 and 2 in a temperature field with unit gradient. The absolute TEMF characterizes conductor materials similarly to electrical resistivity or thermal conductivity [2]. It depends on temperature, composition, and material physicochemical state.

The TEMF in a circuit with multiple conductors equals the algebraic sum of TEMFs in sub-circuits (Fig. 2). These sub-circuits consist of conductor 3 paired with conductors 1 and 2, as described by Equation (2).

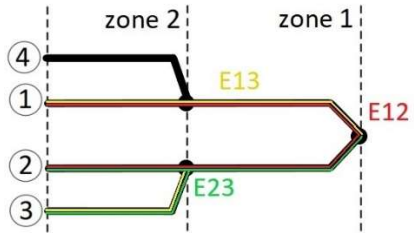

Fig. 2. Calculation TEMF of the circuits in zone 1.

$$E_{T1}(T_1,T_2) = E_{13}(T_1,T_2) + E_{23}(T_1,T_2)\,. \quad (2)$$

The temperature in zone 1 of the thermoelectric converter is determined by TEMF E_{T1} [3]. Zone 2 temperature calculations use primary TEMFs E_{14} and E_{23}. Supplementary TEMFs E_{13} and E_{24} compensate for temperature gradient effects between zones 1 and 2 (Fig. 3). Combining Equations (1) and (2) gives:

$$E_{T_2} = E_{14} - \frac{E_{13}}{2} \qquad E_{T_2} = E_{23} - \frac{E_{24}}{2}\,. \quad (3)$$

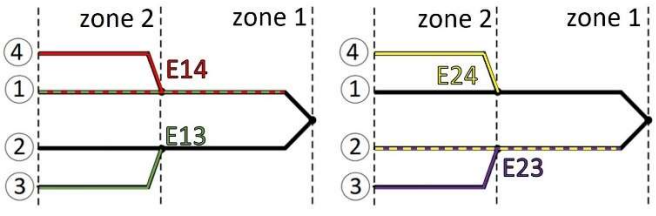

Fig. 3. Calculation of TEMF of the circuits in zone 2.

III. Multipoint Thermocouple Self-Diagnosis Method

The TEMF generated in a circuit with two dissimilar thermocouple conductors (1 and 2) equals the algebraic sum of EMFs from sub-circuits in zone 2 formed by a third conductor (3) with conductors 1 and 2. Fig. 4 demonstrates this principle in a multi-point converter measurement circuit.

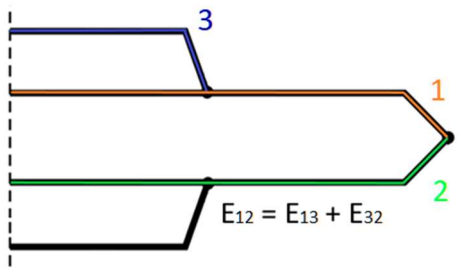

Fig. 4. Using three conductors for diagnostics.

Theoretical analysis shows this algebraic sum equals the EMF generated by the third conductor (Equation 4). Equation 5 detects partial or complete junction failure when the equality fails. Each measured EMF permits two diagnostic equality variations for conductor and junction assessment.

$$E_{12} - \left(E_{13} + E_{32}\right) \cong \varepsilon \quad (4)$$

where E_{12}, E_{13}, E_{32} – measured TEMF values for each pair of multipoint thermocouple wires.

1,2,3 – multipoint thermocouple conductors

ε– permissible deviations according to GOST R 8.585-2001 [4].

The diagnostic procedure involves the following steps:

1. Verification of Equation (4) compliance.

2. Identification of junction integrity. If the equality fails, this indicates partial or complete junction failure in the measurement circuit.

3. Analysis of individual EMF contributions to measurement junctions.

Junction integrity violations occur when equalities are unsatisfied. The impact of measured EMFs on junction integrity is zone-dependent:

- zone 1 junction failure affects measurements: E_{12}, E_{24}, E_{13}, E_{34};
- first Zone 2 junction failure affects measurements: E_{14}, E_{24}, E_{34};
- second Zone 2 junction failure affects measurements: E_{23}, E_{13}, E_{34}.

IV. Problems with the Operation of a Multipoint Thermocouple

Field experience with thermocouple temperature measurements reveals multiple factors increasing measurement errors [4]. Temperature gradients along thermoelectrodes significantly affect measurement accuracy [5]. This effect stems from thermoelectric inhomogeneity in thermocouple wires.

Fig. 5 shows the furnace exit section (points 2-3) contributes most to the resultant TEMF. This section experiences the maximum temperature gradient. For homogeneous thermoelectrodes, the total TEMF follows Equation 1 due to constant differential TEMF throughout the wire.

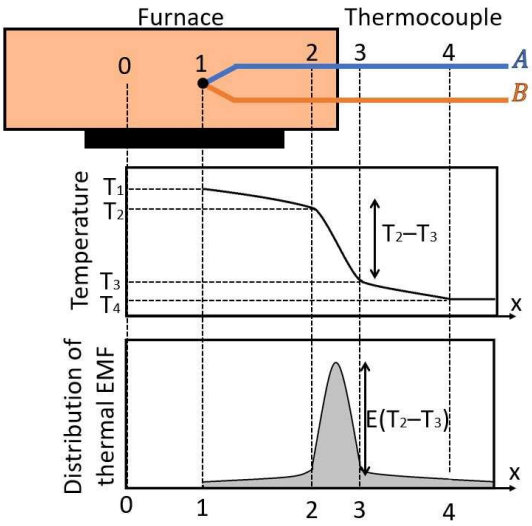

Fig. 5. Effect of temperature gradient on the resulting TEMF.

Thermocouple materials undergo progressive degradation during operation, particularly in high-temperature zones. This deterioration creates thermoelectric inhomogeneity along the thermoelectrodes. When such inhomogeneous sections occur in regions with maximum temperature gradients, the resulting thermoelectromotive force may deviate significantly from nominal process temperature values [6].

This effect persists even when hot and cold junction temperatures remain constant for inhomogeneous thermocouple materials. The maximum TEMF deviation is observed when the thermoelectric converter is not overheated at the junction and when the junction is locally overheated relative to the entire thermocouple structure [7].

Junction temperature remains the primary factor determining TEMF, temperature gradients along the electrodes also affect measurement accuracy.

V. A Correction Model for Multipoint Thermocouple Based on the Decision Tree Algorithm

This paper presents a novel correction model for measurement data based on a decision tree machine learning algorithm. The decision tree approach systematically corrects measurement inaccuracies through pattern recognition and data-driven correction rules. This machine learning system offers advantages over conventional correction methods, including adaptive learning capabilities and handling of nonlinear relationships in thermocouple measurement systems.

To address temperature gradient issues, we developed a machine learning-based correction model. The model uses two primary input datasets: measured thermoelectromotive force (TEMF) values and calculated temperature values from measurements (Fig. 6):

$$T_1 = f\left(T_1^*, T_2^*, E_{34}, E_{14}, E_{24}, E_{13}, E_{23}, E_{12}\right), \quad (5)$$

where T_1*, T_2*– calculated temperatures before correction in zone 1, 2;

E_{34}, E_{14}, E_{24}, E_{13}, E_{23}, E_{12} – measured TEMF values for each pair of thermocouple wires.

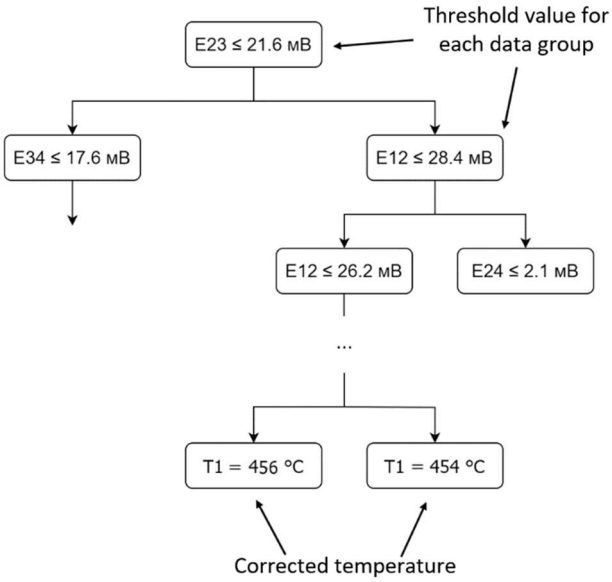

Fig. 6. The structure of the decision tree model.

A decision tree model was implemented for measurement data correction. Decision trees represent a machine learning method that partitions large input datasets into smaller homogeneous groups based on specific conditions.

The decision tree algorithm is a non-parametric supervised learning method. It can handle systematic errors, noise, missing data and other biases [8]. The decision tree construction process involves five steps:

1. Feature selection, the algorithm selects either TEMF values (E_{12}, E_{24}, E_{14}, E_{13}, E_{23}, E_{34}) or measured temperature (T_1, T_2). At each step, it picks the TEMF or temperature that separates the measured data into more homogeneous groups better.

2. Data separation. The measurement data divides into subgroups according to the selected TEMF or temperature parameter.

3. Tree nodes creation. Each subgroup generates a tree node representing the split result.

4. Tree formation stop. Data partitioning and subgroup construction continues until one of the stopping conditions is met, such as reaching a certain tree depth set by the user or data exhaustion.

5. Evaluation and prediction. The constructed tree classifies new measurements. Each measurement processes through the tree from root to leaf nodes, where final corrected temperature values are determined.

VI. Experimental Evaluation of the Temperature Gradient Effect on Thermoocuple Precision

Deviation of measured data can occur when operating both multi-point and single thermoelectric converters. Examples of experiments in which the measured TEMF deviation occurs are presented on Fig 7. There, the thermocouple in zone 2 is overheated relative to zone 1 (Fig. 7a), and when the measurement junction in zone 1 is significantly overheated relative to the whole structure (Fig. 7b).

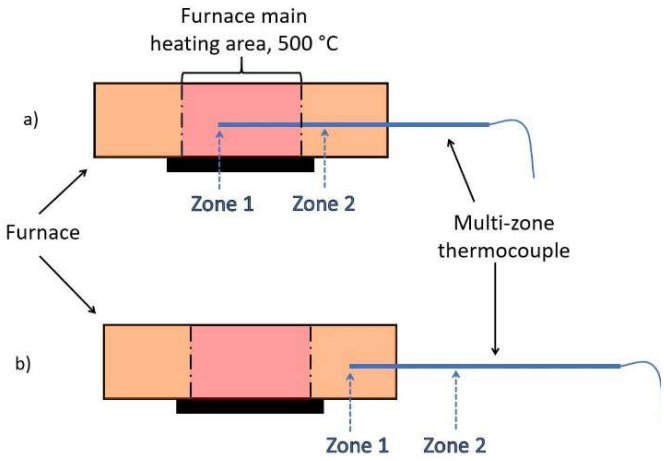

Fig. 7. Scheme of multi-zone thermoelectric converter placement in the furnace. a - the area of main heating falls on zone 2; b - overheating of zone 1 relative to the whole structure.

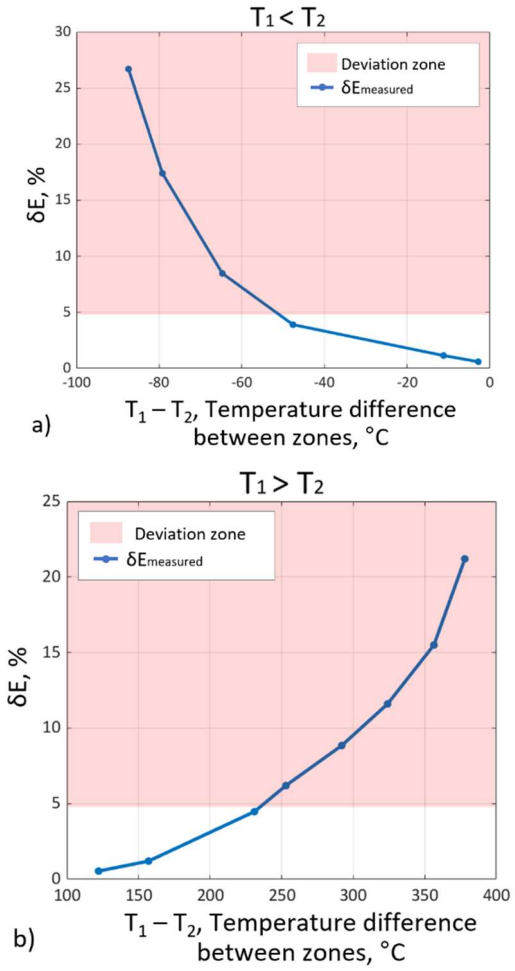

Fig. 8. Scheme of multi-zone thermoelectric converter placement in the furnace. a - the area of main heating falls on zone 2; b - overheating of zone 1 relative to the whole structure.

Conventional and multi-zone thermoelectric transducer were used in the experiment. During the experiment the following EMFs were obtain ned for the multizone transducer: E_{12} for zone 1, E_{14} and E_{23} for zone 2, auxiliary EMFs: E_{34}, E_{13}, E_{24}. The results of the experiment on the chromel-copel thermocouples at overheating of zone 2 show on Fig. 8a, and for the experiment at overheating of zone 1 relative to the whole structure show on Fig. 8b. The both experiments were carried out with the furnace heated to 500 °C.

The experiments demonstrate thermocouples TEMF deviation. The TEMF measurement result in zone 2 deviates from the TEMF reference value and the deviation value reaches 26.7% when the thermoelectric converter in zone 2 is overheated by 50 °C or more relative to zone 1, (Fig. 8a). The measured TEMF deviates in zone 1 and the deviation reaches 22.5%, when zone 1 is overheated by 230 °C and more degrees relative to zone 2 (Fig. 8b).

VII. Experimental Verification of the Proposed Correction Model

Several tests were conducted to validate the proposed decision tree-based correction method. The experiments used multizone thermoelectric converters with chromel-alumel and chromel-copel materials. Tests examined two overheating conditions: in zone 2 and in zone 1.

The model was trained using experimental data collected from 52 independent trials. Each trial incorporated temperature measurements at six distinct points, which allowed a comprehensive dataset for algorithm development. The dataset was partitioned into training and testing subsets, consisting of 290 and 23 measurement points respectively, ensuring robust model evaluation.

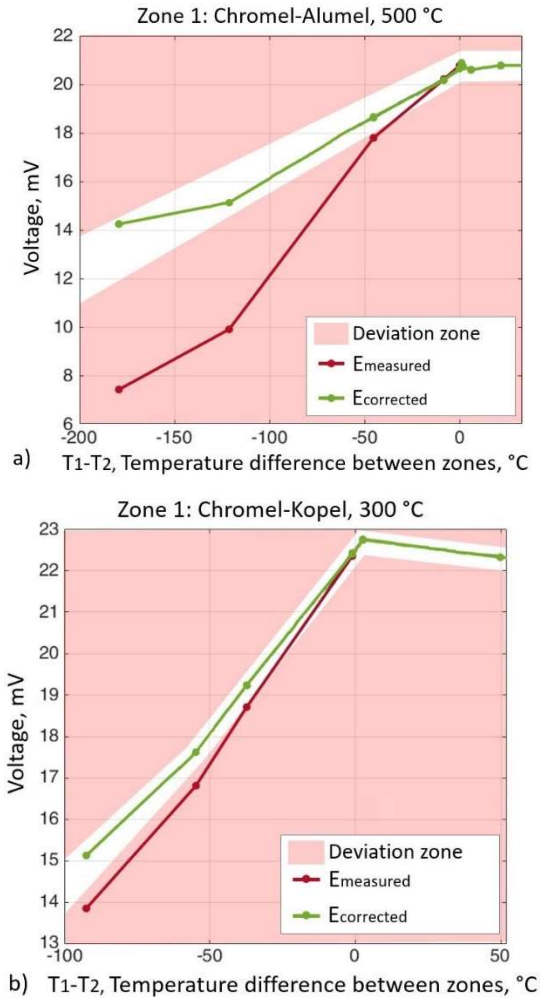

Fig. 9. Introduction of correction of zone 1 thermoelectric converter readings in the event of overheating in zone 2. a - Chromel-alumel thermocouple; b - Chromel-copel thermocouple.

Estimation of performance for the proposed decision tree-based correction method were studied at several tests for the multipoint thermocouples. The examined thermocouples of chromel-alumel and chromel-copel materials were overheating in zone 2 and overheating in zone 1 correspond. The results for the decision tree correction model are presented on Fig. 9 and 10.

The results of the experiment with overheating in zone 2 are presented for the chromel-alumel converter at the temperature point of 500 °C (Fig. 9a) and for the chromel-copel converter - at the temperature point of 300 °C (Fig. 9b). Criteria of acceptable deviations in each case are constructed according to GOST 8.585-2001 [4]. The results of tests on thermoelectric converters show that there is a significant deviation of TEMF values in zone 1 due to overheating of zone 2. After correction of the measurements, the deviations of the obtained results do not exceed the permissible deviations for each type of multi-zone thermoelectric converter.

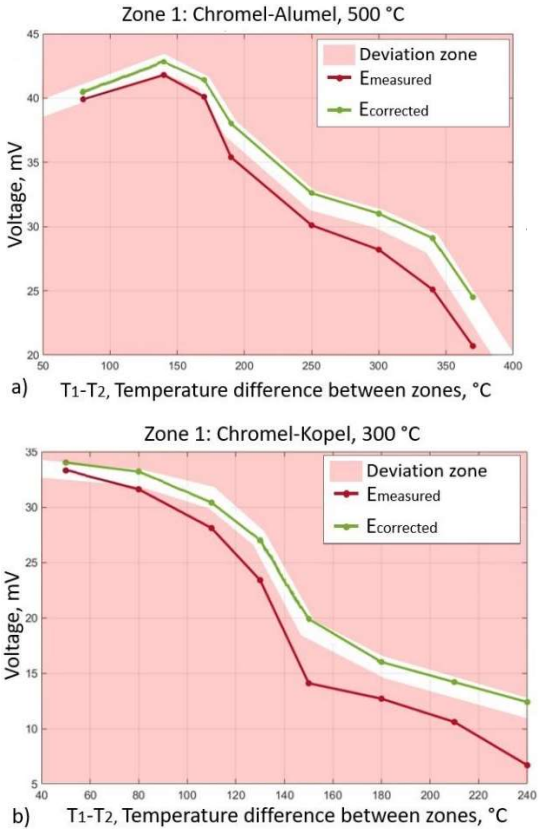

Fig. 10. Introduction of correction of thermoelectric transducer readings in the event of overheating of zone 1 with relation to the whole structure. a - Chromel-alumel thermocouple; b - Chromel-copel thermocouple.

The decision tree method was also used to correct for overheating in zone 1 relative to the whole structure. The chromel-alumel experiments show a temperature point of 500 °C (Fig. 10 a) and for the chromel-copper experiment - a temperature point of 300 °C (Fig. 10 b). The results of the thermoelectric transducers show that there is a deviation of the TEMF values in zone 1. However, after correction of the measurements, the data obtained do not exceed the permissible deviations for chromel-copel and chromel-alumel thermocouples [5].

Implementation of the decision tree-based correction algorithm demonstrated significant improvement in measurement accuracy (Fig. 11). Post-correction analysis revealed an average temperature deviation of less than 3,4 % across all test cases, validating the effectiveness of the proposed methodology.

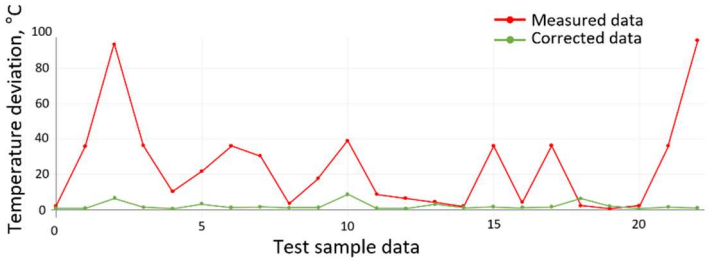

Fig. 11. Test sample for the decision tree method

VIII. Conclusion

This study presents a novel measurement circuit design for multipoint thermocouple systems. The design enables measurement correction through acquisition of additional data. The developed circuit incorporates two key improvements this machine learning-based correction model using decision tree algorithms and a new self-diagnostic method for junction integrity verification. Theoretical analysis confirms that the algebraic sum of EMFs in the circuit equals the EMF generated by the third conductor. This principle enables detection of partial or complete junction failures when the equality is violated. The decision tree-based correction model was experimentally validated using chromel-copel and chromel-alumel thermocouple materials. Results demonstrate the model's effectiveness in temperature correction for both zone 1 and zone 2. The average measurement error decreased significantly from 26.7% to below 3.4%. These findings confirm the decision tree algorithm's capability for accurate thermocouple signal processing. Future research will explore alternative machine learning architectures, hyperparameter optimization, and adaptive learning techniques to further improve the correction model, with potential applications extending to various thermocouple types and configurations. The proposed methodology shows significant promise for enhancing temperature measurement accuracy across industrial and scientific applications.

References

[1] S.A. Korolev and V.P. Mikheev, “Sensors and detectors of physical and energy installations: textbook” Moscow, NRN, 2011, p. 232. (in Russ).

[2] I.L. Rogelberg, and V.M. Beilin, “Alloys for thermocouples reference book” Moscow, Metallurgy, 1983, p. 356. (in Russ).

[3] Pat. US11187592B2 United States. Thermocouple arrangement and method for measuring temperatures / Tomáš Gajdarus, Vitesco Technologies GmbH – № WO2018/210580; 30.11.21.

[4] GOST R 8.585-2001, State System for Ensuring the Uniformity of Measurements. Thermocouples. Nominal Static Conversion Characteristics. Introduced 2002-07-01. Moscow: Standards Publishing House, 2001, 78 pp. (in Russ).

[5] A. M. Belenkiy, A. M. Bursin, and V. V. Kurnosov, Metrology and Thermotechnical Measurements: Textbook. Moscow: MISIS, 2018, 396 pp. (in Russ).

[6] S. N. Dyakov, Physical Foundations of Control and Testing Methods: Textbook. Ryazan: RGRTU, 2014, 96 pp. (in Russ).

[7] A. A. Ryzhova and V. V. Kuzmin, Temperature and Mechanical Quantities Sensors: Educational and Methodological Guide. Kazan: KNITU, 2018, 116 pp. (in Russ).

[8] A. V. Semerikov, Classification of Objects Based on a Neural Network: A Study Guide. Ukhta, Russia: USTU, 2022, 68 pp. (in Russ).

AUTOMATED METROLOGY VERIFICATION AND DIAGNOSTICS OF PRESSURE TRANSDUCERS

1st Lyuboslav Hristov
Metrology
Assurance
Kozloduy NPP EAD
Kozloduy, Bulgaria
lhhristov@npp.bg

2nd Momchil Lazarov
Metrology
Assurance
Kozloduy NPP EAD
Kozloduy, Bulgaria
mglazarov@npp.bg

3rd Ivan Ivanov
Metrology
Assurance
Kozloduy NPP EAD
Kozloduy, Bulgaria
ipivanov1@npp.bg

Summary This report examines the commissioned automated workplaces for metrological verification and diagnostics of the САФІР transducers at the Kozloduy NPP Metrology Assurance Department. A short description of the software platform is made. The structure, hardware components, bench operating modes and working interfaces are described.

Keywords: Automated verification, subject to inspection, diagnostic, automated workplaces, САФІР

I. INTRODUCTION

Accuracy and reliability of measurements of controlled technological parameters are an important factor for safe operation of nuclear facilities, protection of personnel health and environment. Thousands of measurements are made every second at Kozloduy NPP. For this purpose, more than 50,000 measurement instruments and systems, approved for use by Kozloduy NPP metrologists, are used. The automation of activities is the solution to the problem of the large number of verification checks carried out during the limited period of the outage. Today, there are more than 12 automated workplaces in the laboratories of the department.

II. AUTOMATED WORKPLACES

The automated workplaces have a number of advantages compared to the traditional workplaces, such as:

- decreased probability of error occurrence during processing of the obtained results;
- lack of operator's errors;
- large scope of the performed operations;
- high productivity;
- options for the development of additional interfaces and modification of the existing interfaces;
- reliable data archiving and its visualization on graphic displays;
- archive data analysis;
- possibility to modify and supplement both software and hardware without significant costs.

The САФІР pressure transducers used at the automated workplaces of the Metrology Assurance Department for metrological verification and diagnostics have been developed by the equipment manufacturer.

III. AUTOMATED INSPECTION BENCH

Referring to the large-scale modernisation at the Kozloduy NPP and replacement of more than 4400 pressure transducers (sensors), the Kozloduy NPP Metrology Assurance Department purchased two automated benches manufactured by ООО"Манометр" plant, Kharkiv, Ukraine.

Benches are modular and consist of separate elements, the use of which depends on the assigned tasks.

The following operations can be performed using the bench:

- verification of the absolute error and variation of the output signal of pressure transducers;
- verification of the influence of the maximum operating pressure on differential pressure transducers;
- inspection and diagnostics of the pressure transducers and their components – measuring unit and electronic module.

Fig. 1 Automated inspection bench

The automated benches for inspection and diagnostics of Сафір pressure transducers include the following modules:

- installation for verification of the influence of the maximum operating pressure on differential pressure transducers;

- 10 bar automatic pneumatic pressure system with all necessary components (compressor to create the required pressure, manifold, filter, regulator, pressure gauge, etc.);
- ПТС"Сафір" current signal transducer, a set of cables and automated workplace software installed in advance on PC, as well as USB/RS232 transducer;
- ЭК-2 electronic commutator, a set of cables and a connecting cable with a personal computer LPC300-KAB-USB;
- ППД-2 instrument for diagnostics and operability check of the Сафір pressure transducers, a set of cables;
- hydraulic four-way valve manifold with quick connect couplers for transducers;
- pneumatic four-way valve manifold with quick connect couplers for transducers;
- LR-Cal electronic pressure calibrator, model LPC300, together with a set of connecting cables, adapter, charger and LPC-cal software manufactured by Druck&Temperatur Leitenberger GmbH ;
- LPC-S external standard pressure modules for LPC300 calibrator;
- LSP-1000 hydraulic device for creating pressure (up to 1000 bar);
- LPP 60-T pneumatic device for creating pressure (up to 60 bar);
- GW Instek GDM-8245 precise digital multimeter;
- personal computer together with a power supply unit, keyboard, mouse, Windows 10 operating system, MS Office and any software needed for the operation of the automated workplace programme for metrological verification of the pressure transducers;
- printer or MFP device for printing the records from the metrological inspection;
- standard multi-value resistors P4831 type, enabling measurement of the output signal from the transducers as a voltage drop.

The main characteristics of the LPC-S external standard pressure modules for the LPC300 calibrator are the following:

- minus 1÷10 bar;
- 0÷0,25 bar;
- 0÷1 bar;
- 0÷2,5 bar;
- 0÷10 bar;
- 0÷25 bar;
- 0÷60 bar;
- 0÷250 bar;
- 0÷600 bar.

The accuracy class for all LPC-S external pressure modules is 0.025 % of the range.

Absolute error limits when measuring constant voltage in the 0÷10 V ~~mV~~ range for LPC300 calibrator $\leq \pm 1$ mV and resolution 0,1 mV.
Absolute error limits when measuring direct current in the 0÷20 mA range for LPC300 calibrator $\leq$ 5 μA and resolution 0.1 μA.

Fig. 2 LR-Cal reference standard electronic pressure calibrator

IV. SOFTWARE FOR AUTOMATION

During the automated inspection, the specialised automated workplaces program for metrological inspection of pressure transducers is used.

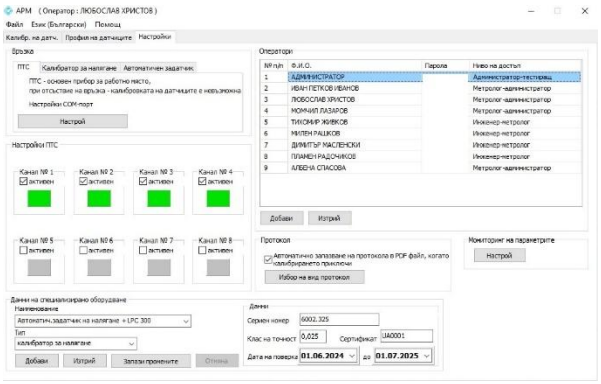

Fig. 3 User menu settings

The Settings menu enables entering information for:

- Operators – name, password and access level;

- Standard data – name, type, serial number, accuracy class and calibration data;

- Connection and adjustment of the direct current (DC) system;

- Each of the listed submenus has an option to perform adjustments and to add or remove records.

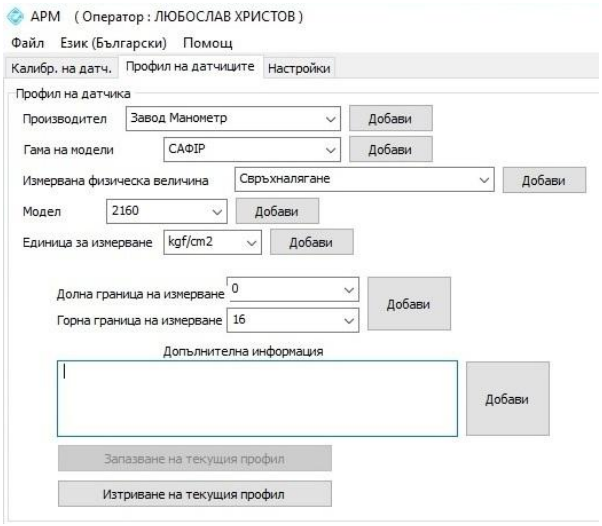

Fig. 4 Sensor profile

The Sensor Profile menu enables the user to enter information for:
-Manufacturer;
-Product range;
-Measured physical quantity;
-Model.
Unit of measurement:
-Lower measurement threshold;
-Upper measurement threshold;
-Additional information.

V. PRESSURE TRANSDUCERS VERIFICATION

According to the type and range, transducers are installed on a pneumatic or hydraulic four-way valve manifold with quick connect couplers. The transducers with measurement range up to 10 kgf/cm^2 are inspected with an automatic pneumatic pressure system equipped with all necessary components (compressor for creating pressure, manifold, filter, regulator and pressure gauge);

Fig. 5 Installation of transducers

Sensors are connected to a САФІР direct current (DC) signal transducer that energises them with 36 V and measures the output signal.

Fig. 6 ПТС Сафір current signal transducer

We start the automated workplaces application for the metrological verification.

We select:

- The group profile data from the available pressure transducer parameters that were entered into the program.
- Standard that we will use during the inspection.
- Number of inspection points.

We enter:

1. The data for each individual transducer:

- Factory number;
- Technological position;
- Date of manufacture.

2. Environmental parameters:

- atmospheric pressure;
- air temperature;
- relative humidity.

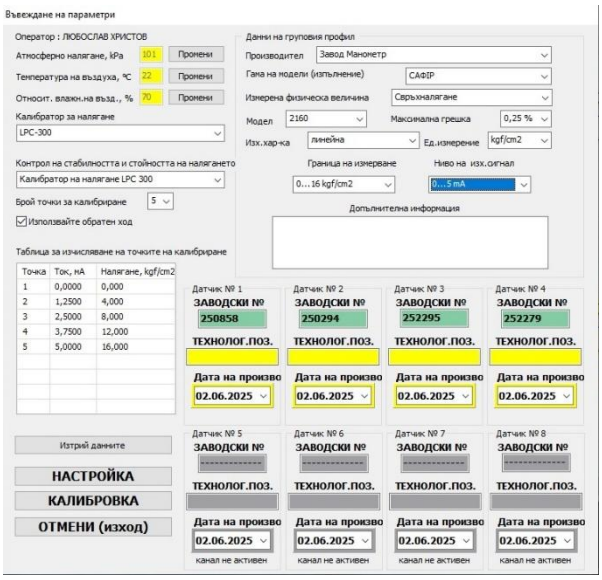

Fig.7 Entering parameters

We start the automated calibration procedure.
The automatic pneumatic pressure system increases the pressure to the upper threshold of the transducers range to inspect the air tightness of the system. When leaks are detected, the system starts to automatically set the pressure within the limits that correspond to 0, 25, 50, 75 and 100 % of the measurement scope. The two thresholds (0 and 100 %) are compulsory.

Fig. 8 User screen of calibration procedure

The automated workplace program performs the following:

- Using the direct current transducer, ПТС"Сафір" simultaneously measures the output signal for all pressure transducers;
- it calculates the measurement errors for all pressure transducers;

- it concludes on the suitability or unsuitability of the transducer depending on whether the maximum measurement error is within the permissible limits;
- it displays the results of the verification, the errors and the conclusion (visually and in words);
- it records all results in a file type (.pdf);
- it creates reporting documents for the performed inspections.

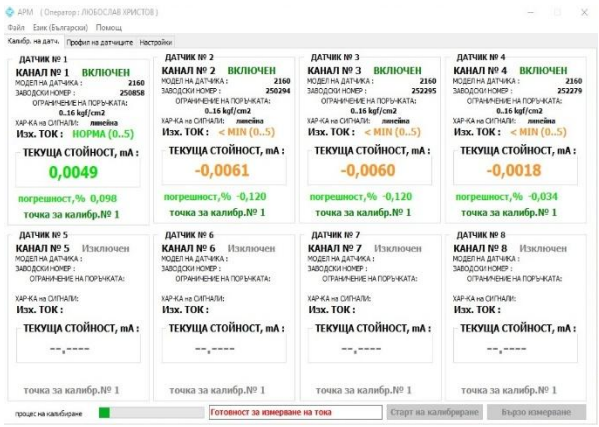

Fig. 9 Inspection

VI. METROLOGY VERIFICATION REPORT

"АЕЦ КОЗЛОДУЙ" ЕАД
ОТДЕЛ "МЕТРОЛОГИЧНО ОСИГУРЯВАНЕ"
ЛАБОРАТОРИЯ "ИЗМЕРВАНЕ НА НАЛЯГАНЕ, РАЗХОД И НИВО"

ПРОТОКОЛ ОТ МЕТРОЛОГИЧНА ПРОВЕРКА
№ _____

Дата на проверка:	02.06.2025
Температура на околната среда:	22 °C
Атмосферно налягане:	101 kPa
Технологична позиция:	РЕЗЕРВ
Средство за измерване	Преобразувател на налягане
Тип	2160
Идентификационен номер	252294
Горна граница на измерване	0/16 kgf/cm2
Обхват на изходния сигнала	0-5 mA
Максимално допустима грешка	0,25 %
Документ по който е извършена проверката:	82.MO.00.MT.371 Методика за метрологична проверка на преобразуватели на налягане
Еталон: Калибратор	LPC-300
Идентификационен номер:	6002.322
Клас на точност	0,025
Дата на калибриране	25.06.2024

Стойност на налягането, kgf/cm2		Пресметнати стойности на изх.сигнал, mA		Измерени стойности на изх.сигнал, mA		Основна грешка , %
Повишаван на налягането	Понижаване на налягането	Повишаване	Понижаване	Прав ход	Обратен ход	
-0,0002	-0,0003	-0,0001	-0,0001	-0,0009	-0,0017	-0,031
4,0360	4,0607	1,2613	1,2690	1,2595	1,2661	-0,057
8,0437	8,0395	2,5137	2,5123	2,5098	2,5077	-0,092
12,0647	12,0303	3,7702	3,7595	3,7660	3,7543	-0,104
16,0672	16,0709	5,0210	5,0221	5,0170	5,0183	-0,079

Резултати от проверка: Максимална основна грешка = -0,104 %

ЗАКЛЮЧЕНИЕ: СИ е метрологично ГОДНО/НЕГОДНО и се/не се допуска за използване

Извършил проверкат:
Експерт метролог ДИМИТЪР МАСЛЕНСКИ _____

Фиг.10 Report

VII. CONCLUSION

The implementation of automated workplaces enabled decrease of the subjective error factor when assessing and processing the measurement results, reduction of the time needed for metrological control and timely development of the reporting documents following the activity. Conditions have been created for the accumulation of data from metrological verifications.

The automated workplaces ensure the quality performance of the metrological control activities regardless of the reduced times for service and maintenance of the facilities.

References

[1] https://manometr-kharkiv.com/
[2] 82.MO.00.MT.371 Methodology for metrological verification of pressure transducers using direct current electrical input signal

SECTION III
MEASUREMENT AND INFORMATION SYSTEMS AND TECHNOLOGIES

Development of Air Purification Drone

1st Popov Teodor Georgiev
dept. Foreign Languages and Applied Linguistics
English Language Faculty of Engineering
Sandanski, Bulgaria
tpopov@tu-sofia.bg

2nd Dzhudzhev Bozhidar Petkov
dept. Information and Measurement Technology
Technical University of Sofia
Sofia, Bulgaria
b.djudjev@tu-sofia.bg

3rd Pandelova Antonia
dept. Information and Measurement Technology
Technical University of Sofia
Sofia, Bulgaria
apandelova@tu-sofia.bg

4th Stoyanov Nikolay
dept. Information and Measurement Technology
Technical University of Sofia
Sofia, Bulgaria
n_stoyanov@tu-sofia.bg

***Abstract*—The paper presents the elements and their characteristics used for developing the air purification drone. Furthermore, conclusions on the capabilities and limitations of the air purification drone are done, as well as the primary challenges encountered in the course of development and testing, along with prospective solutions and improvements that would greatly contribute to system performance in future designs.**

Keywords—air purification, drone, PM 10, Python

I. INTRODUCTION (*HEADING 1*)

Air pollution is one of the most significant environmental and public health challenges of the 21st century. According to the World Health Organization, nearly 99% of the world's population breathes air that does not meet safe pollution standards, and it causes more than 7 million premature deaths each year [1]. Both natural sources—such as volcanic eruptions, wildfires, and dust storms—and anthropogenic sources—like the burning of fossil fuels, agriculture, and industrial processes—contribute to pollution [2]. Air quality is especially poor in urbanized and industrial areas, where seasonal and spatial variation renders static monitoring and filtration systems ineffective.

Conventional air cleaning technologies are typically stationary, depending on ambient airflow to direct contaminated air into contact with filters. Such approaches are inadequate in dynamic environments such as construction sites, wildfire zones, or busy urban corridors, where contaminants are both highly localized and transient [3]. Stationary systems are also hard to deploy quickly in response to emergencies and are of limited utility in open or semi-open spaces.

To overcome these drawbacks, this paper presents a mobile air filtration system using an unmanned aerial vehicle (UAV). The drone is fitted with a high-efficiency particulate air (HEPA) filter and a ventilator, which enables it to actively capture and clean airborne particles during flight. The mobile strategy permits direct intervention in pollution hotspots and provides responsiveness to fluctuating air quality in real time. The project has several aims: to create and design an energy-efficient, lightweight drone that can sustain an operational air filtration unit; to measure its performance in relation to conventional static filters; and to determine its potential for use in urban, rural, and emergency environments. Recent studies have demonstrated that the use of mobile filtering units can decrease concentrations of PM 2.5 by as much as 20% within a matter of minutes in enclosed spaces [4], illustrating the effectiveness of this method in enhancing air quality.

By combining filtration and mobility, the project proposes a novel, scalable, and versatile solution to air-borne pollution. It adheres to the United Nations' global sustainability objectives, specifically SDG 3 (Good Health and Well-being) and SDG 11 (Sustainable Cities and Communities), through the facilitation of decentralized and fast-response air cleansing technologies [5].

II. SYSTEM ARCHITECTURE AND CORE ELEMENTS

The portable air purification system developed for this project revolves around a small quadcopter drone equipped with necessary modules for airborne particulate elimination. Every component was chosen on the basis of factors such as weight, power consumption, modularity, and affordability, to be appropriate for aerial use in varied environments. What follows is a comprehensive description of each component and its function within the system.

A. Drone Platform: GLOBAL DRONE GD95

At the center of the system is the GLOBAL DRONE GD95, which is a light consumer-level quadcopter drone initially designed for aerial photography. Its moderate lift and physical design made it the perfect candidate as a filtration drone prototype. Some of the important specifications are:

- Frame material: ABS plastic
- Motor configuration: X-shape quad layout (4 brushed DC motors)
- Maximum thrust capacity: ~320–400 g
- Max altitude: ~40 meters
- Flight duration (with payload): 15–20 minutes
- Battery type: 3.7V, 2000mAh Li-ion rechargeable battery
- Control range: ~100 meters

Although it had a limited payload capacity and lacked GPS/autonomous navigation, the GD95 served as a stable testbed for early experimentation, especially in indoor and low-wind environments. Weight balancing was done with cable ties and sticky strips, enabling rapid prototyping and field modification.

Identify applicable funding agency here. If none, delete this text box.

978-1-6654-7799-4/25/$31.00 ©2025 IEEE

Fig. 1. Global Drone GD95

B. Ventilation Unit: SUNON PMD2406PTV1-AU Fan

In order to generate directed airflow through the HEPA filter, the system employs a SUNON PMD2406PTV1-AU axial fan, a small but powerful DC ventilator widely applied in industrial and electronics cooling:

- Operating voltage: 24V DC (tested at 12V for power and weight optimization)
- Current draw: ~160mA at 24V
- Airflow capacity: A maximum of 20 L/min (at full voltage)
- Noise level: ~45–55 dB
- Weight: ~60–70 g

Though the fan was nominally rated for 24V, the fan operated acceptably at 12V provided by an auxiliary battery at decreased—but adequate—airflow. Installed at the drone's front, it actively drew ambient air through the filtration apparatus without degrading flight dynamics when properly balanced.

Fig. 2. SUNON PMD2406PTV1-AU Fan

C. Filtration Module: Standard Black HEPA Filter

Filtration was accomplished with a typical black HEPA (High-Efficiency Particulate Air) filter, which can trap 99.97% of particles ⩾0.3 µm in diameter [6]. The module was attached alongside the fan's exhaust trajectory with adhesive and cable ties, creating a portable active filtration system.

- Filtration efficiency: 99.97% @ ⩾0.3 µm
- Weight: ~30 g
- Resistance to airflow: Moderate

Later models are planned to feature white filters, enabling visual observation of particulate accumulation, and modular cartridges for simple replacement or upgrade with activated carbon or UV-C sterilization modules.

Fig. 3. HEPA Filter

D. Power System: Dual Battery Architecture

In order to operate power requirements separately for flight and filtration, they adopted a dual battery system.

Main Flight Battery

- Type: Li-ion rechargeable
- Voltage: 3.7V
- Capacity: 1800mAh (~6.67 Wh)
- Discharge rate: 5–10C
- Function: Powers all motors and core drone systems
- Auxiliary Fan Battery

Fig. 4. Flight Battery

Energizer A23 alkaline battery

- Voltage: 12V

- Capacity: 55mAh
- Runtime (with fan load): ~4–6 minutes
- Function: Operates ventilation system alone

Fig. 5. Energizer A23 alkaline battery

This isolation guaranteed that the operation of fans would not disrupt the drone's primary flight systems, increasing operational stability and safety [7].

E. Sensor Unit: SDS011 PM Sensor (For External Use Only)

While not onboard mounted because of weight constraints, the system employs the Nova SDS011 PM sensor in experimental configurations to track PM2.5 and PM10 levels. The sensor is interfaced with a nearby laptop over USB and takes real-time readings of air quality, represented using a Python-based GUI:

- Detection range: 0.3 – 10 µm
- PM accuracy: ±15%
- Sampling time: 1–3 seconds
- Weight: ~100 g (too heavy for the drone's lift capability)

Fig. 6. SDS011 PM Sensor

The drone is flown manually close to the sensor during experiments, and the variation in particle concentration is measured and analyzed [8].

F. Auxiliary Components and Mounting Solutions

In order to build and stabilize the system, the following components were incorporated:

- Wiring and switches: Utilized for power routing and fan control
- On/off toggle: Manual activation of the ventilator
- Cable ties and double-sided tape: Attached parts without damaging the structure
- Protective ring: Propeller protection standard for drones Every attachment was tested for weight, resistance to vibration, and simplicity of mounting. Low-cost, modular design was given priority to ensure replicability and fieldworthiness.

III. System Assembly and Operational Workflow

The success of the drone-based filtration system is not just in the choice of effective components but also in the manner they are assembled, integrated, and coordinated in use. In this chapter, the physical assembly of the system, the rationale for integration, and the procedure used in operation during testing are described. Modularity, power segregation, and special adaptations necessary to achieve stable and safe drone operation while conducting real-time air purification are highlighted.

A. Component Integration and Mounting

The assembly starts by transforming the base GLOBAL DRONE GD95 into a modular filtration module. Due to the restricted payload capacity (~250 g), components were placed strategically over the frame for a balanced center of gravity and minimal aerodynamic disturbance.

The SUNON PMD2406PTV1-AU ventilator was mounted at the front using cable ties and adhesive. This ensured maximum exposure to ambient air and a clean path for airflow.

The HEPA filter was placed beside the exhaust outlet of the fan with the aid of light plastic holders. The snug fit guaranteed that air sucked in would go straight through the filter, guaranteeing particle collection.

A 12V Energizer A23 battery and a small on/off switch were also mounted on the top side of the frame. These supplied power to the ventilator independent of the drone's flight system.

Cables were routed through small clips and tied beneath the drone’s arms, ensuring no interference with propeller motion.

The flight battery (3.7V 2000mAh Li-ion) was kept in its original housing.

This gave us a completely modular design in which every component could be removed and replaced in a matter of minutes, enabling field repairs, upgrades, or experimental modifications.

Fig. 7. Complete assembly of the Air filtering drone

B. Control System and Sensor Interfacing

In contrast to more sophisticated UAVs, the GD95 lacks onboard computational capability or sensor interfacing. Due to this, air quality sampling was carried out externally, where the SDS011 PM sensor was positioned in a stationary position, connected by USB to a laptop where a Python-based script was being executed.

The Python script does the following:

- Initiates the USB serial communication with the SDS011 sensor
- Reads PM2.5 and PM10 readings at 1-second intervals
- Plots live measurements on a graph using matplotlib
- Incorporates a 3-minute measurement period to normalize test times

This arrangement provides controlled test conditions, with the drone flown towards the sensor in different patterns (e.g., linear, circular, vertical) to measure how efficiently the filter system lowers particulate concentrations over time [9].

Using this configuration allowed for:

- Measurement of pollution concentration changes during drone proximity
- A repeatable methodology across multiple test scenarios
- Comparisons of the performance between tests with/without ventilator on

Python was selected over Arduino due to the USB interface of the sensor, the requirement for graphical output of data, and the reality that Arduino integration would have introduced complexity and weight without benefit [10].

C. Experimental Protocol

In order to examine the filtration system, seven experimental trials were crafted. All of them involved introducing controlled pollution (e.g., through the use of incense smoke) and measuring the changes in air quality as the drone was activated.

Each test adhered to the following general protocol:

- Sensor setup and baseline measurement of air quality (usually PM2.5 and PM10 under clean room conditions).
- Introduction of pollutions (e.g., lighting a small incense stick close to the sensor).
- Deployment of drones after delay or immediate approach, as per the test version.
- Real-time plotting of PM concentration for a steady period (3 minutes).
- Data logging and averaging across five trials for each experiment to reduce noise.

The drone was operated manually with its 2.4 GHz remote control at all times, and the ventilator was turned on with the physical switch. In a few instances, the ventilator was kept off in order to examine the effect of airflow created by drone motion alone.

D. Observed Workflow Limitations

During testing, several limitations emerged:

- The short flight time of the drone (~10 minutes) under payload rendered long-duration testing impossible.
- The ventilator auxiliary battery life (~4–6 minutes) placed time constraints and necessitated quick setup and performance.

External environmental factors such as airflow turbulence or slight sensor misplacement could lead to data variability. Because the sensor was stationary, tests did not represent onboard sensing—a compromise required by the low payload tolerance of the drone. In spite of these constraints, all configurations unequivocally proved the system's potential to decrease local PM concentrations in quantifiable manners. Controlled test flights affirmed up to 20–30% decrease in PM2.5 concentration within 2–3 minutes of arborial drone activity, based on the type of experiment [11].

IV. Conclusions

While the drone-based air purification system showed evident functionality in controlled testing, it is necessary to acknowledge its present limitations and points of optimization. These involve weight, energy, filter design, and reliability of operation concerns—all of which affect the system's feasibility in real-world use.

A. Payload and Power Constraints

One of the main limitations of the present platform is the low payload capacity of the GLOBAL DRONE GD95. The plastic frame, along with coreless motors, sustains a maximum added payload of approximately 200–250 g prior to the onset of flight instability. Consequently, the system is not able to carry more massive or additional modules, such as onboard sensors, cameras, or higher capacity batteries.

Likewise, power segregation between flight and filtration systems causes coordination issues. The 2000mAh lithium-ion battery enables flight for about 10 minutes under load, whereas the 12V Energizer A23 battery for the ventilator only lasts 4–6 minutes. In a more integrated design, a central power management system—or a higher capacity lithium-polymer (Li-Po) battery—could drive both the motors and the ventilator, if voltage regulators are implemented to align load demands [12].

B. B) Ventilator and Filter Efficiency

The chosen SUNON PMD2406PTV1-AU fan, while small, operates below its optimum capacity since it is powered by a 12V battery as opposed to its rated 24V. This diminishes

airflow and filtration capacity, restricting how fast contaminated air can be purified throughout drone flybys.

Also, the HEPA filter utilized in the system is a standard and black filter, which makes it hard to judge visually contamination. It would be better if this was replaced with a white or translucent filter so that operators can more easily monitor pollution accumulation. The filter is also secured in position with tape, which makes replacement in the field troublesome. A clip-in cartridge system would enable maintenance to be quicker and minimize operator error on assembly [13].

C. Sensor and Control System Constraints

The SDS011 sensor was operated offboard because of weight constraints and USB-only connectivity. Although this allowed testing to proceed successfully, it constrains the drone from being able to fly autonomously or change its flight path according to real-time air quality feedback.

A more long-term solution would be the incorporation of lighter, serial-output PM sensors (e.g., PMS7003) directly on the drone, along with a microcontroller like an ESP32 or Arduino Nano, which would enable wireless communication and rudimentary onboard data logging or decision-making.

This would also pave the way for using feedback-controlled autonomous routing, where the drone can target areas of pollution hotspots based on GPS or real-time AQI feedback.

D. Structural and Mechanical Enhancements

The GD95 frame is not set up for modular attachments, so adhesives, tape, and cable ties were used. Though useful, they are less than ideal for long-term durability or reuse of components. A future iteration of the drone might use:

- 3D-printed filter and fan mounts
- Shock-absorbing landing gear
- Carbon-fiber propellers or reinforced arms for better lift and less vibration

These upgrades would enhance the mechanical robustness and reproducibility of test results, particularly for outdoor or field use.

E. Possible Real-World Applications and Scalability

Despite these limitations, the system holds significant promise for real-world deployment in areas with:

- Limited infrastructure (e.g., disaster zones, remote rural areas)
- Rapid temporal change in the level of pollution (e.g., urban rush hour, wildfire areas)

Small but urgent requirements (e.g., spot filtration in schools, hospitals, refugee camps) To realize these use cases, the system needs to be more miniaturized, independent, and self-managing, with increased flight duration and increased filtration capability. Future versions should also look into the deployment of drone swarms, where several units operate in parallel, either manually synchronized or as part of a swarm-based routing algorithm. The platform also holds promise outside of civilian uses, such as in military, industrial, and humanitarian situations, where air quality intervention is required nimbly and without extensive infrastructure.

REFERENCES

[1] World Health Organization. (2021). Air pollution. Retrieved from: https://www.who.int/news-room/fact-sheets/detail/ambient-(outdoor)-air-quality-and-health

[2] U.S. Environmental Protection Agency (EPA). (2023). Fast Facts about Transportation Greenhouse Gas Emissions. Retrieved from: https://www.epa.gov/greenvehicles/fast-facts-transportation-greenhouse-gas-emissions

[3] European Environment Agency. (2022). Sources and emissions of air pollutants in Europe. Retrieved from: https://www.eea.europa.eu

[4] Zheng, Y. et al. (2021). "Airborne Filtration using Mobile Robotic Units in Confined Urban Zones." Environmental Pollution Research, 28(3), 243–252.

[5] MIT Environmental Robotics Lab. (2019). Mobile UAV deployment for particulate removal during industrial events. Retrieved from: https://environmentalrobotics.mit.edu/research/mobile-uav-filtration

[6] GLOBAL DRONE. (2023). Product Manual – GD95 Quadcopter Drone. Manufacturer Specifications Sheet. Retrieved from: https://globaldrone.com/GD95

[7] Sunon Inc. (2022). PMD2406PTV1-AU Fan Specifications. Datasheet. Retrieved from: https://www.sunon.com

[8] Nova Fitness Co., Ltd. (2021). SDS011 Laser Dust Sensor – Technical Manual. Retrieved from: https://www.inovafitness.com/sds011

[9] Vassilev V., Komarski D., Nikolova H., Motion and control of surface-shaping mechatronic neural network, International Scientific and Technical Conference Automation of Discrete Production Engineering ADP 2025, Sozopol, Bulgaria, 2025, pp. 138-148, doi: 10.53656/adpe-2025.12

[10] Energizer. (2022). A23 Alkaline 12V Battery Data Sheet. Retrieved from: https://data.energizer.com

[11] [Zhang, H., & Lee, J. (2022). "Compact Environmental Drone Design with Active Filtration." Journal of Emerging Engineering Systems, 11(1), 51–62.

[12] Wang, H., & Zhao, Z. (2022). "Optimization of Li-Po Battery Usage for Multi-Rotor UAV Systems." IEEE Access, 10, 56842–56855.

[13] Zhang, L., & Feng, X. (2021). "Design Considerations for Modular HEPA Filter Cartridges in Mobile Air Purification Devices." Journal of Environmental Engineering Technology, 45(3), 229–237.

System Of Index Identification Of Parameters Of The Equivalent Model Of Substitution Of Objects With Distributed Parameters

Maryna Miroshnyk
dept. of Theoretical and Applied System Engineering
V. N. Karazin Kharkiv National University
Kharkov, Ukraine
m.miroshnyk@karazin.ua
0000000222312529

Anatolii Miroshnyk
dept. of Design Automation
Kharkiv National University of Radioelectronics
Kharkov, Ukraine
anatolii.miroshnyk@nure.ua
0000 – 0001 – 5702 – 9611

Borys Sytnik
dept. of Information technologies
of the Ukrainian State University of Railway Transport)
Kharkov, Ukraine
bts12021947@gmail.com,
0000 – 0002 – 9664 – 5617

Yurii Pakhomov
dept. of Design Automation
Kharkiv National University of Municipal Economy
Kharkov, Ukraine
abc050073@gmail.com
0000-0002-8319-8061

Volodymyr Bryksin
dept. of Information technologies
of the Ukrainian State University of Railway Transport)
Kharkov, Ukraine
vladimir.bryksin@gmail.com,
0000 – 0002 – 8036 – 8811

Andrei Shafranskyi
dept. of dept. of Theoretical and Applied System Engineering
V. N. Karazin Kharkiv National University
Kharkov, Ukraine
shafranskyi.andrei@student.karazin.ua
0009-0004-7725-3556

***Abstract*—**The system of parameter identification of simplified digital models of objects with distributed parameters for digital adaptive controllers is proposed. The methods of realization of models and regulators with controllable tuning parameters are used for distributed software control. Formulas linking the optimal settings of the regulators to the settings of the object models and the adaptive filter are given. The research has shown that the proposed identification system has determined with high accuracy the parameters of the simplified model of objects with distributed parameters.

***Keywords*—** *identification, digital regulator. delay. distributed parameters, irrational transfer function, adaptation, filter, model*

I. INTRODUCTION (*HEADING 1*)

Identification, approximation, interpolation, extrapolation, modeling in digital control systems of the central control system – a set of methods for constructing mathematical models of a dynamic system based on observational data.
value

Problem Statement. For distributed software control it is necessary to use methods of implementation of substitution models of objects with distributed parameters and regulators with controlled tuning parameters. Therefore, a system of parameter identification of simplified digital models of objects with distributed parameters for digital adaptive controllers is needed.

II. ANALYSIS OF RECENT STUDIES

Many thermal, mechanical, and transportation facilities with distributed parameters (DPFs) can be described by linear systems of partial differential equations and lagged partial differential equations (PDEs) [1 - 8].

For example, by heat conduction equations, Fourier mass-conduction equations or Thompson cable equation, which can characterize the signal propagation speed in railroad track circuits, long electric RC - circuits, thermal and mechanical systems (e.g., trains [9]). For a multidimensional analog model of the object with distributed parameters (ODP), it has the following form [1-7]:

$$\frac{\partial^2 e}{\partial x^2}+\frac{\partial^2 e}{\partial y^2}+\frac{\partial^2 e}{\partial xz^2}\text{-RC}\frac{\partial e}{\partial t}=\varphi(x,t), \qquad (1)$$

where $0 \le t \le t_{max}$, $-\infty \le x,y,z \le +\infty$, x,y,z – coordinates for the node points of the mesh RC-model of the object, and for the one-dimensional model

$$\text{-RC}\frac{\partial e}{\partial t}=\varphi(x,t)\ 0 \le t \le t_{max}\ , -\infty \le x \le +\infty. \qquad (2)$$

III. MAIN PART

In [9], the problem of developing fast noise-protected control loops (CLs) for moving objects taking into account distributed mass and the presence of wave-like processes in the propagation of signals and forces along the length of the train is substantiated. The following statement is formulated.

If the controlled ODP contains irrational links in the transfer function, then the controller having proportional, half differential, half integral, half inertial and other irrational links in its structure can optimize the transient process in the closed CHP unit.

The variant of the ODP numerical difference model corresponding to equation (9) has the following form [8]:

$$\begin{cases} \frac{e_m^{n+1}-e_m^n}{\tau}-\frac{e_{m+1}^n-2e_m^n+e_{m-1}^n}{h^2}=\varphi(mh,n\tau) \\ e_m^0=\psi(mh,n\tau) \end{cases}, \qquad (3)$$

where $\tau=\frac{tmax}{\Delta t}$, $h=\frac{lmax}{\Delta x}$, m-number of the model node, n-number of modeling tact.

The heat and mass transfer equations (1), (2) describe the so-called damped links (or half delayed, half inertial, half integral, etc.). The transfer functions of the models of such links may contain operators of the following form [3, 4, 5, 9]:

$W_o(x,s)=K_0 exp(-x\sqrt{s})$,

$W_o(x,s)=K_0(x\sqrt{s})^{-1}$, $W_o(x,s)=K_0(\sqrt{RCs})^{-1}$;

$W_o(x,s)=K_0\left(1+\frac{x}{n}\sqrt{s}\right)^{-n}$, $W_o(x,s)=K_0(1+x\sqrt{s})^{-n}$;

$W_o(x,s)=K_0\sqrt{s}$, $W_o(x,s)=\frac{K_0}{(1+\sqrt{RCs})}$;

$$W_o(x,s)=\frac{K_0}{(1+x\sqrt{s})}, \quad (4)$$

where s – Laplace operator, x – dimensionless relative coordinate (for one-dimensional problem) of the node point of the grid RC-model of the object.

In [9] there is a comparison between two object models: an object with transfer function $W_{01}(x,s)$, consisting of a series-connected semi-exponential link with transfer function $W_1(x,s)=k_0 exp(-x\sqrt{s})$ (4) and aperiodic link $W_0(x,s)=\frac{1}{b_0 s+1}$ [3], [4]

$$W_{01}(x,s)=W_1(x,s)W_0(x,s)=\frac{k_0 e^{-x\sqrt{s}}}{b_0 s+1} \quad (5)$$

and object with transfer function $W_{02}(x,s)$, cconsisting of series-connected links with a pure lag [2] $W_2(x,s)=k_0(x)e^{-\tau(x,s)s}$ and a similar aperiodic link of the form

$$W_{02}(x,s)=W_2(x,s)W_0(x,s)=\frac{k_0 e^{-\tau(x,s)s}}{b_0 s+1}=\frac{k_0}{[b_0 s+1][\frac{\tau(x,s)}{i}s+1]^i}=\frac{k_0}{[T_i s+1]^i}. \quad (6)$$

The equality condition [9] of transfer functions $W_{01}(x,s)=W_{02}(x,s)$ is satisfied if

$$\tau(x,s)=\frac{x}{\sqrt{s}}. \quad (7)$$

The original expression (7) according to [5] is defined by the formula

$$\tau(x,t)=\frac{x}{\sqrt{\pi t}} \quad (8)$$

Thus, the link with irrational transfer function (semi-exponential link) can be replaced by a link with equivalent delay.

The lag value $\tau(x,t)$ в (8) in (8) is a variable function of time t and spatial coordinate x ODP

To determine the value of the equivalent delay, the corresponding (6) differential equation of the object is considered in [9]

$$\sum_{i=1}^{n} b_i(x)V^{(i-1)}(x,t)+V^{(n)}(x,t)=K_0\varphi_0[t-\tau(x,t)] \quad (9)$$

from which the lag value $\tau(x,t)\in(0,t)$ is determined by the inequality

$$0\le t=\tau(x,t)=\frac{x}{\sqrt{\pi t}}, \quad (10)$$

The magnitude of the equivalent lag $\tau(x)$ is determined in [9] from equation (9) at time $t=\frac{x}{\sqrt{\pi t}}$.

Table 1 shows the values of the equivalent lag $\tau(x)$ of the $t=\tau(x)$ object determined from formula (10) by the formula

$$t=\tau(x)=[\tau(x,t)^2 t]^{\frac{1}{3}}=(\frac{x^2}{\pi})^{\frac{1}{3}} \quad (11)$$

Table 1. The values of the equivalent delay $\tau(x)$ of the object determined on the x coordinate by the formula (21)

x	0.1	0.2	0.3	0.4	0.5	0.6	0.7	0.8	0.9	1.0
$\tau(x)$	0.233	0.306	0.371	0.430	0.4858	0.5384	0.5885	0.6366	0.6829	0.7277

In general, the ODP models in [9] are represented by an example of two kinds of mechanical conveyors (Fig.1):

- with length l(v2) varying with velocity v2 according to the law (8) depending on coordinate x and delay time τ(x,t) (upper conveyor belt);
- with constant length corresponding to constant equivalent delay τ(x) (lower conveyor). Linear velocities of both conveyor belts are the same and equal to v1.

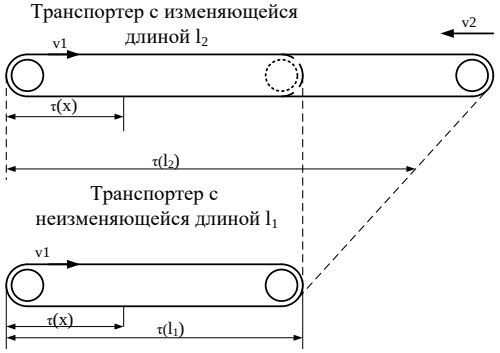

Fig. 1. Mechanical ODP models in the form of conveyors

The time dependences of the upper conveyor length change correspond to (8). Thus, the variable lag time of ODP is modeled by decreasing the length of the upper conveyor. At the same time, the angular velocities of rotation of both conveyors are the same. At the time defined by (11), the variable lag of the upper conveyor is equal to the constant equivalent lag $\tau(x)$ of the lower one. Thus, the movable objects (MO) model described by partial derivative equations was replaced in [9] by an ordinary differential equation with an equivalent constant (for a given relative coordinate x) delay $\tau(x)$. This allowed, on the one hand, to simplify the mathematical models of ODPs (to replace the grid model of ODPs of high dimensionality with a model with equivalent delay), and, on the other hand, to apply to the synthesis of adapative regulators for ODP models with equivalent delay $\tau(x)$. the known [9-12] analytical synthesis methods developed for objects with constant delay time to the synthesis of adapative regulators for ODP models with equivalent delay $\tau(x)$.

In [9] the stability of control loops (CL) is considered with similar facilities. In the dynamics of a closed control loop CL with a transfer function of the form

$$W(q)=\sum_{i=1}^{2n+1} ResA(q_i)(q-q_i) =\frac{A(q^2)}{B(q)}, (q=\sqrt{s}), \quad (12)$$

containing a regulator having in its structure proportional, differential, integral, inertial and other links with operators s, and an ODP having in its structure proportional, semi-differential, semi integral, semi inertial and other irrational links with operators $q=\sqrt{s}$ (4).

Parameters of such e change in time, for example, temperature and properties of cured rubber-technical product [7], train length, distribution of train mass along its length [9], etc. Moving objects (MO) of high-speed rail transportation are complex objects functioning under the influence of

disturbances of variable intensity. Therefore, control loops (CL) with such objects should be characterized by simplicity of realization and high dynamic characteristics. Determination of forces arising in distributed MOs at transient modes of motion is important for designing effective control loops. Transient modes include starting and braking of trains, movement through longitudinal profile fractures, movement during traction force changes, etc. In these modes, due to the necessity of MO speed growth [9,12], it is necessary to take into account the forces arising between the cars, restrictions on their maximum (modulo) values [9-12], and on the speed of transient processes. Manual control is unacceptable here because of the limited psychophysiological reactions of the drivers, as it takes less than 10 ms to evaluate the situations and make a decision to develop new controls. In [9] the method of synthesis of adaptive proportional-half-integral PI controller is proposed and the method of synthesis of digital noise-protected adaptive proportional-half-integral analog PI controller is used [9-13] for a closed control loop containing an adaptive filter with time constant varying to the optimal ratio useful signal / interference and ODP.

Ha Fig. 2 the scheme of the proposed system of index identification of parameters (Kj, Ti, i) of the equivalent substitution model is presented ODP.

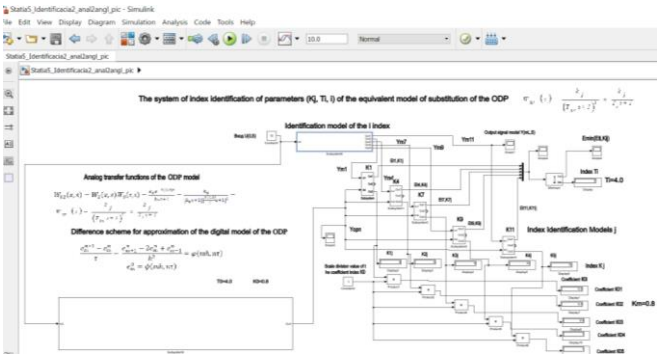

Fig.2 Proposed system of index identification of parameters (Kj, Ti, i) of the equivalent substitution model ODP

If in a closed control loop the object model is described by a transfer function Kj, Ti, i

$$W_m(s) = \frac{k_j}{(T_i s+1)^i} \tag{13}$$

then the expression for the optimal value of the maximum degree of stability is found in [13]

$$I_{onm} = \frac{3}{T_i(i+1)} \tag{14}$$

and allow to obtain expressions for optimal settings of a continuous PID controller with transfer function

$$W(s) = \frac{u(s)}{e(s)} = K_p(1+\frac{K_i}{s}+K_d s) \tag{15}$$

as follows:

$$K_{d\,onm} = \frac{1}{2K_j}\times\left(i(i-1)T_i^2 I_{onm}(1-T_i I_{onm})^{i-2} - 2iT(1-T_i I_{onm})^{i-1}\right)^{i-2} \tag{16}$$

$$K_{ponm} = \frac{1}{K_j}[(1-T_i I_{onm})^i - \mathrm{i}T_i I_{onm}(1-T_i I_{onm})^{i-1} - 2K_j K_{donm} I_{onm}] \tag{17}$$

$$K_{ionm} = \frac{1}{K_j}[K_{ponm}K_j I_{onm} - K_{donm}K_j {I_{onm}}^2 + (1-\mathrm{T}_i {I_{onm}}^i)] \tag{18}$$

Discrete transfer function of PID controller (15) at $s=\frac{1-z^{-1}}{T}$ with independent settings in the form of Z-transformation has the form:

$$D(z) = \frac{u(z)}{e(z)} = K_p\left[1+\frac{K_i T}{(1-z^{-1})}+\frac{K_d}{T}(1-z^{-1})\right], \tag{19}$$

and its corresponding difference equation is of the following form:

$$u[nT] = u[(n-1)T] + (K_p + \frac{K_i T}{2} + \frac{K_d}{T})e[nT] - \\ -(K_p + \frac{2K_d}{T})e[(n-1)T] + \frac{K_d}{T}e[(n-2)T]. \tag{20}$$

IV. Results and their discussion

A system for identifying parameters of simplified ODP numerical models for digital adaptive controllers is proposed.

The difference model of the ODP (train), reflecting the real processes in the train, is justified, since the delay inside the train, which must be taken into account, depends not only on the point (coordinate) defining the process of formation and transmission of control signals, but also on time. In addition, the model takes into account the propagation of the oscillation wave to both ends of the train, which can be reflected by the sequential connection of elastic elements instead of rigid ones..

The conditions under which the MO model containing an aperiodic link and a link with an irrational transfer function can be replaced by a model with an equivalent transfer coefficient *Kj* and a constant (for given indices *i* and *j*) delay $\tau_i=\tau(x)$ using the index identification model are proved. This will allow, on the one hand, to simplify the mathematical models of MO (to replace the discrete grid model of high dimensionality by a single equation), and on the other hand, to apply to the synthesis of regulators for ODP the known analytical methods developed for objects with constant lag time.

The methods of model realization and regulators with controllable tuning parameters are used to control distributed MOs. Formulas linking the optimal settings of regulators with the settings of object models and adaptive filter are given.

The studies have shown that the proposed identification system determined the parameters of the simplified model with high accuracy ODP: *Kj*=*Ko*=0.8, *Ti*=*Ti*=4.

Acknowledgment *(Heading 5)*

A system of parameter identification of simplified digital models of objects with distributed parameters for digital adaptive controllers is proposed.

References

[1] Попович М. Г., Ковальчук О. В. Теорія автоматичного керування: Підручник. — 2-ге вид., перероб. і догі. — К.: Либідь, 2007. — 656 с.

[2] Мірошник А.М. Удосконалення моделі та методу структурної ідентифікації параметрів інерційних об'єктів. / Ситнік Б. Т., Мірошник А.М. // Інформаційно-керуючі системи на залізничному транспорті, 2024, №1.

[3] Аблесімов О. К. Теорія автоматичного керування: навчальний посібник / О. К. Аблесімов – К. : «Освіта України», 2019. – 270 с.

[4] Мірошник А.М. Структурно-параметрична індексна ідентифікація в адаптивних системах управління рухомими об'єктами. / Ситнік Б. Т., Мірошник А.М. // Інформаційно-керуючі системи на залізничному транспорті, 2023, №4, с.3-8.

[5] Дискретні системи автоматичного керування : конспект лекцій / укладачі : Г. В. Кулінченко, А. В. Павлов, П. В. Леонтьєв. – Суми : Сумський державний університет, 2023. – 64 с.

[6] Бесекерский В.Л., Попов Е. II. Теория систем автоматического управления. / Изд. 4-е, перераб. и доп. СПб.: Изд-во «Профессия», 2003. 752 с.

[7] А.О. Бобух. Автоматизовані системи керування технологічними процесами: Навч. посібник. – Харків: ХНАМГ, 2006. - 185 с.

[8] Кутнів М. В. Триточкові різницеві схеми високого порядку точності для систем нелінійних звичайних диференціальних рівнянь другого порядку на півпрямій / М. В. Кутнів, О. І. Паздрій // Математичні методи та фізико-механічні поля. - 2013. - Т. 56, № 1. - С. 40–51. -

[9] Сытник Б.Т. Синтез адаптивных дискретних регуляторов для подвижных объектов с распределенными параметрами и запаздыванием [Текст] / В.А. Брыксин, Г.И.Загарий, С.В.Панченко, Б.Т.Сытник // Науково-технічний журнал "Інформаційно-керуючі системи на залізничному транспорті". – 2009. – №5. – С. 44-55.

[10] Б.Т. Ситнік, Мірошник А.М. Структурно-параметрична індексна ідентифікація в адаптивних системах керування рухомими об'єктами // Інформаційно-керуючі системи на залізничному транспорті. – 2023. – № 4. – С.64-70.

[11] Загарій Г. І. Критерій якості ухвалення рішення по керуванню в складній ієрархічній системі / Г. І. Загарій, С.В. Панченко, Б.Т. Ситнік, В. А. Бриксін // Інформаційно-керуючі системи на залізничному транспорті. – 2009. - № 3. – С. 54-58.

[12] П.О. Качанов, Б. Т. Ситнік, Мірошник А.М. Синтез апаратних та програмних засобів адаптивних дискретних систем управління високого порядку на основі моделі бажаного перехідного процесу гарантованого ступеня стійкості // Вісник Харківського національного технічного університету "ХПІ", 2024, №1-2(11-12),- с.122-139.

[13] Мірошник, А., Качанов, П., Ситнік, Б. (2023). Синтез структури та моделювання адаптивних цифрових формуючих фільтрів. Вісник Харківського національного університету імені В.Н. Каразіна, серія «Математичне моделювання. Інформаційні технології. Автоматизовані системи управління», 59, 35-48. https://doi.org/10.26565/2304-6201-2023-59-04

[14] Новосядлий С. П., Мельник Л. В. Адаптивні фільтри в цифровій обробці сигналів сучасних телекомунікаційних систем / С. П. Новосядлий, Л. В. Мельник // Восточно Европейский журнал передовых технологий. – 2013. – №2/9. – С.48–54.

Device for Rapid Testing of Lithium-Ion Batteries

1st Velev Boris
Institute of Mechanics
Bulgarian Academy of Sciences
Sofia, Bulgaria
b.velev@imbm.bas.bg

2nd Dzhudzhev Bozhidar
Faculty of Automatics
Technical University of Sofia
Sofia, Bulgaria
b.djudjev@tu-sofia.bg

3rd Kamenov Vladimir
Technical University of Sofia)
Sofia, Bulgaria
vladokamenov@tu-sofia.bg

4th Dimitrov Vladimir
Technical University of Sofia
Sofia, Bulgaria
dimitrov@tu-sofia.bg

***Abstract*— A device is presented for rapid testing, evaluation, and grouping-based qualification of "good" and "weak" cells of various types of lithium-ion batteries. The types of essential qualification tests required for identifying "weak" cells are listed. For the purpose of testing the device, rapid qualification tests were conducted to measure the internal resistance R_{in} and assess the functionality (State of Health, SOH) of prismatic LFP cells. The graphical (visual) identification of "weak" cells is carried out using the LabVIEW graphical program and the U3 test board for data acquisition by LabJack. In addition to rapid qualification testing, the device can visually determine the remaining capacity, operating range, and state of charge (SOC) of the cell or lithium-ion battery pack by graphically plotting the charge/discharge curve.**

Keywords*— Internal Resistance (Rin), State of Health (SOH), State of Life (SOL), State of Charge (SOC), Open Circuit Voltage (OCV)

I. Introduction (*Heading 1*)

The lithium-ion battery packs assembled in electric vehicles (EVs) have a long service life — more than 8 years. However, the time is approaching when the parameters of many of these batteries will no longer meet the operational requirements of EVs and will need to be replaced with new ones. The worn-out battery packs are subject to recycling or disposal.

From an economic standpoint, it is reasonable to reuse some of the functioning cells from old, worn-out battery packs for other applications — for example, for assembling packs to power small electric vehicles or for energy storage in autonomous photovoltaic systems (renewable energy installations).

To do this, rapid qualification tests of the worn-out cells must be conducted in order to determine their suitability for a specific application. A single worn-out lithium-ion battery pack from an EV with a high-voltage architecture (400V–1000V) contains hundreds of cells [7], many of which are still suitable for other uses.

Economically, it makes sense to group and qualify these cells by similar characteristics for defined applications, and only the ones that are unfit for reuse should be disposed of. Therefore, it is necessary to develop a specialized device for rapid identification of the "functioning" cells through qualification testing, using graphical programs such as LabVIEW and LabJack.

II. Types of Basic Qualification Tests

A. Load Testing

This test is performed to verify whether the cell can deliver the required power when needed. The load typically represents expected usage conditions under which the cell may operate. It may be a constant or a pulsed load at higher current or power values. Low-power testing is usually done with resistive loads. For testing very high-power outputs with variable loads, other techniques may be used [2].

A cell may demonstrate a higher capacity during intermittent discharging compared to continuous discharging. This is because the cell can recover during idle periods between heavy bursts of current demand. Therefore, testing a battery's capacity using constant high-current discharge may not accurately reflect the capacity achievable under the actual application profile. These profiles may involve simple pulsed loads or more complex high-power load patterns.

B. Functionality Testing

This test checks whether the cell continues to perform as required after being used in its designated application.

There are no simple direct measurements—such as placing a voltmeter across the terminals—that can reliably determine battery condition. A voltmeter reading may give some indication of the state of charge (albeit with a large margin of error), but it cannot determine how well the battery will deliver current when demanded.

The relaxation rate of the cell can quickly provide insight into its state of functionality (SOH).

C. Internal Resistance (R_{in}) Determination

A "weak" cell always has higher internal resistance and lower capacity. To identify such a cell within a battery pack, the actual internal resistance must be measured. However, this cannot be done using a simple ohmmeter, since the current generated by the cell itself interferes with the measurement.

For large cells, an electrical method [1] is used to determine R_{in}. First, the Open Circuit Voltage (OCV) of the cell is measured. Then, a load is connected across the cell, causing a current to flow. This current results in a voltage drop due to the internal resistance (IR drop). The cell's voltage is then measured again while the current is flowing.

The internal resistance is calculated using Ohm's Law, based on the difference between the two voltage measurements and the measured current.

978-1-6654-7799-4/25/$31.00 ©2025 IEEE

D. Open Circuit Voltage (OCV)

The open-circuit voltage of a cell is not a reliable indicator of its ability to deliver current. As the cell ages, its internal resistance increases, which reduces its ability to accept and retain charge. However, the OCV may still appear normal despite the reduced capacity.

Comparing the actual internal resistance to that of a new cell reveals any degradation in functionality.

E. Additional Qualification Tests

In addition to the above, other tests are needed, such as: Determining the state of charge (SOC), Cell balancing and other tests required for assembling the viable cells into packs for specific applications [3,4].

These are key characteristics that must be monitored and managed by the Battery Management System (BMS) and are not the subject of the current study.

III. Objective of the Work

The main objective of this work is to develop and study a device for rapid testing, evaluation, and group-based qualification of "functioning" cells from various types of worn-out lithium-ion battery packs. The device should perform qualification tests to measure internal resistance (Rin), load response, and functionality of prismatic LFP cells, in order to visually identify "weak" cells through the use of the graphical programming environment LabVIEW and the U3 data acquisition board from LabJack [5,6].

In addition to the aforementioned qualification tests, the device should also be capable of determining the remaining capacity and the operating range (SOC) of the cell by graphically plotting the charge/discharge curve.

IV. Development of a Conceptual Diagram for a Lithium-Ion Battery Testing Device

A "weak" cell always has higher internal resistance and lower capacity. To identify a weak cell with elevated internal resistance, the actual internal resistance of the cells within the battery pack must be measured. Internal resistance can be determined using a pulse current test [1].

This method involves performing a series of internal resistance measurements on lithium-ion cells. During the test, a pulse current of 1.5C is applied, where C is the nominal capacity of the cell, for a duration of 2 seconds. A 2-second pulse is long enough to allow the cell voltage to relax and stabilize, yet short enough to have a negligible impact on the state of charge (SOC).

The downside of the method is that it is labor-intensive, slow, and the analog pulses are displayed on an oscilloscope with significant external noise [1].

These disadvantages are avoided in the proposed device by digitizing the measured quantities and pulses using the graphical programs LabVIEW and LabJack [5].

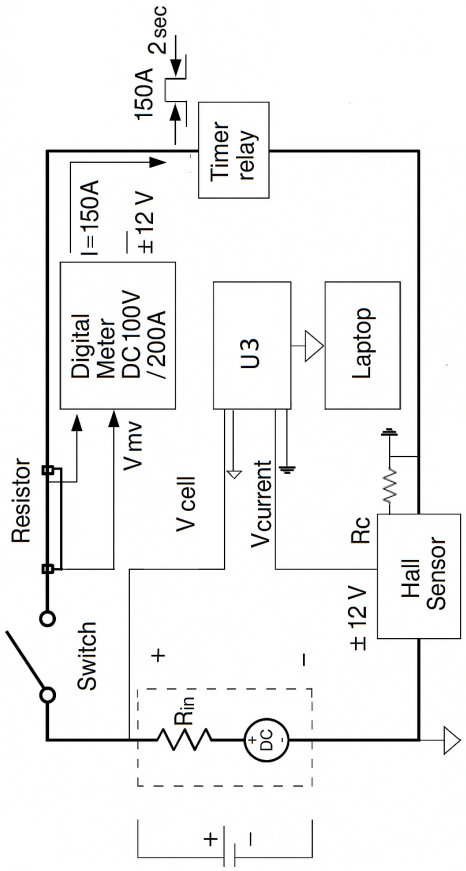

Fig. 1. Block Diagram of a Device for Graphical Measurement of Battery-Cell Internal Resistance

Description of the Elements:

Switch – Manually controls the connection and disconnection of the tested cell to the load circuit.

Resistor (Shunt Element) – Used to measure the voltage drop and determine the current.

Digital Meter DC 100V/200A – Displays the instantaneous values of voltage and current during the test.

U3 Board – Test board from LabJack, used for control and data acquisition.

Timer Relay – Defines the duration of the current pulse at 1.5C (e.g., 150 A for 2 seconds).

Hall Sensor – Measures the current waveform passing through the load resistor Rc.

Rc (Load Resistor) – Dissipates the energy of the current pulse and allows measurement of voltage and current.

Figure 1 shows the block diagram of the device, where the lithium cell is modeled as a voltage source with a small series resistance. A current pulse of 1.5C is converted to a much lower current level passing through a small Shunt Resistor. The voltage across the Shunt Resistor and the voltage of the cell are measured using the graphical programs LabVIEW and LabJack via the U3 data acquisition hardware, and displayed on the PC monitor. Using LabVIEW, equations (1) and (2) are applied to determine the internal resistance Rin:

$$\frac{1}{5000} = ratio = \frac{Vcurrent/Rc}{I} \quad (1)$$

$$Rin = \frac{\Delta Vcell}{I}, I = 150A \quad (2)$$

According to this scheme, a fully charged cell is connected to the load resistor *Rc* and the internal resistance measuring device, as shown in the diagram in Figure 1. For example, for prismatic LFP ($LiFePO_4$) cells with a capacity of 100 Ah, pressing a switch activates a relay timer, causing a current pulse of 150 A to flow through the load resistor *Rc* and the tested cell for 2 seconds.

A Hall sensor sends the voltage of the current pulse to the LabJack U3 testing board within the LabVIEW graphical program, while the cell voltage at open-circuit voltage (OCV) is also input there. The digital voltage signals from the U3 board are sent to the PC, where the internal resistance *Rin* is calculated using the LabVIEW program according to the algorithm based on formulas (1) and (2).

The internal resistance *Rin* can be displayed on the PC monitor or on a digital indicator. The measurements use a graphical user interface (GUI) based on LabVIEW and the LabJack U3 testing board. The voltage and current pulse waveforms can be graphically displayed on the computer monitor for evaluating the state of health (SOH) and state of life (SOL) of the cell and for identifying the "functioning" cells.

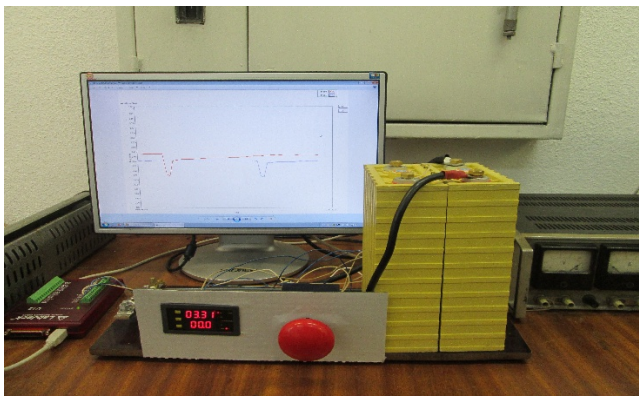

Fig. 2. Photo of the lithium-ion battery cell testing device

The device can operate independently or be integrated as a subsystem into a battery testing stand in laboratory conditions. The device for measuring internal resistance, determining functionality (SOH), and state of life (SOL) of the cell can be applied to all types and sizes of lithium-ion cells.

V. Developing and Testing of the Lithium-Ion Battery Testing Device

Figure 2 shows a photo of the device for testing and evaluating the internal resistance (impedance) *Rin* of two LiFePO4 / 100Ah cells. The determination of *Rin* uses equations (1) and (2) and the schematic in Figure 1. For comparative analysis of the two cells, the internal resistance *Rin* can be displayed graphically or directly in milliohms (mΩ) on the PC monitor.

Figure 3 presents the output data used to calculate the internal resistance Rin. It shows the voltage response of two LFP cells under the application of short load pulses with a current of 1.5C. On the Y-axis the voltage is plotted, while on the X-axis the measurement time is shown. Although the graph displays voltage versus time, these pulses are what make it possible to characterize the internal resistance values of the cells. The method for determining Rin is based on measuring the instantaneous voltage drop (ΔUcell) at a known current (I) and calculating the internal resistance using Ohm's law through formula (2)

Figure 3 graphically shows the internal resistance pulses of the two tested prismatic LiFePO4 cells. The first cell (red line) has a higher internal resistance—65 mΩ—as well as more uneven and slower relaxation to a stable state (load test). It also has a higher open-circuit voltage (OCV), therefore it is a "weak" cell.

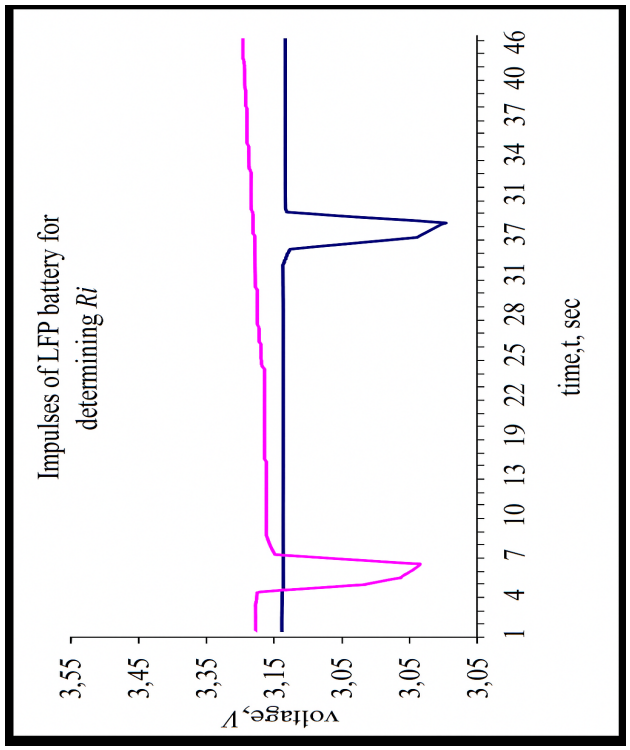

Fig. 3. Internal resistance pulses of two LiFePO4 cells

The second cell (black line) has an internal resistance of 45 mΩ, which is closer to the previously recorded internal resistance of a new cell—39 mΩ—and it immediately transitions to a stable state after loading. Therefore, this cell is still "fit" to perform its functions.

Probably, the cells with higher internal resistance were not well balanced during operation, have reduced capacity, and may self-discharge.

Using this method, "weak" and "fit" cells from a worn lithium-ion battery pack can be quickly identified. After further qualification tests, the cells are grouped by similar

characteristics for specific applications, for example, photovoltaic systems or light vehicles with low-voltage architecture [7].

Figure 4 shows the discharge curve of a lithium-ion battery pack of the LFP type with a low-voltage architecture. It consists of 32 prismatic cells with the electrochemical formula LiFePO4, a nominal open-circuit voltage (OCV) of 96V, and a capacity of 100 Ah.

The fully charged LFP battery pack is subjected to continuous discharge with a current I≈0.25CI \approx 0.25CI≈0.25C depending on the state of charge (SOC), where CCC is the capacity of *the* battery pack — in this case approximately I=20AI = 20AI=20A.

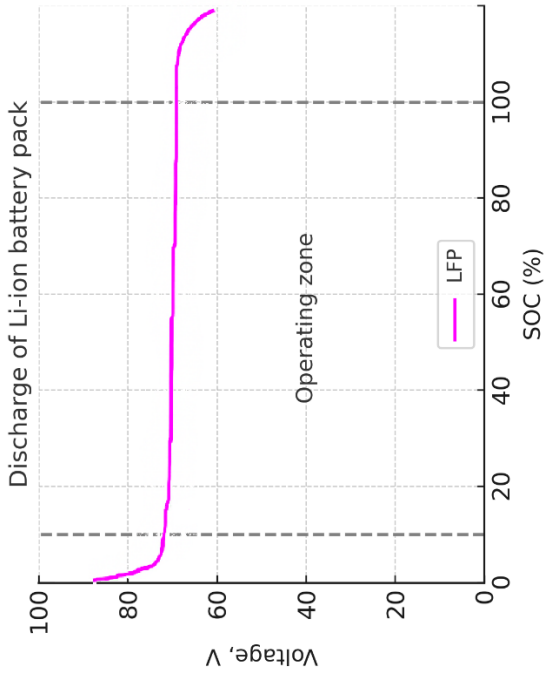

Fig. 4. Discharge curve of a LiFePO4 battery pack

The visualization allows determining the working voltage range of the battery's *open*-circuit voltage (OCV), which is necessary for subsequent functional tests. The small slope of the working range is visible, and it should be between 10% and 90% SOC for this LiFePO4 battery pack.

VI. Conclusions

A device has been developed to perform rapid qualification tests for determining the internal resistance (Rin), load testing, and functionality of lithium-ion cells with the purpose of graphically (visually) identifying "weak" and "good" cells.

The types of main qualification tests that can be conducted with the device are presented, which are necessary to determine the "weak" and "good" cells in lithium-ion battery packs.

The device can also be used for visual determination of the remaining capacity and the working range of the state of charge (SOC), both for individual cells and for packs of different types of lithium-ion batteries intended for specific applications, by graphically plotting the charge/discharge curve.

References

[1] W. Zhu, A Smart Battery Management System for Large Format Lithium Ion Cells, Ph.D. dissertation, University of Toledo, 2011.

[2] D. Doerffel, Testing and Characterisation of Large High-Energy Lithium-Ion Batteries for Electric and Hybrid Electric Vehicles, Ph.D. dissertation, University of Southampton, Faculty of Engineering, 2007.

[3] P. Svens, Methods for Testing and Analyzing Lithium-Ion Battery Cells intended for Heavy-Duty Hybrid Electric Vehicles, Doctoral Thesis, 2014 KTH Royal Institute of Technology Applied Electrochemistry Department of Chemical Engineering and Technology SE -100 44 Stockholm, Sweden, 2014.

[4] www.mpoweruk.com/testing.htm.

[5] https://en.wikipedia.org/wiki/Graphical_user_interface.

[6] www.ni.com/pdf/manuals/373427f.pdf.

[7] B. Velev, B. Dzhudzhev , V. Dimitrov , N. Hinov ; Comparative Analysis of Lithium-Ion Batteries for Urban Electric/Hybrid Electric Vehicles; Batteries, 2024.

AUTOMATED WORKPLACE FOR METROLOGICAL VERIFICATION OF RESISTANCE THERMOMETERS

1st Krasimir Bosilkov
Metrology Assurance Department
Kozloduy NPP EAD
Bulgaria
kkbosilkov@npp.bg

2nd Snezhana Spasova
Metrology Assurance Department
Kozloduy NPP EAD
Bulgaria
sgspasova@npp.bg

3rd Elena Nikolova
Metrology Assurance Department
Kozloduy NPP EAD
Bulgaria
enikolova2@npp.bg

***Abstract* - The verification of resistance thermometers (RTDs) is a process that requires considerable time and short-term temperature stability during measurements at specific temperature points. In most laboratories, the verification process is not automated, which necessitates the presence of a specialist during the procedure as well as for the subsequent calculation of measurement error. This article presents a new automated workplace for the metrological verification of RTDs. The workplace enables the entire verification process, within a range from minus 20 °C to 650 °C, to be controlled by a computer after setting the verification parameters.**

The automated workplace can reduce the risk of human error and deliver real-time data for analysis and reporting. It also offers a solution to the challenge posed by the large number of RTDs.

Keywords - Verification/Metrology/ Automated Measurement and Automated workplace / Software for Process Automation.

I. INTRODUCTION

Accuracy and stability are key characteristics of any measurement process, especially in temperature control. At Kozloduy Nuclear Power Plant (NPP), hundreds of resistance thermometers (RTDs) are used due to their high precision and stability across a wide temperature range. The operating principle of RTDs is based on the change in electrical resistance of the sensing element depending on the variation in the measured temperature. Some types of RTDs used at Kozloduy NPP are shown in fig. 1.

In the "Temperature Measurements" laboratory at Kozloduy NPP, metrological verification is performed on RTDs - platinum, copper, and nickel types.

To improve efficiency, a computer-controlled data acquisition workplace has been developed that automates the verification process fig. 2. This report presents the automated workplace and the results of its application in verifying RTDs within a temperature range from minus 20 °C to 650 °C.

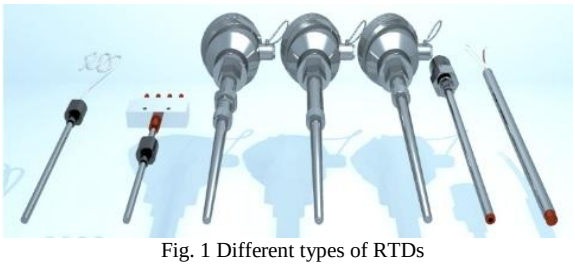

Fig. 1 Different types of RTDs

II. DESCRIPTION OF THE AUTOMATED WORKPLACE

The automated workplace for verifying RTDs in the laboratory uses a comparative method - it compares the temperature measured by a reference thermometer with the temperature measured by the resistance thermometer under verification.

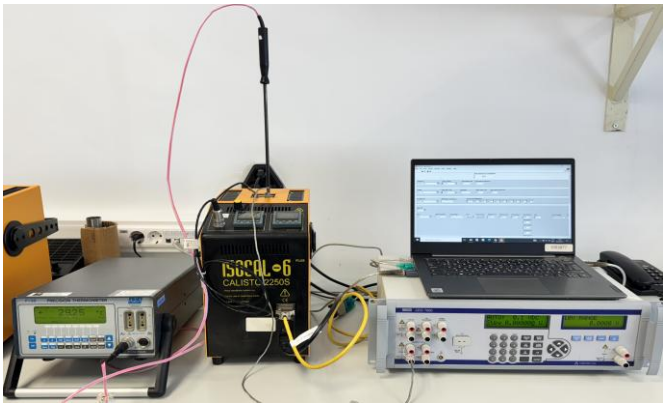

Fig. 2. Automated workplace for the metrological verification of RTDs

The automated workplace includes:

- A digital multimeter with ≥ 4.5 digits for resistance measurement;
- A Dewar vessel or zero thermostat with stability of ±0.01 °C;
- Liquid thermostats with an operating range from minus 30 °C to 250 °C and stability from ±0.025 °C to ±0.05 °C;
- Furnaces with an operating range from 30 °C to 650 °C and stability from ±0.03 °C to ±0.25 °C;
- A reference thermometer;
- A personal computer running LabVIEW;
- A scanner for channel switching.

The workplace can be used with temperature baths and furnaces that have a computer interface. To cover the temperature range from minus 20 °C to 650 °C, four furnaces and baths are used in the laboratory. The reference temperature is determined using a digital reference thermometer with a range corresponding to that of the thermometer under verification.

The block diagram of the workplace is shown in fig. 3.

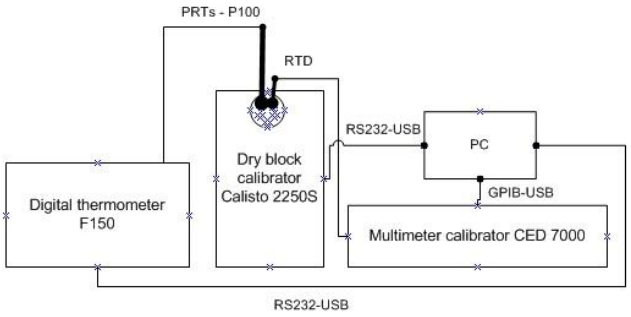

Fig. 3 Block scheme

Compared to non-automated verification, the system offers several advantages, listed below:

- Elimination of human influence in the verification process (the operator only sets the initial verification parameters, after which the measurement system takes full control of the process);
- Automatic storage of measurement results in a database;
- Automated processing of results and generation of a report upon completion of the verification.

III. VERIFICATION PROGRAMME AND PROCEDURE

A. Verification programme

The front panel, as shown in fig. 4, allows the user to configure the standards used, select the type of communication, enter the serial number of the reference digital thermometer, the serial number and scanning channel of each thermometer under verification, choose the temperatures to be measured, and define the acceptable temperature limits.

For a given measurement temperature, the program groups up to three thermometers and the reference thermometer into a single measurement block. If more than three thermometers require measurement at the same temperature, the program will create multiple measurement blocks to accommodate the additional RTDs.

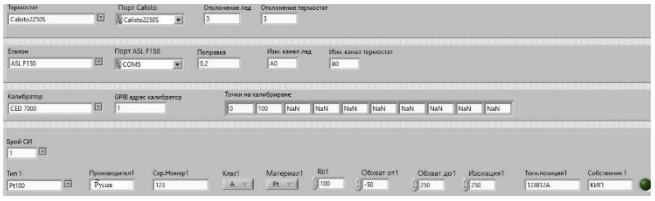

Fig. 4. Front panel of the LabVIEW virtual instrument

B. Verification Proccedure

To determine the reference temperature in the comparative furnace, a reference digital thermometer is used, providing high measurement accuracy. A digital multimeter (DMM) is employed to measure the electrical resistance of the RTD under verification.

Each reference value is calculated as the average of ten consecutive measurements. For each current direction, the DMM readings are also averaged over ten samples to minimize the influence of noise and instability.

The obtained resistance is converted into temperature using a specialized software calculator based on standard conversion tables (e.g., БДС EN 60751 for platinum RTDs).

If the measured values fall outside the predefined acceptable limits, the system continues measuring until stability is achieved. Once an acceptable value is reached, the temperature is stored, and the furnace automatically adjusts to the next temperature point in the verification program.

IV. SOFTWARE FOR THE AUTOMATION OF RESISTANCE THERMOMETER VERIFICATION PROCESS

The software for automating the RTDs verification process is implemented in the LabVIEW environment and provides the following functionalities:

- Configuration of communication and measurement parameters;
- Initialization of system components;
- Calculation of errors and generation of reports;
- Archiving of reports and raw data.

The permissible measurement errors are defined according to international standards and are presented in Table 1.

TABLE I. TOLERANCE CLASSES

Type RTD	Tolerance class	Temperature range, °C	Tolerance values, °C
Platinum	A	-100 ÷ 450	$\pm (0{,}15 + 0{,}002 \cdot \lvert t \rvert)$
	B	-196 ÷ 660	$\pm (0{,}3 + 0{,}005 \cdot \lvert t \rvert)$
	C	-196 ÷ 660	$\pm (0{,}6 + 0{,}01 \cdot \lvert t \rvert)$
Copper	A	-50 ÷ 120	$\pm (0{,}15 + 0{,}002 \cdot \lvert t \rvert)$
	B	-50 ÷ 200	$\pm (0{,}3 + 0{,}005 \cdot \lvert t \rvert)$
	C	-180 ÷ 200	$\pm (0{,}6 + 0{,}01 \cdot \lvert t \rvert)$
Nickel	C	-60 ÷ 180	$\pm (0{,}6 + 0{,}01 \cdot \lvert t \rvert)$

The designation of the material of the sensitive element, the temperature coefficients and the standards for platinum resistance thermometers are given in Table 2.

The temperature coefficient α defines as:

$$\alpha = \frac{R_{100} - R_0}{R_0 . 100}$$

Usually written as α = 3,851x10-3 C-1, where R_0 is the resistance at t = 0 °C and R_{100} at t = 100 °C.

TABLE II. TYPE DESIGNATIONS, TEMPERATURE COEFFICIENTS AND TOLERANCE CLASSES OF RTDs AND SENSING ELEMENTS

Type IPRTs	Material of the sensitive element	Temperature coefficient, α, °C-1	Standard
Platinum	Pt	0,00385	БДС EN 60751, DIN 43760, GOST 6651
	П	0,00391	GOST 6651
Copper	M	0,00428	GOST 6651
Nickel	H	0,00617	GOST 6651

The LabVIEW application allows the configuration of various communication parameters for all peripheral programmable devices (system multimeter, scanner, and furnace controller). Devices can be connected via COM

ports or GPIB interface. Upon software startup, these parameters are preset to default values, but the operator must adapt them according to their specific hardware configuration.

The software provides the operator with a choice between two types of temperature probes: thermocouples or RTD thermometers. Depending on this selection, the program automatically sets the appropriate measurement type (voltage or resistance) and the measurement range of the system multimeter.

The operator defines:

- The number of measurements for each sensor;
- The total number of cycles for the entire process;
- The directory for storing the results.

After configuration, pressing the START button initiates the verification process. The LabVIEW application automatically sets the temperatures, performs the measurements, and records the results without requiring further operator presence.

V. RESULTS

The measurement data generated by the workplace are automatically recorded using a developed LABVIEW virtual tool for connection to a Microsoft Access database.

Fig. 5 presents a user screen of the database containing administrative and measurement data from a metrological check of resistance temperature transducers (RTDs).

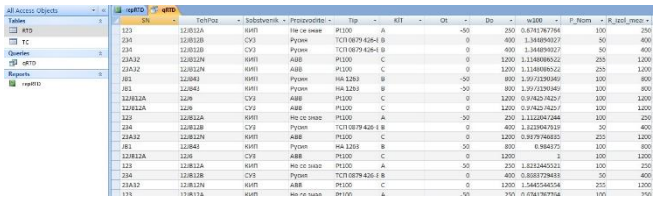

Fig. 5. RTDs database user screen

After the completion of the measurements, the LabVIEW application automatically generates a report that includes:

- Configuration parameters of the measurement;
- Recorded values for each temperature point;
- Calculated errors compared to the permissible; values according to the accuracy class;
- Date, time, and storage directory.

Conclusion regarding compliance or non-compliance of the transducer with the requirements

The report can be archived and used for preparing documentation and future reference.

VI. CONCLUSION

This paper presents an automated workplace for metrological verification of RTDs in a Laboratory for metrology. The workplace is developed in Lab VIEW environment. This automated workplace provides full control of the process and report generation with only initial assistance of laboratory staff. Results show that using this automated system time-consuming verification process for thermometers can be done without full-time presence of laboratory staff.

The implementation of the automated workplace ensured limitation of the subjective factor for making mistakes in the evaluation and processing of the measurement results thermometers. The system archives measurement data, which allows for additional processing for the purpose of analyzing the measurement data.

This is especially important when working with a large number of RTDs, where manual verification would be laborious, time-consuming and prone to inaccuracies. The system ensures high accuracy, efficiency and safety, as measurements are performed in real time and the results are stored in a file for subsequent processing.

REFERENCES:

[1] EN IEC 60751 Industrial platinum resistance thermometers and platinum temperature sensors;

[2] GOST 6651 Термопреобразователи сопротивления. Общие технические требования и методы испытаний;

[3] ISO/IEC Guide 99 International vocabulary of metrology. Basic and general concepts and associated terms (VIM);

[4] 82.MO.00.MT.1229 Proccedure for metrological verification of resistance temperature termometers.

AUTOMATED SYSTEM FOR SILICA MEASURING – "AMI SILICA" TYPE

1st Stoyan Doynov
Technological Measurements and Automation Section
Kozloduy NPP EAD
Bulgaria
sydoynov@npp.bg

2nd Philip Philipov,
Metrology Assurance Department
Kozloduy NPP EAD
Bulgaria
fgfilipov@npp.bg

Abstract: Three-channel system for the automatic and continuous measurement of silicate content in water was installed at the water treatment plant of Kozloduy NPP. The goal was to provide an early warning of depleted anion filter and to prevent silicon dioxide (SiO_2) from entering the circuit in the Turbine halls of Units 5 and 6. This report details the operation and results of this system.

The main objectives are safe operation of the equipment and significant reduction in manual sampling from once every hour to approximately once per shift (every eight hours).

Keywords: Silicates, anion filter, silicon dioxide

I. INTRODUCTION

Danube water is an extremely important resource for the operation of Kozloduy NPP, as it is converted into chemically demineralised water through the Water Treatment Plant (WTP) and is used as a coolant in the main equipment of the nuclear plant. During normal operation, the production rate is 100-200 m³/h, and the maximum capacity is 400 m³/h. The chemical treatment of such quantities of water is a complex multi-step process involving passing the water through various filters and dosing of reagents.

On Fig. 1 we will examine a simplified diagram of the WTP and the positioning of the analysers.

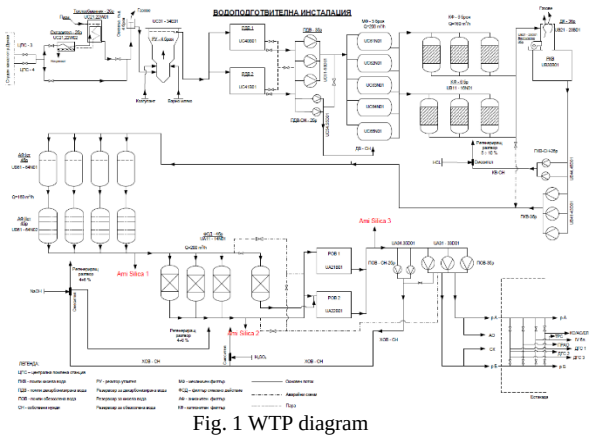

Fig. 1 WTP diagram

One of the important processes is the early capture of dissolved silicon dioxide (SiO_2) in water and limiting its supply to the circuit. Silicates in contact with heat engineering equipment are deposited on the walls and can lead to blockages in the primary circuit or imbalance in the turbine of the secondary circuit.

The first single-channel analyser measures silicates every 10 minutes and takes a sample after the ion exchange filters. Its range is from 0 to 250 ppb, with silicates between 5 ppb and 10 ppb during normal operation. As the anion resin is depleted, they begin to increase and another filter must be put into operation. Such a process can be observed in Fig. 2, where silicates increase smoothly every 10 minutes from 10, 12, 18, 22, 32, 48, 76 and at 102 ppb the filter is stopped for regeneration. Regenerated filter is put into operation and the measured silicates are again below the normal level of 10 ppb.

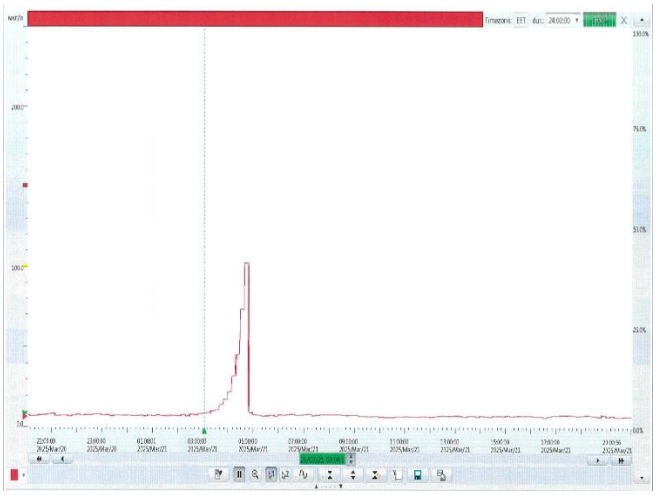

Fig. 2 Trend screen with points loaded from the database.

The second dual-channel analyser measures silicates after mixed-action filters and demineralised water tanks. Its range is 0 to 15 ppb and the channel measurement result is available in 20 minutes. This measurement is primarily preventive because silicates are filtered out by ion exchange filters. According to an internal instruction the norm for silicates at the outlet of the WTP is up to 15 ppb, however, the daily values are 0÷3 ppb.

On Fig. 1 we can see the location of the sampling points.

II. MEASUREMENT

A. Technical characteristics and description

- Power supply voltage: 100÷240 VAC (±10%); 50/60Hz;
- Operating power: max 35 VA;
- Ambient temperature: -10 ÷ +50 °C;
- Humidity: - 10 ÷ 90 % non-condensing;
- Display: backlit LCD, 75 mm x 45 mm;
- Current output: 4 ÷ 20mA;
- Measurement method: colorimetric, molybdeseilicate;
- Measurement range: 1 ÷ 5000 ppb
- Reproducibility: ±1 ppb, or ±5 %, whichever is greater;

Requirements to the sample:
- Sample flow rate: - min. 10 l/h;
- Pressure: 0.15 ÷ 2 bar (2 – 28 PSI);
- Temperature: up to 50°C (122°F).

One cycle of the Ami Silica system lasts 10 minutes, with the following reagents being dosed at different stages:
Reagent 1 – Ammonium molybdate

$_4MoO_{3.3}H_2MoO_{4.4}H_2O.{}_6H_3N$“:

16 g sodium hydroxide pellets + 56 g

ammonium molybdate tetrahydrate;

Reagent 2 – ‘Sulphuric acid – H_2SO_4’:

200ml Sulphuric acid of 25% concentration

Reagent 3 – ‘Oxalic acid NO_2C-CO_2H’:

40g Oxalic acid dihydrate;

Reagent 4 – „Ammonium iron sulphate

$(NH_4)_2Fe(SO_4)_{2.6}H_2O$“: 80ml Sulphuric acid

25%+13g - Ammonium iron sulphate

hexahydrate.

Description:
Swan AMI Silica is a comprehensive system for automatic, continuous measurement of silicate content in water in power plants and desalination facilities.
Silicates are determined by photometric analysis of molybdenum blue at 810 nm.
Silicates and orthophosphates react at low pH with ammonium molybdate, resulting in yellow silicomolybdic acid or phosphomolybdic acid, respectively. Phosphomolybdic acid is broken down by oxalic acid before silicomolybdic acid is reduced with ferroammonium sulphate to a complex molybdenum blue compound.
The necessary reagents are added in three steps to the sample in the photometer, where they enable accurate measurement of the silicate content in the sample after the chemical reactions have been completed.

Fig. 3 shows the general appearance, dimensions and components of the analyser.

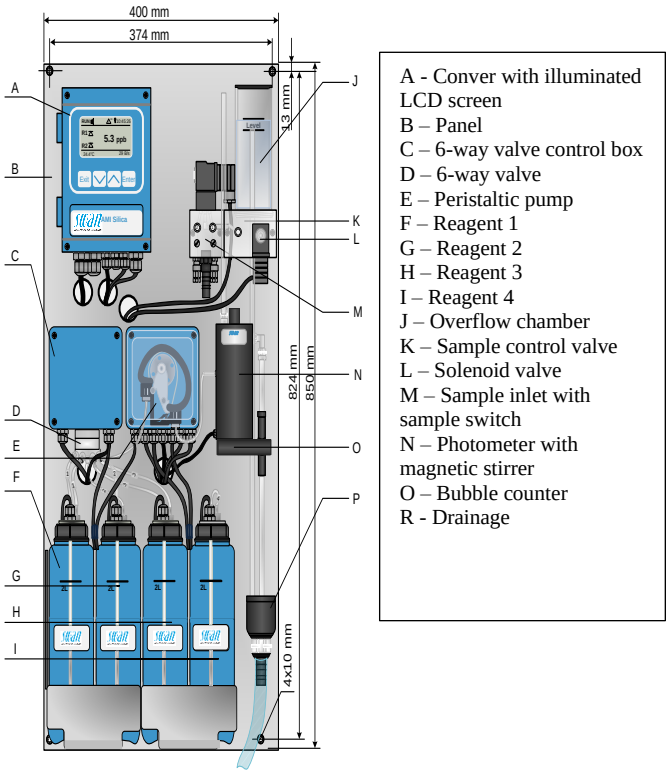

Fig. 3 Swan AMI Silica Analyser

B. Measurement with Swan AMI Silica Analyser

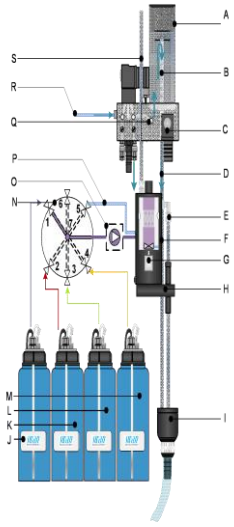

Fig. 4 Legend to Fig. 3

The sample flows through the inlet [R] and the flow control valve [Q] into the overflow chamber [A]. The flow control valve is adjusted so that a small portion of the sample always flows through the overflow tube [B] into the drain [I]. This setting ensures a sufficient flow rate of the sample through the measuring chamber of the photometer [F]. If no measurement is performed, the sample passes through the outlet [E] of the photometer, where it will be vented through the air inlet [S] to generate bubbles. The sample then passes through the bubble counter [H] in the drain [I]. If a measurement cycle starts, the solenoid valve [C] is activated and the sample inlet [D] of the photometer is closed. The 6-way valve [N] automatically rotates to position 1 and a precisely defined amount of reagent from vessel [J] is pumped into the measuring chamber by the peristaltic pump

[O]. Immediately afterwards, the 6-way valve is turned to position 2 and reagent 2 from vessel [K] is pumped into the photometer and mixed with reagent 1 and the sample by the magnetic stirrer [G]. This procedure is repeated with the 6-way valve in position 3 and reagent 3 [L] and the 6-way valve in position 4 and reagent 4 [M]. After completion of the measurement, the electromagnetic valve opens and the measuring chamber is flushed. The level of reagents in the vessels is controlled by reagent level detectors [N].

The quantities of reagents are determined precisely by a specific number of rotations of the peristaltic pump. Once the preset amount of reagent has been sucked out of the vessel, the 6-way valve is turned to position 5, where a sample from the photometer is sucked into line [P]. Together with the sample from the line, the reagents are pumped into the photometer. The sample is measured as follows:

- The sample flows through the overflow chamber in the photometer.
- Measurement cycle begins:
- The sample inlet is closed by activating the electromagnetic valve [C].
- The zero point is measured.
- The 6-way valve is in position 1:
- reagent 1 is sucked out of the vessel [J].
- The 6-way valve is in position 2:
- reagent 2 is sucked out of the vessel [K].
- The 6-way valve is in position 5: sample is sucked into the line and the entire amount of reagent is pumped into the photometer.
- The reagents are mixed with a magnetic stirrer and the first reaction begins.

After 150 sec.

- The 6-way valve is in position 3:
- reagent 3 is sucked out of the vessel [L].
- The 6-way valve is in position 5:
- sample is sucked into the line and the entire amount of reagent is pumped into the photometer.
- The reagents are mixed with a magnetic stirrer and the second reaction begins.

After 90 sec.

- The 6-way valve is in position 4:
- reagent 4 is sucked out of the vessel [M].
- The 6-way valve is in position 5:
- sample is sucked into the line and the entire amount of reagent is pumped into the photometer.
- The reagents are mixed with a magnetic stirrer and the third reaction begins.

After 90 sec.:

- The sample is measured.
- The sample inlet is opened by deactivating the electromagnetic valve.
- The measuring cell of the photometer is flushed
- The 6-way valve is in position 5:
- The reagent inlet tube is flushed with a sample.
- The peristaltic pump rotates for a certain period of time until the reagent inlet tube is filled with a sample.

The measurement cycle takes **10 minutes.**
The diagram below shows the measurement process on the time axis.

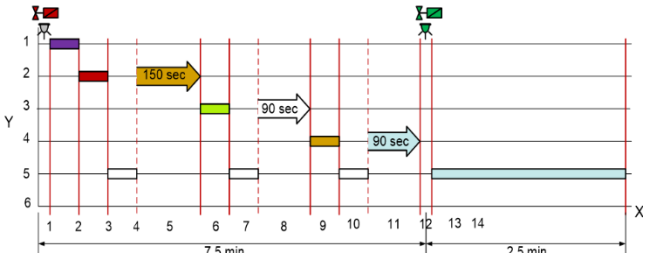

Fig. 4 Measurement cycle

The analysers undergo an internal metrological inspection once a year. To do this, the sample flow is stopped and item 4.1 is selected from the menu. “Manual measurement” is selected from the menu, and a pre-prepared solution with a concentration of 100 ppb is poured into the overflow chamber. The calibration procedure is similar, with the flow being stopped, the standard being poured in and item 3.1.1. Calibration is selected.

III. Conclusion

The implementation of the AMI Silica automated silicate measurement system at Kozloduy NPP has significantly improved the reliability and efficiency of control of silicon dioxide content in the water. The system provides early warning of ion exchange filter depletion and allows timely intervention, which prevents silicates from entering the Unit circuits and minimises the risk of deposits and process disruptions. Significant reduction in the need for manual sampling has been achieved, work of the personnel has been optimised and the overall chemical safety of the process has been improved.

References

[1] Instruction for Maintenance and Repair of the Automated Silica Measurement System Type "AMI Silica"

[2] Technical Documentation for Silica Measurement System Type "AMI Silica"

SECTION VII
MEASUREMENTS IN THE ECOLOGY, BIOTECHNOLOGY, MEDICINE, AND SPORT

Research of applicability of the electronic colorimetry method in medical diagnostics

Iurii Y. Khoroshailo
Department of Design and Operation of Electronic Devices
Kharkiv National University of Radio Electronics (NURE)
Kharkiv, Ukraine
horoshajlo@ukr.net

Yuriy P. Gnidenko
V.N. Karazin Kharkiv National University,
Kharkiv, Ukraine
yuriy.p.gnidenko@karazin.ua

Maksym V. Korbetskyi
Department of Information and Measuring Technologies
Kharkiv National University of Radio Electronics
Kharkiv,
Ukraine
maksym.korbetskyi@nure.ua

Oleksandr B. Galat
Department of Microelectronics, Electronic Devices and Appliances, NURE
Kharkiv, Ukraine
oleksandr.galat@nure.ua

Oleksandr Degtiarov
Department of Information and Measuring Technologies
Kharkiv National University of Radio Electronics
Kharkiv, Ukraine
oleksandr.degtiarov@nure.ua

Abstract **– The article considers the application of colorimetry in medicine, its basic principles, methods and development prospects. Modern technologies for analyzing biological samples based on changes in the optical properties of substances are described, which allow for quick and accurate determination of the concentration of biomarkers. Considerable attention is paid to the development of a new colorimeter, in particular its technical characteristics, data processing algorithms and potential areas of application. The advantages of using colorimetric methods in diagnostics, quality control of medicines and monitoring of patients are discussed. The prospects for improving colorimetry through digital technologies and artificial intelligence are also considered.**

Keywords - colorimetry, electronic colorimeter, color range, medical object, digital electronic converter, ICG technology, fluorescence imaging.

I. INTRODUCTION

Colorimetry, the quantitative study of color perception, has become a key tool in medical research, allowing for the accurate measurement and analysis of colors in a variety of biological contexts. Colorimetry is the science and technology of quantifying and describing colors using precise mathematical and physical principles. In medicine, it is a powerful tool for the objective analysis of colors in organisms and tissues. The value of colorimetry lies in its ability to provide reproducible and accurate data on color phenomena that are often associated with important biological processes such as photosynthesis, pigmentation, and light signaling. As an interdisciplinary field, colorimetry combines physics (the behavior of light), chemistry (molecular interactions), and biology (the functional and ecological role of color). The advent of modern instruments in the 20th century, such as spectrophotometers and tristimulus colorimeters, revolutionized the field. These instruments enabled precise, reproducible color measurements and expanded the scope of applications to include molecular biology, environmental monitoring, and clinical diagnostics. Recent advances in computer imaging, hyperspectral techniques, and portable colorimetric devices have further expanded its capabilities, making colorimetry an integral component of modern biological research.

This paper discusses the possibilities of using the electronic colorimetry method in medicine for the diagnosis of diseases. Electronic colorimetry is widely used in medical diagnostics for the analysis of biological fluids, such as blood, urine, and others [1–5]. . The method measures the intensity of light absorbed by a solution to determine the concentration of certain biomolecules, facilitating real-time diagnosis and monitoring in medical procedures. It is used to detect various compounds in liquids, which can help in the diagnosis of various diseases. Some of the analytical methods in medical practice that use electronic colorimetry include:

- measuring blood efficiency: it is an important parameter for controlling diabetes levels;
- cholesterol measurement: high cholesterol levels can be associated with cardiovascular disease.
- urine protein level test: Elevated urine protein levels can detect kidney problems.
- determination of blood iron levels: high or low iron levels can reveal the presence of anemia or other diseases.
- analysis of the content of drugs in the blood: this is important for monitoring drug therapy and side effects.
- determination of hemoglobin concentration or identification of pathogenic microorganisms.

Colorimetry also plays a vital role in monitoring physiological conditions during surgery and therapy. By providing real-time data on tissue and organ function, it ensures patient safety and improves surgical outcomes. Tissue color is influenced by the levels of oxygenated (bright red) and deoxygenated (dark red) hemoglobin.

By analyzing the reflection of light at specific wavelengths, colorimetric systems quantify the oxygenation status of tissues, offering a direct measurement of perfusion.

The aim of the study [5] was to investigate the potential impact of filters on the intrinsically sensitive retinal cells of people with low vision (ipRGC). The authors also analyzed colorimetric changes in the light transmitted by these filters, emphasizing differences depending on the manufacturer.

It is noted in [2] that intracellular levels of biothiols are associated with various diseases, including cancer, and biothiols are considered to be tumor biomarkers. Due to the similarity of the molecular structure of biothiols, the

development of simple, rapid, efficient, and sensitive colorimetric sensors has great prospects for clinical cancer diagnostics.

Since 2020, ICG (indocianin green) technology has been widely used in oncology, which significantly increases the accuracy of minimally invasive surgical operations.

Indocyanine green (ICG) is a fluorescent dye used in surgery to assess blood flow and tissue perfusion. Its colorimetric properties allow visualization of perfusion in real time using imaging systems. In this work, we propose to use for ICG diagnostics a developed electronic colorimeter calibrated in this color range, which monitors the appearance and shades of green substance in human organs, the reflection of which is observed during the examination. Taking into account the interest of the world community in colorimetry, the task of developing electronic colorimeters for specific purposes in medical practice arises.

II. THEORETICAL FOUNDATIONS OF COLORIMETRIC ANALYSIS

Colorimetric analysis is based on measuring the amount of light absorbed by a colored solution. If the substance is colored, its concentration in the solution can be determined directly; if the substance is colorless, it is converted to a colored compound by adding an appropriate reagent. The dependence of the amount of light absorbed by a solution on the thickness of the solution layer and its concentration is expressed by the Lambert-Beer law (1)

$$I \cdot C \cdot k = \lg \frac{J_o}{J}, \qquad (1)$$

where I - layer thickness, cm,

C – concentration, mol/l,

J_0 and J – respectively, the intensity of the light flux before and after its passage through the solution,

k – some constant, which may correspond to the molar absorption coefficient ε.

For a colored solution, the characteristic values are the optical density ($\lg J_o/J$ - the logarithm of the ratio of the initial intensity of the luminous flux to its intensity after passing through the solution) and extinction (e - the optical density of a molar solution at a layer thickness of 1 cm) in this case, k is equal to e. The numerical value of e ranges from 500 for lightly colored solutions to 100000 - 2000000 for strongly colored solutions. Colorimetric analysis is carried out in monochromatic light, which is most fully absorbed by the solution, so it is recommended to use a light filter with a maximum absorption in the region complementary to the color of the analyzed solution [6].

Currently, colorimetry is actively researching the perceived differences between colors and their relationship with tristimulus coordinates. The goal of these studies is to develop a formula that allows calculating the degree of visible differences between colors based on their coordinates. Similar formulas have already been proposed and, judging by the results, demonstrate satisfactory accuracy. However, until their final refinement, they remain the main tool for practical application.

The most successful formula of this type is probably that proposed by Schrödinger, which is expressed as follows (2):

$$\Delta = \sqrt{\lg\left(\frac{h_1}{h_2}\right)^2 + 4\left(\arccos\frac{\rho\sqrt{r_1 r_2} + \gamma\sqrt{g_1 g_2} + \beta\sqrt{b_1 b_2}}{\sqrt{h_1 h_2}}\right)^2}, \qquad (2)$$

where Δ is the magnitude of the apparent difference between two colors;

r_1, g_1, b_1 and r_2, g_2, b_2 – elementary stimuli corresponding to colors;

h_1, h_2 – denote the lightness (brightness) of the compared colors, expressed in heterochromic units; ρ, γ, β – lightness coefficients, i.e. in other next mathematical expression:

$$h_2 = \rho r_2 + \gamma g_2 + \beta b_2.$$

However, a simplified formula (3) has been proposed in which the unit color vectors are chosen as follows: white, red (x), corresponding to the color of the extreme spectral red, and yellow (y), corresponding approximately to the spectral radiation with a wavelength of 569 nm:

$$\Delta = \sqrt{K \cdot \lg\left(\frac{h_1}{h_2}\right)^2 + \left(\frac{x_1}{h_1} - \frac{x_2}{h_2}\right)^2 + \left(\frac{y_1}{h_1} - \frac{y_2}{h_2}\right)^2}, \qquad (3)$$

where h_1, h_2 - remain the same as before (heterochromic lightness), and the coefficient K is determined experimentally.

Formula (3) may be less accurate than formula (2), but both require detailed experimental verification, which is currently being carried out. The main practical value of formulas (2) and (3) is that they allow quantitative evaluation of color deviations corresponding to the subjective perception of the difference by eye. This is especially important for industries where color plays a key role and it is necessary that visually perceived deviations do not exceed the permissible level.

In cases where color is an indirect indicator, the objective difference, rather than the subjective one, becomes a priority. Therefore, in such measurements, the degree of deviation from the norm can, in essence, be expressed by the vector of the difference between two given colors.

However, in this case it is necessary to agree in advance what angles are formed by the vectors representing the standard colors and used as coordinate axes. The most convenient option is to take them as mutually perpendicular. By determining the coordinates of the remaining colors relative to these three, it is possible to calculate the degree of difference between any two colors using the formula (4) for distance in a rectangular coordinate system:

$$L^2 = x^2 + y^2 + z^2. \qquad (4)$$

As is known from analytical geometry, in the case of using oblique coordinates, the distance formula includes coordinate angles.

This method of calculating deviations causes certain difficulties, even if the subjective assessment of differences does not play a decisive role. Since color measurement is carried out subjectively in most cases (with the exception of the developed device with photocells), the accuracy of measurements is determined rather by the magnitude of perceived, rather than objective optical differences.

Consequently, if too narrow tolerances for color deviations are set, according to formula (4), they may go beyond the limits of measurement accuracy for some colors, while for others they will be excessively rough from the point of view of visual perception.

The study presents noninvasive methods for solving a practical problem of metrological control of colorimetric devices using dispersion analysis of measurement results. The analysis is carried out using the example of an

electronic colorimeter containing a digital sensor for measuring the permeability of optical media. The diagram of the developed digital sensor for measuring the permeability of optical media is presented and the principle of its operation is given.

In works [7-8], experimental data were obtained on three channels for measuring the permeability of a control liquid containing biological objects.. A statistical analysis of the series of observation results was carried out, which allowed us to establish the levels of unbiased estimates of variances for the three measurement channels. Graphs of voltage changes along the three measurement channels, namely, the red, green, and blue photodiode channels, were constructed. Changes in the voltage across the channels are associated with changes in the composition of the control fluid containing a certain amount of biological objects. Graphical representations of the laws of distribution of voltage measurement errors across the measuring channels were obtained. The selection of a larger variance from many was made by applying the Cochran criterion, which is used to check the homogeneity of the variances of three or more samples. One of the conditions for using this criterion is that it requires the same number of experiments in each sample.

By comparing the results of the control with the results of the test samples, researchers can identify and correct any sources of error that may have affected the results of the experiment. Colorimetric enzyme assay is a method widely used in biochemical research to quantify enzyme activity. By measuring the change in color of a substrate or product in response to enzyme activity, researchers can determine the concentration of the enzyme in a sample.

Given the global interest in colorimetry, the task of ensuring high accuracy of the results obtained with the help of appropriate measuring instruments arises. This task can be solved by implementing dispersion analysis methods. The feasibility of this assumption is based on the results presented in a number of papers [7 – 8].

An electronic colorimeter plays an important role in medical research, providing accurate measurement of color parameters of biological samples. Unlike subjective evaluation methods, such as visual comparison, an electronic colorimeter eliminates the influence of the human factor, increasing the accuracy and reproducibility of measurements.

This device is especially important in diagnostics, where minimal color deviations can indicate pathological changes. For example, when analyzing blood or urine, color parameters allow you to identify hidden diseases at early stages. In addition, in dermatology, a colorimeter helps to evaluate skin pigmentation, monitor the dynamics of treatment and select cosmetics.

Development of an electronic colorimeter for medicine requires high sensitivity of sensors and software algorithms that take into account the characteristics of biomaterials. Modern technologies make it possible to create a device that will provide objective color control, improving the quality of diagnostics and increasing the effectiveness of treatment. Therefore, research aimed at developing an electronic colorimeter is relevant.

III. STATEMENT OF THE RESEARCH PROBLEM

The purpose of the study is to analyze the necessity of using the electronic colorimetry method for the diagnosis and treatment of diseases in oncology, dermatology, ophthalmology, etc. It is also proposed to use electronic colorimeters developed by the authors for these purposes.

IV. DEVELOPMENT OF A DIGITAL ELECTRONIC COLORIMETER FOR RAPID CONTROL OF BIOLOGICAL OBJECTS IN MEDICINE

The control and measurement of biological objects in medicine by the colorimetric method can be carried out in different optical ranges (depending on the specifics of use). In this paper, we consider an electronic colorimeter operating in the ultraviolet range.

Ultraviolet radiation covers the range from 10 nm to 400 nm. It plays a special role in the life of people and plants. In small doses, this radiation is beneficial to biological objects used in medicine. In high doses, it causes undoubted harm, but even in this mode, it is possible to obtain practical benefits, such as disinfection.The method is used to detect biological fluids (blood, urine, semen, saliva). Both medical and forensic applications use this radiation, for example, to identify and record fingerprints, since handprints also contain various fluorescent substances that are the product of human activity. Detecting biological fluids that glow under ultraviolet light is one of the main challenges faced by forensic scientists. Since reflection occurs during irradiation and the color changes, this makes it possible to analyze the reflected signal. The utility model relates to sensors for measuring the reflection from biological materials and obtaining reliable information about this material. the method of controlling biological substances is an electronic colorimeter, the main part of which is a digital sensor.

The authors know the design of a digital sensor for measuring color [1], The digital sensor contains a lens with an aperture, a light-dividing prism, three light filters, three photoresistors, the light flux passing through the lens with the aperture is focused on the light-dividing prism, and through red, green, and blue light filters is transmitted to photoresistors sensitive to the visible spectrum of radiation; it has a normalizing amplifier, microcontroller, interface, computer, and analog multiplexer.

The disadvantages include the fact that the design consists of discrete elements, it takes up more space than microprocessor technology, requires a certain selection of elements, and requires devices for communication with a computer, and they are “wired.” All of this dramatically reduces the convenience and reliability of operation.

The closest is a UV dermoscopy device for detecting skin cancer [2], which is mobile and includes an emitter, electronic circuitry, batteries, and a magnifying glass.

The disadvantages include the following: the analysis is carried out optically, i.e. by a specialist. This, in turn, imposes requirements on his qualifications. The result is a subjective conclusion.

The device is based on the task of creating a mobile automatic control of biological samples, with the ability to connect to a computer network, which can work without the presence of an operator to perform analysis. The operator is only required to approach the sample under test.

This is achieved by the fact that the digital sensor for rapid monitoring of biological objective lens, which contains a housing, with an emitter located inside, a control circuit and a power supply, according to the utility model, has a hinge between the handle for holding and the location of the measuring unit, the measuring unit has a place for attaching the stop, the measuring unit consists of three or

four separate emitters for different wavelengths on one side of the magnifying glass, optical receivers are placed in the same plane at the other end of the magnifying glass, a microprocessor with a built-in Wi-Fi modem and low power consumption is added to the electronic circuit.

Figure 1 shows the design of a portable device for detection and rapid analysis of biological objects. The body of the device contains two compartments connected by a swivel hinge 1, the first compartment, inside which is located the electronic control of the device 2, containing a microprocessor 3, with a built-in Wi-Fi radio communication module 4,on the outer side of this compartment, which is made in the form of a cylinder, there are two control buttons: power button 5 and start measurement button 6, as well as a beeper 7 and power supply 8.The second compartment contains radiation sources 9 (in three or four different ranges to cover the entire ultraviolet spectrum), receivers of this radiation 10 in the appropriate quantity, and a small lens 11 for visual inspection. The communication interface 12 from the microprocessor to the radiation sources and the reception of the reflected signal passes through both compartments. The directions of radiation movement to the analyzed object 13 and the signal reflected from it 14, the object itself is marked 15. In addition, devices that can operate as a recorder are indicated: a smartphone 16 or a computer 17.

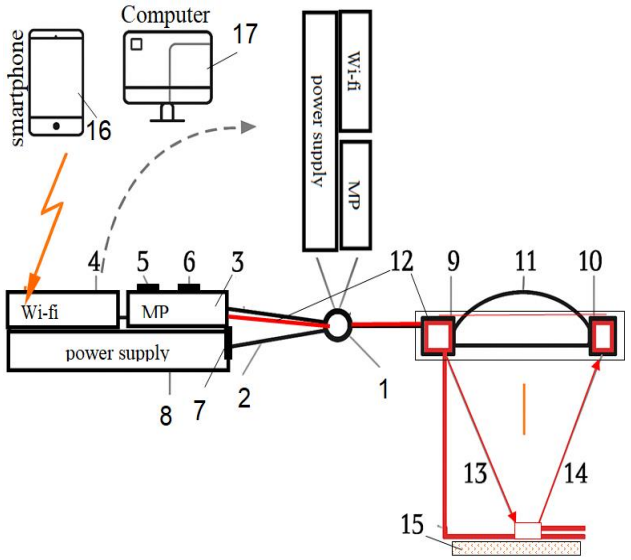

Fig. 1 Block diagram of the developed electronic colorimeter

The device works as follows: the handle - the device holder is set to a convenient working position. A bracket is installed that determines the determined distance to the object under study and the device is raised to the stop in this object. The "on" button is pressed, power is supplied to the electronic control circuit, and when the system is ready for operation - a sound signal sounds. The second button is pressed, the object is irradiated for a short time, and the reflected signal is received by the radiation receivers. When the analysis is completed, the device automatically turns off the irradiation and a sound signal is given. Next, the read information is processed in the microprocessor, depending on the algorithm, or immediately transmits the results of the study to the recording device (smartphone, personal computer, router), or is recorded in the internal memory of the processor. Later, in a stationary place it is transmitted to the recording devices.

The use of this design will make it possible to easily find and obtain information about the presence and condition of biological substances, almost automatically (except that the device must be brought to the object). In addition, the task of entering this data into databases will be facilitated. The algorithm of primary information processing can be easily replaced - by simple reprogramming of the processor.

IV CONCLUSIONS

1) An analytical review of the use of the colorimetric method in medicine has shown that:

- colorimetric Monitoring helps surgeons assess the blood supply to flaps or grafts, ensuring their viability.
- conducting Perfusion Assessment helps detect vascular occlusion or ensure proper organ function after transplantation.
- treatment of burns and trauma: Monitoring tissue viability helps determine the extent of injury and guides debridement or reconstructive interventions.

2) A digital electronic colorimeter has been developed for express control in medicine. The developed device provides:

- non-invasive and continuous: real-time measurement reduces the need for invasive procedures and provides continuous feedback at critical moments.
- increased accuracy: quantitative perfusion data minimizes the risk of postoperative complications and improves recovery outcomes.

REFERENCES

[1] Campos C.M., Hoffmann W.R., Correia F.d.S., Lengowski E.C., Silva M.J.d., Natalino R., Oliveira A.C., Pereira B.L.C. Radial Variation in Colorimetric Parameters, Chemical Composition, and Biological Resistance of Teak Wood Extracted from 13- and 22-Year-Old Teak Trees. *Forests.* 2025. Vol. 16, P. 177. DOI: https://doi.org/10.3390/f16010177.

[2] Sanchez-Cano A, Orduna-Hospital E, Aporta J. Colorimetric and Photobiological Properties of Light Transmitted Through Low-Vision Filters: Simulated Potential Impact on ipRGCs Responses Considering Crystalline Lens Aging. *Life*. 2025.Vol. 15(2). P. 261. DOI: https://doi.org/10.3390/life15020261

[3] Xiaowei Huang, Haroon Elrasheid Tahir, Zhihua Li, Shi Jiyong, Zou Xiaobo, Chapter Eight. Colorimetric sensors for poultry and red meat quality control.*Colorimetric Sensors, Academic Press*. 2024. P. 161–185. ISBN 9780443132186. DOI: https://doi.org/10.1016/B978-0-443-13218-6.00013-6.

[4] Kokoro Matsushita,Chihiro Honda,Yoriyuki Nakamura, Shigenori Kumazawa, Comparison of colorimetric methods for the analysis of total polyphenols in black tea extracts. *Food Science and Technology Research*,Article ID FSTR-D-24-00220, Advance online publication January 22, 2025, Online ISSN 1881-3984, Print ISSN P. 1344–6606, DOI: https://doi.org/10.3136/fstr.FSTR-D-24-00220.

[5] Yin Li,a Yumeng Liu,d Yueqin Zhang,d Mengmeng Dong,e Lidong Caobcand Kai Jiang. A simple Ag–MoS2 hybrid nanozyme-based sensorarray for colorimetric identification of biothiols andcancer cells. *RSC Adv*. 2024. Vol. 14.P. 31560–31569. DOI: https://doi.org/10.1039/d4ra05409a.

[6] Kavindra Borgaonkar, Ranjit Patil. Clinical importance of control in colorimetric estimationof enzymes Quest Journals.*Journal of Medical and Dental Science Research*. Vol. 11.Issue 3. 2024. P. 09–12. ISSN (Online): 2394-076X ISSN (Print):2394-0751.

[7] S. Efimenko Y. Horoshajlo, I. Sezonova, V. Chumakov and G. Levitskaya. ThePossibility of Using the Concept of Colorimetric Functions in Applied Research.*IEEE 8th International Conference on Advanced Optoelectronics and Lasers (CAOL)*, 2019, P. 225–227 DOI: https://doi.org/10.1109/CAOL46282.2019.9019456, electronic ISSN: 2160–1534, print on Demand(PoD) ISSN: 2160-1518).

[8] Serhii Yefymenko, Ihor Hrihorenko, Iurii Khoroshilo, Svitlana Hryhorenko, Inna Petrovska. Evaluation of informativeness of indicators in colorimetric control using discriminative analysis models. *IEEE XXXII MHC «MMA 2022»*, Sozopol, Bulgaria. P. 1–4.DOI: https://doi.org/10.1109/MMA55579.2022.9992712.

SECTION VIII
METROLOGY PRACTICE

Verification procedure for low speed automatic instruments for weighing road vehicles in motion and measuring axle loads

1st Ivaylo Stoyanov
Regional department of DG MMI - Ruse.
Bulgarian Institute of Metrology
Sofia, Bulgaria
i.stoyanov@bim.ggovernment.bg

Abstract — Low-speed automatic weighing in motion instrument (LS WIM instruments) is a measuring instrument, that determines the vehicle mass, axle loads or the axle-group loads of a road vehicle while the vehicle is crossing over the load receptor of the weighing instrument. Different technical equipment (measurement standards and auxiliary devices) is used for carrying out metrological control of LS WIM instruments. Reference vehicles are used for carrying out in field testing as well. This paper presents the verification procedure, compliant with the requirements of the International recommendation OIML R 134:2006 and the Ordinance on measuring instruments subject to metrological control in order to prove compliance with the requirements for them during initial and subsequent verifications carried out by the Bulgarian Institute of Metrology (BIM).

Keywords — weighing in motion instrument, testing, technical equipment, reference vehicles, metrological control.

I INTRODUCTION

In accordance with the Law on measurements, for ensuring accuracy and reliability of measurements, legal metrological control is carried out on measuring instruments responding to reasons of public interest, public health, safety and order, protection of the environment and the consumer, of levying taxes and duties and of fair trading.

The requirements to technical and metrological characteristics, testing and methods for control of LS WIM instruments are laid down in Section III of the Ordinance on measuring instruments subject to metrological control.

II SCOPE AND FIELD OF APPLICATION

SL WIM instruments are used in Bulgaria by the Customs Agency for control of the vehicles' mass and axle loads when crossing the country's borders, and determining the fees to be paid and fines for their overloading.

This procedure applies to SL WIM instruments:

- which are installed in a controlled weighing area;
- which are used for determining and indicating the vehicle mass, the single-axle loads, and if applicable the axle-group loads of a road vehicle in motion.

This procedure does not apply to SL WIM instruments that:

- determine individual axle loads by multiplying a single wheel load of an axle by two; or
- are installed on-board vehicles to measure axle load.

Measured quantities:

The quantities measured in verification of SL WIM instruments are total mass (m), axle loads/axle-group loads (m) and speed (v).

Measurement units of the International system of units, SI, are used for the measured quantities:

- for mass – kilogram (kg) and ton (t);
- for speed of the reference vehicles – kilometer per hour (km/h)

Accuracy classes:

For determination the vehicle mass, SL WIM instruments may be of the following accuracy classes: 0,2, 0,5 and 1.

For determination of the axle-loads and group-axle loads SL WIM instruments may be of the following accuracy classes: A, B, C and D.

SL WIM instruments may have different accuracy classes for single-axle loads and axle-group loads. The relation between the accuracy classes for single-axle load and axle-group load, and the accuracy classes for vehicle mass is shown in Table 1.

TABLE 1 RELATION BETWEEN THE ACCURACY CLASSES FOR SINGLE AXLE-LOAD/AXLE-GROUP LOAD AND THE ACCURACY CLASSES FOR VEHICLE MASS

Accuracy class for single-axle load and axle-group load	Accuracy class for vehicle mass		
	0,2	0,5	1
A	x	x	
B	x	x	x
C		x	x
D			x

Maximum permissible errors (MPE):

The MPE for the vehicle mass determined by in-motion weighing, shall be one of the following values, whichever is greater:

- the value calculated according to Table 2, rounded to the nearest scale interval;
- 1 d × the number of axles in the totalization in the case of initial verification or 2 d × the number of axles in the totalization in the case of subsequent verification.

TABLE 2 RELATION BETWEEN THE ACCURACY CLASSESS AND MPE OF THE VEHICLE MASS

Accuracy class for vehicle mass	Percentage of conventional value of the vehicle mass	
	Initial verification	Subsequent verification
0,2	± 0,10 %	± 0,20 %
0,5	± 0,25 %	± 0,50 %
1	± 0,50 %	± 1,00 %

The maximum difference between the indicated single-axle load for in-motion tests and the conventional true value of the static reference single-axle load shall not exceed one of the following values, whichever is the greater:

- the value from Table 3 rounded to the nearest scale interval;
- 1 d in the case of initial verification, 2 d in the case of subsequent verification.

TABLE 3 RELATION BETWEEN ACCURACY CLASSES AND MPE OF THE STATIC REFERENCE SINGLE-AXLE LOAD

Accuracy class for single-axle load	Percentage of conventional true value of the static reference single-axle load	
	Initial verification	Subsequent verification
A	± 0,25 %	± 0,50 %
B	± 0,50 %	± 1,00 %
C	± 0,75 %	± 1,50 %
D	± 1,00 %	± 2,00 %

For all reference vehicles, except for the two-axle rigid reference vehicle, the maximum difference between the recorded value of the single-axle load or axle-group load during weighing in-motion and the corrected average value of the single-axle load or the corrected average value of axle-group load shall not exceed the greater of the following values:

1. the value from Table 4 rounded to the nearest scale interval;
2. 1 *d* x n in the case of initial verification, 2 *d* x n in the case of subsequent verification, where n is the number of the axles in a group, and n = 1 for one axle.

TABLE 4 RELATION BETWEEN THE ACCURACY CLASSES AND MPE OF THE SINGLE-AXLE LOAD OF OTHER VEHICLES

Accuracy class for single-axle load and axle-group load	Percentage of corrected average value of the single-axle load or the value of the axle-group load	
	Initial verification	Subsequent verification
A	± 0,50 %	± 1,00 %
B	± 1,00 %	± 2,00 %
C	± 1,50 %	± 3,00 %
D	± 2,00 %	± 4,00 %

III VERIFICATION METHODS

The method for carrying out the verification is comparative.

Verification is carried out according to the procedure described in OIML R 134:2006:

- weighing of the total mass of the reference vehicles, VM_{ref};
- determination of static reference single-axle load for the two-axle rigid reference vehicle;

In-motion tests:

- weighing of the total mass of the reference vehicles;
- weighing in-motion with the two-axle rigid reference vehicle;
- weighing in-motion with all other types of reference vehicles.

Control instrument:

Control instruments are used for determination of the total mass of the reference vehicles and the static reference single-axle loads. They shall ensure that the true mass value of the reference vehicles is measured with an error smaller or equal to 1/3 of the smallest MPE for weighing in-motion.

Reference weights:

The reference weights used in the verification of SL WIM instruments in static mode or of separate control non-automatic instrument shall comply with the metrological requirements of OIML R 111 for the respective accuracy class, they shall be calibrated and their uncertainty shall be not bigger than 1/3 of the applicable MPE of the instruments under test.

Reference vehicles:

Two-axle rigid vehicle

The two-axle rigid vehicle is a reference vehicle used in determination of the conventional true value of the static reference single-axle loads and as one of the reference vehicles for weighing in-motion.

Other reference vehicles:

Besides the two-axle rigid vehicle, at least two other reference vehicles from the listed below shall be used in the verification:

- one three/four-axle rigid;
- one four-or more axle articulated;
- one two/three-axle rigid vehicle and a two/three-axle draw-bar trailer.

Auxiliary measuring instruments:

- thermometer with a temperature range from minus 15 °C to 50 °C, resolution 1 °C and expanded uncertainty ± 1 °C;
- measurement standard for linear speed with following characteristics:
  - accuracy ≤ 1 km/h;
  - maximum speed ≥30 km/h;
  - minimum speed ≤ 1 km/h;
  - resolution ≤ 0,1 km/h.
- steel measurement tape with a range no less than 20 m, division 1 mm and expanded uncertainty U = ± 2 mm.

IV METROLOGICAL EXAMINATION

Verification of the control instrument.

The condition of the control instrument for determining the full mass of the reference vehicles (VM_{ref}) is established and checked whether it meets the requirements of BDS EN ISO 45501 for MPE for the relevant accuracy class of the scale used.

The total mass, VM_{ref}, of the reference vehicles is determined.

Verification of the SL WIM instrument in static mode.

Before starting the verification, SL WIM instrument shall be loaded close to the Max.

The instrument under test shall be set to zero before each measurement and the zero shall not be corrected unless a significant malfunction has occurred. After each measurement, the scale shall be left for a sufficient time to recover before the next measurement..

Test loads from zero to Max are applied then unloaded back to zero. When the size of the load receptor does not allow uploading to Max, the decreased load shall be noted and it cannot be smaller than 50 %. Five different loads shall be chosen. The chosen loads shall include 50 % of Max and Min, and loads close to ones in which MPE is changed.

If it is impossible to eccentrically load the scale on each bearer, it is divided into two segments and loaded with the maximum possible safe placement of the standards on them.

Repeatability error is defined at load equal to 50 % of max.

Determination of the static reference single-axle load for two-axle reference rigid vehicle.

For verified instruments which will be used for applications requiring measurements of single-axle loads, the actual value of the static reference single-loads is determined for two-axle rigid vehicle including at least two different axle loads, using the following method:

Each axle of the static two-axle reference vehicle is weighed by the control instrument and the indicated single-axle load is recorded. After the two axles are weighed, the vehicle mass (VM) is calculated by summing the recorded two values, and the sum is recorded. This operation is repeated five times with the vehicle and, if applicable, it is carried out in reverse direction as well.

For each of the above-mentioned weighing operations, the vehicle shall be motionless and the axle-wheels entirely positioned on the load receptor, the engine is off, the gear lever is in neutral and the brakes are released. If it is necessary, wheel chocks are used to prevent the vehicle from moving.

The average static reference single-axle load for each axle of the two-axle reference rigid vehicle is calculated by formula (1):

$$\overline{Axle_i} = \frac{\sum_1^n Axle_i}{n} \quad (1)$$

where:

i – number in order of the single load;

n – number of weighing of each static axle;

*Axle*i – recorded load for this axle.

Both average single-axle loads are added by formula (2) in order to define the average value of the vehicle static mass.

$$\overline{VM} = \sum_{i-1}^{n} \overline{Axle_i} \quad (2)$$

As an alternative, recorded values for the vehicle mass calculated after each vehicle weighing as described above can be used for calculating the average value of the static mass of the two-axle reference rigid vehicle by formula (3):

$$\overline{VM} = \frac{\sum_1^{10} VM}{10} \quad (3)$$

Corrected average single-axle loads are calculated by formula (4):

$$\overline{CorrAxle_i} = \overline{Axle_i} \times \frac{VM_{ref}}{\overline{VM}} \quad (4)$$

where *VM*ref is the actual value of each reference vehicle mass determined by weighing of the total mass.

Traceability of the actual value of the single-axle loads of the static two-axle reference rigid vehicle is ensured by the fact that the sum of the two corrected average static reference single-axle loads is equal to the actual value of the reference vehicle mass determined by weighing the total mass with the control instrument calculated by formula (5):

$$VM_{ref} = \sum_{i-1}^{2} \overline{CorrAxle_i} \quad (5)$$

The static reference single-axle loads are determined in such a way that the axle-loads cover as far as possible the instrument's measurement range. At least two different axle loads are applied up to the maximum permissible axle load of the two-axle reference rigid vehicle.

In-motion tests:

All weighing operations shall start with the reference vehicle, positioned before the entrance platform, at a distance sufficient for the vehicle to travel at a constant speed before arriving at the platform.

The tests are performed using the two-axle reference rigid vehicle plus at least two other reference vehicles.

The vehicle speed shall be kept as constant as possible during each driving test.

For each vehicle, except for the two-axle loaded reference vehicle, five trial runs are performed (as three of them are in the center, and one on the left and right sides of the load receptor) and, if applicable, three trial runs (center, left, right) in reverse direction, with speeds within the approved range of the instrument.

For the two-axle loaded reference vehicle, the trial runs mentioned above are performed for each of the speed shown below:

- between V_{min} and V_{mid};
- between V_{mid} and V_{max}.

Weighing of the total mass of the reference vehicles:

Indicated or printed readings of the instrument under test shall be recorded and the errors shall be calculated according to the vehicle mass reference values.

No error shall exceed the maximum permissible error for the specified accuracy class shown in Table 2.

Testing in-motion with the two-axle reference rigid vehicle:

The two single-axle loads of a two-axle reference rigid vehicle as indicated or printed by the instrument under test shall be recorded. The difference between each recorded single-axle load and its relevant static reference single-axle load is calculated.

Each calculated difference shall not exceed the applicable maximum permissible errors for the specified accuracy class.

Testing in-motion with all other types of reference vehicles:

Measurements are carried out and the single-axle loads or axle-group loads as indicated by the instrument under test are recorded. For each reference vehicle (except for the two-axle rigid vehicle ant its load condition), the average single-axle loads and, if applicable, the average axle-group loads during the tests are recorded after calculated by formulae (6) and (7):

$$\overline{Axle_i} = \frac{\sum_1^n Axle_i}{n} \quad (6)$$

where:

i is the number in order of the axle loads;

n - number of weighing of each static axle;

*Axle*i - recorded load for this axle.

$$\overline{Group_i} = \frac{\sum_1^n Group_i}{n} \quad (7)$$

The indicated or printed values of the instrument under test are used for vehicle mass, and the average reference mass of the vehicle is calculated by formula (8).

$$\overline{VM} = \frac{\sum_1^n VM_i}{n} \quad (8)$$

As an alternative, the average single-axle loads and axle-group loads can be added for determining the average mass of the vehicle, calculated by formula (9):

$$\overline{VM} = \sum_{i-1}^{q} Axle_i + \sum_{i-1}^{g} \overline{Group_i} \quad (9)$$

where:

q – number of the vehicle single axes;

g – number of the vehicle group axles (it can be zero).

The corrected average single-axle load is calculated and, if necessary, the corrected average axle-group load/-s are calculated by formulae (10) and (11):

$$\overline{CorrAxle_i} = \overline{Axle_i} \times \frac{VM_{ref}}{\overline{VM}} \quad (10)$$

and

$$\overline{CorrGroup_i} = \overline{Group_i} \times \frac{VM_{ref}}{\overline{VM}} \quad (11)$$

where VM_{ref} – conventional true value of each vehicle reference mass determined by weighing the total mass.

Traceability to be ensured, the sum of the corrected average single-axle and axle-group loads of the reference vehicle shall be equal to the conventional true value of the vehicle reference mass calculated by formula (12):

$$VM_{ref} = \sum_{c-1}^{q} \overline{CorrAxle_i} + \sum_{i-1}^{g} \overline{CorrGroup_i} \quad (12)$$

where:

q – number of the vehicle single axes;

g – number of the vehicle group axles (it can be zero).

The deviation between each single-axle load and corresponding corrected average single-axle load and, if applicable, the deviation between each axle-group load and corresponding (if there are more than one axle-groups) corrected average axle-group load is calculated by formula (13):

$$DevAxle = Axle_i - \overline{CorrAxle_i}$$

$$DevGroup = Group_i - \overline{CorrGroup_i} \quad (13)$$

No deviation shall exceed the applicable maximum permissible error for the specified accuracy class.

Processing of the verification results

All calculated results during the verification are entered into the relevant annexes of the verification report. After comparing the final result with the requirements in the regulatory documents, the conclusions as to whether the relevant test has been successfully passed are made and noted as "passed" or "failed". If any measurement result is unacceptable, the verification shall be terminated.

V VERIFICATION OF THE PROCEDURE

Verification of the procedure refers to proving the suitability of the test method described in the verification procedure of LS WIM instruments, as well as its application by different personnel at different locations under different environmental conditions.

The method chosen for verification of the procedure is comparative by using reference vehicles and weights traceable to DG NCM – Sofia.

Objective of verification of the procedure:

To demonstrate that the verification procedure for SL WIM instruments is suitable and reliable for the specific purpose.

On the basis of the measurement results, analysis is to be done to demonstrate that the test method is applicable when implemented by different people under different conditions.

Main requirements to the procedure and the obtained test results are:

- comparability of results within the permissible error limits;
- repeatability – the verification procedure is applied by the same operator under the same conditions;
- reproducibility – the methodology is applied by different operators under different conditions and at different times;
- accuracy – comparison of the average value of multiple measurements with the reference mass of the vehicle;
- sensitivity and speed – verification at different speeds of passage and at different reference masses;
- stability – checking the sensitivity of the procedure to small changes in conditions.

Test conditions:

The measurements were carried out by employees of DG MMI in two stages in the period July 2024 and April 2025:

SL WIM instruments, located at the country's borders and used by the Customs Agency, were randomly selected. The results of the comparative measurements are the basis of the verification of the procedure

The technical equipment and reference vehicles used during the verification of the procedure have proven traceability and are property of BIM.

The employees who participated in the tests have been trained in applying the verification procedure.

Results:

The tests of the individual LS WIM instruments were conducted with the reference vehicles specified in the verification procedure within three working days, with 90 tests for each instrument. After the measurements were completed, an analysis of the data obtained was done by the two teams of employees, which showed the stability and comparability of the results.

IV CONCLUSION:

As a result of the experimental tests carried out, the following conclusions can be drawn regarding the presence of:

- comparability of results within the permissible error limits for the most test loads;
- good repeatability, smaller than 0,3 %;
- accuracy – comparison of the average value from multiple measurements with the vehicle reference mass;
- sensitivity and speed – verification at different speeds of passage and at different reference masses;
- stability – checking the sensitivity of the procedure to small changes in conditions.

Through the applied comparative approach, the presented test results and generally accepted criteria give grounds to declare that the developed verification procedure for LS WIM instruments has been verified.

The general conclusion is that the test method described in the verification procedure is reliable and suitable for control purposes.

REFERENCES

[1] Law on measurements, publ. SG, No. 46/7.05.2002;

[2] Law on technical requirements to products, publ. SG, No. 86/1.10.1999;

[3] Ordinance on the essential requirements and conformity assessment of non-automatic weighing instruments, in force from 20.04.2016, publ. SG, No. 87/31.10.2017;

[4] Ordinance on measuring instruments subject to metrological control, publ. SG, No. 103/06.12.2024;

[5] International Recommendation OIML R 76:2006 „Non-automatic weighing instruments“;

[6] International Recommendation OIML R 111:2004 „Weights of classes E_1, E_2, F_1, F_2, M_1, M_{1-2}, M_2, M_{2-3} and M_3“;

[7] International Recommendation OIML R 134:2006, part 1 and 2 „Automatic instruments for weighing road vehicles in motion and measuring axle loads “;

[8] БДС EN ISO/IEC 45 501:2015 „Metrological aspects of non-automatic weighing instruments“;

[9] Verification procedure for non-automatic weighing instruments, Version 3, No. МП-2/2022 г., in force from 20.04.2022.

Methodology for the Verification of Roller Brake Testers for Road Vehicles

Petko Sinapov
Bulgarian Institute of Metrology (BIM)
Sofia, Bulgaria
p_sinapov@tu-sofia.bg

***Abstract*— This paper presents a verification methodology for roller brake testers used in periodic roadworthiness tests of motor vehicles and their trailers. The methodology is intended for use by accredited laboratories during initial and subsequent verifications and verification after each repair of roller brake testers. The main purpose of the methodology is to determine whether a roller brake tester complies with the requirements laid down in legislation and whether the maximum permissible error of measurements is in accordance with the applicable requirements. The scope of the methodology includes visual inspection of the overall technical condition of the roller brake tester, verification of the diameter and peripheral speed of the rollers, with particular focus given to the verification of the brake force measuring systems, the axle load measuring system, and the air pressure measuring system. The methodology includes specific test procedures and requirements for the measurement standards (etalons) used. The proposed methodology ensures an objective metrological assessment and contributes to maintaining the reliability and traceability of the measurement results.**

Keywords— roller brake tester, methodology, verification

I. Introduction

The purpose of roller brake testers is to determine the braking efficiency of road vehicles. Roller brake testers have a crucial role in assessing the roadworthiness of road vehicle braking systems, allowing for quick and objective diagnosis of potential deficiencies. To ensure accuracy and reliability, the measuring system is subject to initial and subsequent verifications [1-3]. In addition to their use in technical inspections, roller brake testers are also applied in research and development activities for laboratory testing of new brake system designs or vehicle tires.

The basic and validated method for verifying the measurement systems of roller brake testers is the static method, which uses force-generating devices (or, respectively, pressure-generating devices) and measurement standards (etalons) to verify accuracy. Reference [4] presents examples of test devices used in verification (calibration) procedures.

In recent years, however, leading certification and inspection bodies have started using dynamic verification methods to improve inspection efficiency and the accuracy of results. These methods approximately simulate the operating conditions of a moving vehicle, allowing assessment of the measurement system under conditions close to real ones. A detailed example of the proposed dynamic verification method is presented in reference [5].

Despite the growing interest in dynamic methods, the static method continues to be widely used and recognized as the basic approach for the verification of roller brake testers. This is due to its relative simplicity, which allows easy and quick execution of the verification, as well as its high reliability and accuracy of the results. For this reason, the present paper proposes a methodology that can be used in static testing methods.

II. Operating Principle of the Measuring System

A roller brake tester is a measuring machine consisting of two pairs of powered rollers. The rollers drive the wheels of the vehicle by means of friction, with the aim of measuring the braking force exerted by the vehicle during the test . Sample computational models of the mechanical part can be found in [6–9]. Modern brake testers are equipped with force transducers, pressure transducers, angular velocity sensors, and electronic systems for data acquisition and processing, as well as software for visualizing the results.

Fig. 1 shows the main components of the roller brake tester. It consists of the following components:

• Mechanical component (1): Includes the housing, rollers, drive elements, sensors, and other mechanical parts,

• Control panel (2): Contains most of the electronics required for the operation of the brake tester. It houses the main controller PCB and, if necessary, additional PCBs,

• Computer system (3): Responsible for control, processing, storage, and transmission of data,

• Analog display (4).

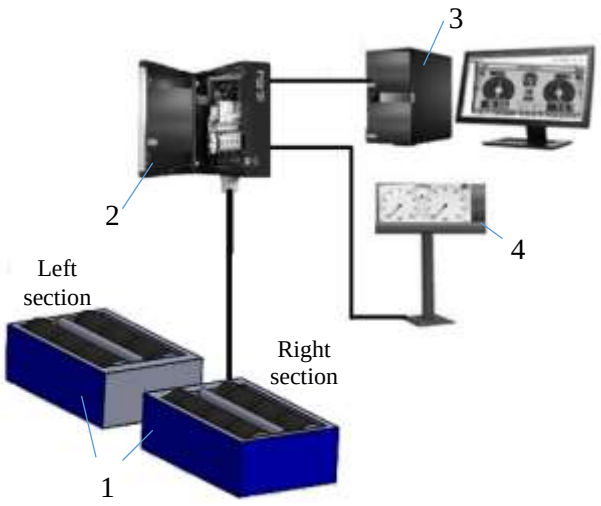

Fig. 1 Illustration of the main components of the roller brake tester

The basic software usually includes several firmware components necessary for the proper functioning of the system. The controller embedded in the control panel contains one or more microprocessors that interact with each other. Computer 3 requires additional software for control and visualization. The software often includes various modules. For more efficient operation, the individual modules are connected to each other through appropriate interfaces. Such systems can be found in [6–8].

978-1-6654-7799-4/25/$31.00 ©2025 IEEE

Some of the more important measured quantities of roller brake testers are:

• Total braking force at the moment of wheel lock-up on a given axle:

$$F = F_L + F_R \quad (1)$$

where:

F_L – measured value of the braking force of the left wheel,

F_R – measured value of the braking force of the right wheel.

• Braking force imbalance on the axle:

$$R = \frac{|F_L - F_R|100}{\text{The larger braking force}} \% \quad (2)$$

• Braking efficiency - depending on the type of braking system, it can be calculated using one of the two formulas below.

- For vehicles with hydraulic brake systems:

$$Z = \frac{\sum F_j}{\text{Test weight of the vehicle in N}} 100 \ \% \quad (3)$$

where $\sum F_j$ is the sum of the braking forces of all wheels.

- For vehicles with pneumatic brake systems:

$$Z = \frac{\left(F_1 R_{p1} + F_2 R_{p2} + F_3 R_{p3} ... + F_n R_{pn}\right)100}{\text{Permissible total weight in N}} \ \% \quad (4)$$

where $F_1, F_2, F_3, ... F_n$ are the measured braking forces for axle 1, 2, 3, 4 ... n, respectively.

The correction coefficient R_{pi} is calculated for each axle using the corresponding measured pressure according to the following formula:

$$R_{pi} = \frac{´p_m - 0.4}{p_i - 0.4} \quad (5)$$

where:

p_m – minimum design brake actuator pressure (in bar) of laden vehicle on axle *i* (for extrapolation purposes),

p_i – is the measured pressure in the brake chambers (cylinders) at which the braking force of the corresponding axle *i* was measured.

Analyses and experimental studies using some of the above-mentioned formulas can be found in [9].

III. METHODOLOGY FOR THE VERIFICATION OF ROLLER BRAKE TESTERS

The verification is carried out in a sequence of three stages, as described in the flowchart in Figure 2.

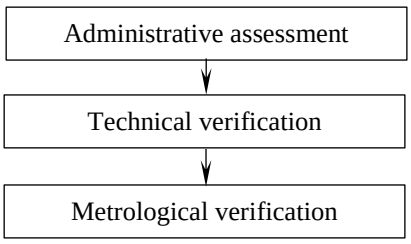

Fig. 2 Sequence of verification

A. *Administrative assessment*

During the administrative assessment, the following checks are carried out:

• compliance with the approved type,

• completeness of the tester,

• presence of markings, labels, and control signs, including the manufacturer's serial number of the tester,

• version and name of the firmware and software installed on the tester under verification.

B. *Technical verification*

For this verification, it is necessary that the technical equipment with measuring functions be traceable. The following activities are carried out:

- Visual inspection – a check of the overall technical condition of the tester [1,2],
- Inspection of all safety facilities– the automatic start function, the automatic stop function, the operation of the automatic slip cut-off system, the emergency stop system, and the safety system of the pit are all tested [1,2],
- Verification of roller diameter – during the roller diameter verification, three measurements of the perimeter are taken for each roller: one in the middle and two at 10 cm from each end, respectively [3]. For the measurement, a circumference tape (pi tape) with a measuring range for diameters of at least 150 mm to 300 mm is used, with a vernier scale division of 0.1 mm and an accuracy class of I,
- Verification of the peripheral speed of the rollers – during this verification, the rotational speed n of each roller is determined using the following formula:

$$n = \frac{60\,m}{t_m} \quad \text{min}^{-1} \quad (6)$$

where:

m – number of rotations of the rollers*;*

t_m – time for *m* rotations, in seconds (s).

The peripheral speed of the rollers is calculated using the following formula [10]:

$$v = 0{,}12\,\pi\,n\,r \quad \text{km/h} \quad (7)$$

where:

n– rotational speed (in min^{-1}) of the rollers,

r – radius of the rollers (in m).

The radius r is determined based on the minimum measured diameter in the respective section.

C. Metrological Verification

1) Verification of the accuracy of brake force and axle load measurement systems

Verifications are carried out using loading devices (Fig. 3 and Fig. 4) and a calibrated force measurement system (Fig. 5) with an expanded uncertainty (coverage factor k=2) not greater than one-third of the absolute value of the maximum permissible error (MPE), in accordance with the requirements for the system under verification. The one-third criterion complies with the recommendations in [11].

The calibration methods for these measurement systems can be found in [12]. Similar measuring systems can be seen in [13].

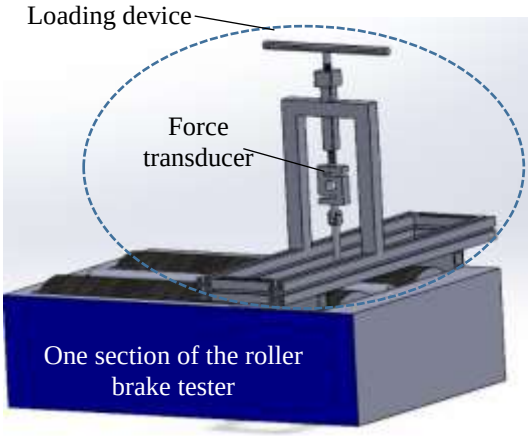

Fig. 3 Loading device for verification of the brake force measurement system.

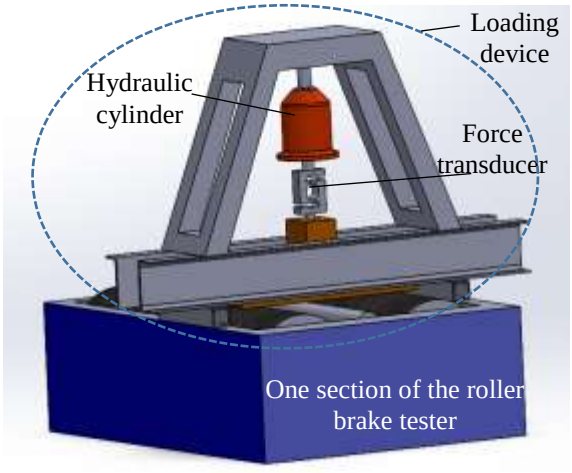

Fig. 4 Loading device for verification of the axle load measurement system

During the accuracy verification of both systems, tests are conducted at no fewer than three points evenly distributed across the measurement range. Three series of measurements are performed with increasing load. The measured force values are compared to the corresponding reference values, and the errors are determined.

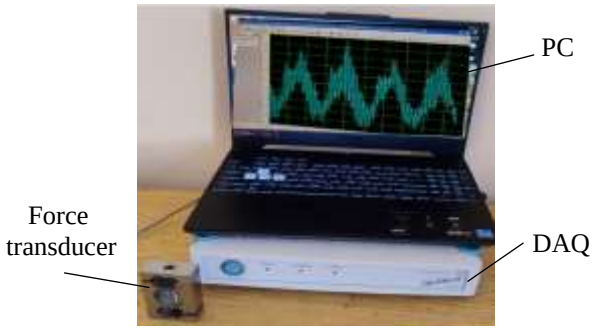

Fig. 5 A measurement system used to determine the reference force values

The formula below is used to determine the absolute error [13]:

$$\Delta F = F_{i,j} - F_{ref} \tag{8}$$

where:

$F_{i,j}$ – measured value at a given test point, recorded by the indicating device of the brake force measurement system, or respectively, by the axle load measurement system,

F_{ref} – reference value recorded by the corresponding measurement standard (etalon).

The following formula is used to determine the relative error in percent:

$$\delta_F = \frac{F_{i,j} - F_{ref}}{F_{ref}} 100\% \tag{9}$$

2) Determination of the difference between the measurements of the left and right sections of the brake force measurement system

The difference between the measurements for the same test force applied to the left and right sections of the brake force measurement stand is determined by the formula:

$$\Delta_R = \frac{F_{\max} - F_{\min}}{F_{\max}} 100\% \tag{10}$$

where:

$F_{\max}$ – the maximum value from the three measurements (of the left or right section) at the same reference force;

$F_{\min}$ – the minimum value from the three measurements at the same reference force, recorded by the other section.

3) Verification of the accuracy of the pressure measurement system of pneumatic brake systems

The verification is performed using a pressure generating device [10], equipped with a calibrated reference pressure measuring instrument (Fig. 6), whose expanded uncertainty (coverage factor k=2) does not exceed one-third of the absolute value of the MPE, in accordance with the requirements of the system under verification.

Fig. 6 Pneumatic Service Kit [15]

During the accuracy verification of the pressure measurement system, tests are conducted at no fewer than three points evenly distributed across the measurement range. Three series of measurements are performed with increasing pressure. The measured pressure values are compared to the corresponding reference values, and the errors are determined.

The formula used to determine the absolute error is:

$$\Delta p = p_{i,j} - p_{ref} \tag{11}$$

where:

$p_{i,j}$ – measured value at a given test point, recorded by the indicating device of the pressure measurement system;

p_{ref} – reference value recorded by the corresponding measurement standard.

The formula for determining the relative error in percent is:

$$\delta_p = \frac{p_{i,j} - p_{ref}}{p_{ref}} 100\% \tag{12}$$

IV. Conclusion

The developed methodology aims to ensure reliability, repeatability, and accuracy in testing roller brake testers. By conducting a series of tests, it is verified whether the testers comply with the requirements of the Ordinance on Measuring Instruments Subject to Legal Metrological Control.

To assess the effectiveness and suitability of the stand for operation, clearly defined acceptance criteria for the test results are applied, which are:

- For each measurement, the diameters must not be less than 98% of the diameter specified in the type approval certificate. If the manufacturer has defined a smaller allowable wear limit for the rollers than the one stated above, it must be taken into account,
- The peripheral speed of the rollers must be in the range from 2 km/h to 6 km/h.
- The measurement errors of the stand must not exceed the maximum permissible errors requirements.
- The difference in brake force measurements between the left and right sections must not exceed 2.5% for the same test force applied to both sections of the stand.

If all acceptance criteria are met, the verification is considered successful. If at least one acceptance criterion is not met, the verification is suspended until the nonconformities are resolved.

The presented methodology contributes to maintaining high standards in the testing procedures of roller brake testers under legal metrological control. The stand's ability to provide accurate and traceable measurements of vehicle braking efficiency will increase confidence in the results obtained, which are extremely important because they indicate the vehicle's ability to brake safely. The roadworthiness of the braking system is a mandatory part of periodic technical inspections. Measuring accurate, highly reliable results when determining the braking efficiency of road vehicles will contribute to the performance of high-quality periodic inspections to check the roadworthiness of road vehicles, which leads to the prevention of accidents and increased road safety. Future work should focus on developing verification methodologies based on dynamic testing methods, enabling more realistic simulation of operating conditions and further enhancing measurement reliability.

References

[1] ISO 21069-1:2004, Road vehicles — Test of braking systems on vehicles with a maximum authorized total mass of over 3,5 t using a roller brake tester Part 1: Pneumatic braking systems.

[2] ISO 21069-2:2008Road vehicles — Test of braking systems on vehicles with a maximum authorized total mass of over 3,5 t using a roller brake tester Part 2: Air over hydraulic and purely hydraulic braking systems.

[3] Bremsprüfstandsrichtlinie. Richtlinie für die Anwendung, Beschaffenheit und Prüfung von Bremsprüfständen. vom 07. Juli 2021.

[4] G. Xu, J. Su, R. Chen, H. Pan, L. Zhang, and X. Wang, "Measurement Performance Assessment: Dynamic Calibration Compared with Static Calibration Method for Roller Tester of Vehicle Brake Force," Advances in Mechanical Engineering, vol. 6, p. 162435, Jan. 2014, doi: 10.1155/2014/162435..

[5] P. L. S. Ferreira, P. R. G. Couto, L. C. Cabral, R. G. Reis, and M. Zillner, "A proposal for dynamic calibration of brake tester," J. Phys.: Conf. Ser., vol. 648, p. 012018, Oct. 2015, doi: 10.1088/1742-6596/648/1/012018.

[6] M. Božić, A. Vučetić, P. Ilinčić, Z. Lulić, " Retrofit Of A Roller Brake Tester At Famena," Transactions of FAMENA, Vol. 38 No. 3, 2014.

[7] R. Maulana Firdaus, B. Supriyo, and A. Suharjono, "Electronic and GUI Developtmen of Roller Brake Tester," J. Phys.: Conf. Ser., vol. 1273, no. 1, p. 012070, Nov. 2019, doi: 10.1088/1742-6596/1273/1/012070.

[8] R. M. Firdaus, B. Supriyo, and A. Suharjono, "Analysis of braking force efficiency measurements for various braking strategy applied for vehicle tested on roller brake tester," J. Phys.: Conf. Ser., vol. 1517, no. 1, p. 012079, Apr. 2020, doi: 10.1088/1742-6596/1517/1/012079.

[9] V. Surblys and E. Sokolovskij, "Research of the Vehicle Brake Testing Efficiency," Procedia Engineering, vol. 134, pp. 452–458, 2016, doi: 10.1016/j.proeng.2016.01.067].

[10] BDS ISO 16327:86, Roller brake testers for measuring brake forces and response time of automotive brake systems. Technical requirements and test methods.

[11] A. Brunelli, Calibration handbook of measuring instruments, First edition. Research Triangle Park, NC: International Society of Automation, 2017, pp. 49–52.

[12] V. Tsonev and N. Kuzmanov, "Design, machining and calibration of a strain gauge loadcell," in AIP Conference Proceedings, Plovdiv, Bulgaria: AIP Publishing, 2022, p. 060006. doi: 10.1063/5.0091463..

[13] S. Slavchev, V. Maznichki, and S. Krastev, "Optimization of railway cantilever based on physical test and non-linear computation model with finite element method," in AIP Conference Proceedings, Sozopol, Bulgaria: AIP Publishing, 2024, p. 060003. doi: 10.1063/5.0201432.

[14] H. Radev, " Metrology and measurement technology, tom 1," 1. izd., Sofia: Softtreyd, 2012, pp. 99–100.

[15] WIKA CPG [CPG-KITP-EU06-5-3ZZ] Pneumatic Service Kit, EU Version, 0.05% FS, 0 to 500 psi (0 to 40 bar) Gauge, https://indomultimeter.com/WIKA-CPG-KITP-EU06-5-3ZZ-Pneumatic-Service-Kit, seen 25.07.2025.

Special Requirements for Calibration of Climate Chambers

Valerii Semenikhin
dept. Information and Measurement Technology
Kharkiv National University of Radioelectronics;
Calibration Laboratory PrJSC MHP
PrJSC MHP
Kharkiv, Ukraine
valerii.semenikhin@nure.ua

Dmytro Taran
Calibration Laboratory PrJSC MHP
PrJSC MHP
Kyiv, Ukraine
d.taran@mhp.com.ua

Inna Moshchenko
dept. Information and Measurement Technology
Kharkiv National University of Radioelectronics
Kharkiv, Ukraine
inna.moshchenko@nure.ua

***Abstract* — According to the requirements of ISO 17025, all equipment used in calibration must be traceable; that is, it must be calibrated. In order to reproduce certain climatic conditions of the environment in the operating range of temperature and relative humidity values, specialized equipment is used, namely: climatic chambers (CC). The study reviewed and analyzed the main requirements of the calibration guideline (CG) "DKD-R 5-7: Calibration of Climatic Chambers" and provided an example of its application to ensure the measurement uniformity during calibration processes of CC.**

Keywords — calibration, calibration methodology, climatic chambers, temperature equipment

I. Introduction

According to the guidelines of the international standard ISO/IEC 17025:2017 “General requirements for the competence of testing and calibration laboratories” [1], all measuring instruments (MI) used in accredited laboratories and affecting the measurement result must be calibrated. Therefore, the analysis of the requirements of the international regulatory framework regarding the CC calibration process is an urgent task for the metrological scientific community.

During the calibration of the CC, deviations of the values of air temperature (AT) and relative humidity (RH) at certain points or parts of the CC, which are indicated by the CC, from the actual values of these climatic characteristics are determined. Also, the tasks of the calibration procedure include determining the parameters that can have an indirect effect on the object of study (heterogeneity, stability, etc.). Calibration results contain important information for CC operators, as they provide an opportunity to take into account the properties of a particular device during the implementation of the measurement process, and determine the measurement result.

For the calibration of test and laboratory equipment used for reproducing and maintaining temperature and/or humidity, it is proposed to use the calibration guideline (CG) “DKD-R 5-7: Calibration of Climatic Chambers” [2], which is recommended by EURAMET Calibration Guide No. 20 [3] from the regional metrological organization "EURAMET”.

Purpose. To present a standardized methodology for calibrating test and laboratory equipment (for reproducing and maintaining temperature and/or humidity) to the metrological community. Additionally, this methodology aims to analyze its special requirements for calibrating this equipment to ensure customers receive high-quality and sufficient information on the metrological characteristics of their equipment based on calibration results, including data on heterogeneity, instability, etc., for its further use. This also aims to ensure the uniformity of measurements within the country by applying a standardized methodology, or methodologies developed on its basis, instead of numerous different methodologies independently developed by various calibration laboratories.

II. Materials And Methods

The proposed guideline [2] establishes the necessary requirements for the calibration process and for determining the measurement error when calibrating CC. This methodology is used for calibrating CC for AT and RH or only for AT. It also considers the calibration of individual measurement points in CC.

A. Main terms

A CC is a technical tool that allows to implement selectively set values of AT and/or RT in a closed volume within the operating range. [2]

The measurement location (ML) is a spatial position in which the sensor is located in a useful volume (UV) for calibration. Thus, ML is a small volume, which is determined by the size of the sensor elements and the accuracy of their positioning.

The reference measuring location (RML) is a position in the UV, for which the deviation between AT and RH and the specified values is indicated. In most cases, the geometric center of the UV is chosen as the RML. [2]

The useful volume (UV) of the CC is the partial volume of the CC covered by the measurement sites of the sensors used for calibration. Depending on the location of the measurement sites, the UV may differ significantly from the total volume of the CC. The CC calibration is valid only for this UV. The necessary requirements for the ML position according to [2] must be fulfilled (Fig. 1).

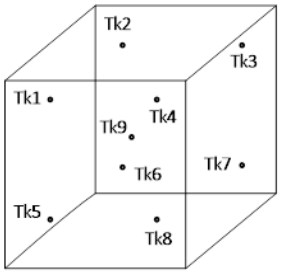

Fig.1. Schematic arrangement of measurement sensors in the UV of the CC

B. *Special requirements for climatic chamber*

To apply this method, it is necessary to assess whether the equipment belongs to CC, since the equipment manufacturer's designation may be different.

CG "DKD-R 5-7" applies to CC that have a UV with a certain size ratio (less than 5). These CC can be fixed or mobile, but their thermal insulation walls must be separate elements, not integrated into buildings or vehicles.

In order for a CC to be calibrated according to CG "DKD-R 5-7", it must meet the following criteria:

- Built-in temperature/humidity sensors and control systems of the calibrated quantities as CC components must be present.
- Technical specifications and documentation from the manufacturer for the categories of sensors must be present (there must be information about the location of sensors, sensor and insulation characteristics, type of temperature stabilization, etc.).
- Ensuring the alignment of atmospheric pressure with the environment.
- Calibration should be done at least three temperature or humidity points within the required range. Calibration at one point is possible, but its results are valid only for that specific point (the information is indicated in the calibration certificate).
- If the dissipation loss occurs in the UV of the CC (e.g., heat input through loading or heat dissipation occurs), this factor should be taken into account in the overall measurement uncertainty.

CG "DKD-R 5-7" classifies CC into two types according to maximum operating and calibration ranges: CC with active air circulation in UV and without active circulation. Both types of CC must have a heating and/or cooling function.

For CC with forced air circulation, additional requirements apply:

- Temperature range: The maximum range is -90 °C to 350 °C.
- Chamber volume: The UV should not exceed 2000 liters.
- Due to the lack of air circulation, the temperature stabilization in the CC is slower. Therefore, measurements can only be started when the temperature at all measurement points has stabilized. This means that there should be no systematic temperature fluctuations for a minimum of 30 minutes.
- To calibrate the UV, measurements must be made at at least nine points, as required by the standard IEC 60068-3-5 [4].
- During calibration, it is necessary to assess how the load affects the uniformity of temperature inside the CC. To do this, measurements are carried out in two modes: 1) Empty chamber: Calibration is done without loading. 2) Loaded CC: Calibration repeats with typical load.
- The load must be at least 40% of the UV (unless otherwise specified by the customer) and must simulate conditions that can lead to the greatest temperature unevenness. All details about the load used must be indicated in the calibration certificate.
- RH calibration is not allowed.
- Heat-generating or absorbing load are not allowed. Active loading with heat dissipation or heat generating is not allowed. [2]

If these specific requirements are met, this Guideline can be used to calibrate this equipment.

C. *Requirements for calibration methods*

Calibration of a CC is the process of determining how much the readings of its temperature and humidity sensors differ from the actual values inside the workspace. This helps not only to understand the accuracy of the CC, but also to evaluate other important characteristics such as uniformity (how much AT and RH are the same throughout the volume) and stability (how much the readings remain constant over time).

Thus, the objectives of calibration are as follows:

- Calibration consists of comparing the temperature/humidity readings of the CC with measurements obtained with reference instruments placed in its working volume. In this way, deviations or necessary corrections are determined.
- When calibrating a CC, measurement uncertainty (MU) must be determined, both for the procedure itself and for the conditions of its use. This includes calculating the temperature and/or humidity uncertainty that occurs during calibration, as well as the uncertainty that may occur during typical use of the CC.
- Calibration may also include checking that the CC meets certain user requirements, set tolerances, or specifications if required by the customer.
- Calibration can only be done at one or a few specific points and not over the entire volume of the CC as required by the customer. In this case, however, some uncertainty factors will not be taken into account, and the calibration result will be valid only for these points and not for the entire CC.

According to this methodology [2], the calibration of a climatic chamber can be carried out by three different methods (the measurements relating always to AT and RH):

Method A: Calibration in the UV of the unloaded CC.

This method is used to calibrate an empty CC and covers measurements over its entire working volume:

- The deviation between the readings of the CC devices and the reference measurements at the control points is determined.
- The spatial heterogeneity (temperature/humidity difference at different points) and temporal instability (variations in readings over time) of an empty volume are measured.

- The effect of radiation on the measurement of AT is evaluated.
- At the customer's request, the impact of loading can be further determined by comparing empty and loaded measurements.

Method B: Calibration in the UV of the loaded chamber.

This method involves load-based calibration, which can simulate typical usage or be at least 40% of the UV. The basic steps are similar to Method A, but all measurements are made with loading:

- The deviation of the CC readings from the reference values in the loaded state is determined.
- The spatial heterogeneity and temporal instability of the loaded volume are measured.
- The effect of radiation is determined.
- The impact of the load itself is estimated by comparing the loaded and empty UV. [2]

Method C: Calibration of individual points of the CC that do not cover UV.

This method focuses on calibrating not the entire volume, but only specific, individually selected points:

- Determination of the deviation between CC readings and reference measurements at selected points.
- Estimation of temporal instability at these points.
- Determination of the impact of radiation at the desired points.
- At the request of the client, the impact of loading on these specific points can be determined by comparing the loaded and empty UV. [2]

D. Calibration procedures

After selecting the calibration method, the calibration procedure begins with the placement of sensors at the measurement points. Calibration of the useful volume using Method A or B is usually carried out by measuring at several locations within the useful volume. The number and spatial arrangement of these locations are set by analogy with the IEC 60068-3-5 [4] standard for chambers with a useful volume of up to 2000 L (Fig. 1). For larger useful volumes, the measurement points must cover a cubic lattice with a maximum lattice constant of 1 m (i.e., the largest distance between adjacent measurement points is 1 m). Other positions are also possible at the customer's request, but the entire useful volume must be covered by the measurement points, and the distance between adjacent measurement points must not exceed 1 m.

The calibration certificate must contain a diagram with the location of the measurement points. The results are valid only for the part of the volume that was covered by these points. The total error specified in the certificate is calculated on the basis of the maximum values of the individual errors, and is valid for the total UV.

Calibration at individual points (Method C) is possible only at the request of the customer. In this case, the result is valid only for these specific locations, and this must be indicated in the certificate of calibration.

Two thermometers are used to measure the local spatial inhomogeneity at each point. They are placed side by side, at a distance of 2 to 5 cm (or at a distance equal to the length of the active sensor). Of these two thermometers, one is used to obtain the main result to be recorded in the certificate, and the other is only used to calculate the heterogeneity. Data from the last thermometer are not included directly in the final calibration result. Each measuring point location must be displayed as a diagram in the certificate.

Spatial heterogeneity is defined as the maximum temperature/humidity difference between measuring points. It is investigated only when calibrating the entire UV (Methods A and B). In Method C, only local heterogeneity is measured to account for in the total error.

Temporal instability is determined by recording temperature/humidity fluctuations within 30 minutes after stabilization. For CC without air circulation, measurements begin 30 minutes after steady-state is reached.

To determine temporal instability, it is necessary to record at least 30 measurements over 30 minutes at approximately equal intervals. These measurements are taken at the center of the UV (or at the reference point) for each calibrated AT or RH. It is important to note that the instability study is mandatory for all calibration methods.

The effect of radiation on measurements can be estimated in methods described in section 7.4 [2]. However, if the AT in the CC is in the range of 0 °C to 50 °C, this effect can be omitted. In this case, an additional uncertainty of 0.3 K is added to the total measurement error to take into account the possible effects of radiation. If the difference between the AT in the CC and the temperature of the environment is more than 30 K, the effect of radiation is mandatory for determination.

The impact of loading is evaluated at the customer's request. With Method B, the calibration result is valid for the loaded state. With Methods A and C, the result is for the unloaded chamber and the impact of the load is taken into account as an additional error. The test load must be at least 40% of the UV and be described in the calibration certificate.

When calibrating for RH in a circulating CC, you can use one of two methods.

Indirect method: you need to measure absolute humidity, dew point (Td) or freezing point (Tf) in the center of the UV. Then, using temperature distribution data, calculate the distribution of RH over the entire volume.

Direct method: you need to measure the RH directly at each point, similar to how it is done for temperature.

It is also imperative to determine the temporal stability of the RH at the reference point of the measurement.

E. Determining uncertainty contributions

The MU specified in the certificate includes several components. It is formed from uncertainties associated with measurements by reference instruments, indicators of the CC, as well as from the unevenness of parameters in time and space (i.e. temporal and spatial distributions).

Spatial heterogeneity (δT_{inhom}; δh_{inhom}) is the maximum deviation of AT or RH at points near the walls or at the corners of the chamber relative to the reference measurement site. According to the IEC 60068-3-5 [4], this value is taken into

account as half the width of a rectangular distributed contribution with a zero mean value [2]:

$$|\delta T_{inhom}| \leq Max|T_{ref} - T_i| \quad (1)$$

$$|\delta h_{inhom}| \leq Max|h_{ref} - h_i| \quad (2)$$

Standard uncertainties (SU) for these factors are determined by the formulas:

$$u(\delta T_{inhom}) = \frac{1}{\sqrt{3}} \times Max|T_{ref} - T_i| \quad (3)$$

$$u(\delta h_{inhom}) = \frac{1}{\sqrt{3}} \times Max|h_{ref} - h_i| \quad (4)$$

Spatial heterogeneity is a mandatory parameter that is taken into account in all calibration methods (from A to C), as well as for all temperature and humidity levels. In methods A and B (total volume calibration), this value is valid for each point inside the CC. In method C (calibration of individual points), it only applies to specific measuring points.

Temporal instability (δT_{instab}; δh_{instab}.) is an indicator that characterizes fluctuations in AT or RH. It is determined by a change in these parameters for at least 30 minutes after stable conditions have been established in the CC.

The maximum difference between any measured value over that 30-minute period and the average value over the same time is treated as half the width of the rectangularly distributed contribution with a zero expected value [2]:

$$|\delta T_{instab}| \leq Max|\bar{T} - T_i| \quad (5)$$

$$|\delta h_{instab}| \leq Max|\bar{h} - h_i| \quad (6)$$

SUs for these factors are determined by the formulas:

$$u(\delta T_{instab}) = \frac{1}{\sqrt{3}} \times Max|\bar{T} - T_i| \quad (7)$$

$$u(\delta h_{instab}) = \frac{1}{\sqrt{3}} \times Max|\bar{h} - h_i| \quad (8)$$

A prerequisite for all calibration methods (A, B, C) and for all calibration values of temperature and humidity is the determination of temporal instability. This indicator must be indicated in the calibration certificate.

Radiation effect $\delta T_{radiation}$. To calculate the uncertainty caused by the radiation effect, it is necessary to estimate the maximum effect of radiation on the uncertainty of the AT measurement. For this purpose, 10% of the determined is considered to be the half-width of the rectangularly distributed contribution with a zero expected value [2]:

$$|\delta T_{radiation}| \leq 0{,}1 \times Max|T_{ref} - T_{wall}| \quad (9)$$

$$u(\delta T_{radiation}) = \frac{0{,}1}{\sqrt{3}} \times Max|T_{ref} - T_{wall}| \quad (10)$$

Loading effect δT_{load}; δh_{load}. The contribution of the load to the total MU is calculated as 20% of the temperature difference measured at the control point between the loaded and empty chamber. This value is considered as half the width of the rectangularly distributed contribution with a zero expected value [2]:

$$|\delta T_{load}| \leq 0{,}2 \times Max|T_{ref} - T_{ref,load}| \quad (11)$$

$$|\delta h_{load}| \leq 0{,}2 \times Max|h_{ref} - h_{ref,load}| \quad (12)$$

SUs for these factors are determined by the formulas:

$$u(\delta T_{load}) = \frac{0{,}2}{\sqrt{3}} \times Max|T_{ref} - T_{ref,load}| \quad (13)$$

$$u(\delta h_{load}) = \frac{0{,}2}{\sqrt{3}} \times Max|h_{ref} - h_{ref,load}| \quad (14)$$

Resolution of indicators δT_{res}; δh_{res}. The resolution of the indicators enters as rectangularly distributed uncertainty contribution. The smallest resolution is 0,5 digit. This is the half-width of a rectangularly distributed contribution with the expectation 0. [2]

Measurement error of standard measuring devices δT_{std}; δh_{std}. This contribution is obtained from the partial budget for the standard measuring devices used. [2]

The resolution of the indicators (δT_{res}; δh_{res}) is taken into account as a rectangularly distributed contribution of uncertainty. Normally, the minimum resolution is 0.5 of the smallest digit, which is half the width of this distribution.

Measurement error of reference MI (δT_{std}; δh_{std}). This contribution comes from the errors present in the reference MI themselves used for calibration. Their uncertainty is taken into account based on their own uncertainty budget:

$$T_{std} = T_{ind,std} + \Delta T_{std} + \delta T_{std} \quad (15)$$

$$\text{with } \delta T_{std} = \delta T_{cal} + \delta T_{drift} + \delta T_{res,std} + \delta T_{heat} + \ldots \quad (16)$$

$$h_{std} = h_{ind,std} + \Delta h_{std} + \delta h_{std} \quad (17)$$

$$\text{with } \delta h_{std} = \delta h_{cal} + \delta h_{drift} + \delta h_{res,std} + \ldots \quad (18)$$

F. Requirements for calibration results

The calibration certificate must indicate the deviation of the measured values from the specified ones or, alternatively, the correction of the readings. These reference values generally refer to the center of the UV of the CC.

The components of the complete calibration result must contain the following elements:

- Correction or deviation of readings: This result is indicated for AT and RH. For Methods A and B, which cover the entire volume, it refers to the reference point in the center. For Method C, which calibrates individual locations, it is provided for each of these points.
- Uncertainty of readings: Indicated for both AT and RH.
- The certificate must also contain information about the characteristics of the CC such as uniformity, stability, exposure to radiation, wall temperature and other relevant data.
- Conformity for AT at customer's request only.
- Conformity for RH at customer's request only.
- Conditions of measurement. [2]

III. Experimental Part

As an experimental work, the calibration of the Binder FD56 CC (see Fig. 2) was carried out at the Calibration Laboratory PrJSC “MHP”. This was done in accordance with the requirements of the standardized methodology discussed in this paper [2], specifically Method A (unloaded chamber), using a multi-channel calibration complex based on a precision thermometer "milliK". This thermometer provides metrological traceability to recognized national standards (see Fig. 3).

Fig.2. Location of temperature measurement sensors in the climatic chamber's useful volume

Fig.3. Calibration complex based on the "millik" precision thermometer

The measurement results, presented according to the requirements of the standardized methodology discussed in this paper [2], are presented in Tables 1–3.

TABLE 1. TEMPERATURE MEASUREMENT RESULTS

Controller adjustment - AT in °C	Temperature standard in the UV in °C	Temperature indication for calibration object in °C	Correction of indication in °C	MU (*U*) in the UV in °C
105	106,2	105	1,2	4,6
130	131,3	130	1,3	5,3

TABLE 2. SPATIAL TEMPERATURE DISTRIBUTION

Controller adjustment - temperature in °C	105	130
Location in the useful volume:	**Temperature - standard thermometer in °C**	
Tk 1	105,70	130,70
Tk 2	104,69	129,80
Tk 3	106,03	130,95
Tk 4	106,08	131,34
Tk 5	105,77	130,65
Tk 6	104,55	129,21
Tk 7	106,77	131,74
Tk 8	110,06	136,00
Tk 9 reference location	106,14	131,43
Measurement uncertainty (*U*) in °C	0,79	0,61

TABLE 3. RESULTS FOR THE CHARACTERIZATION OF THE CC VOLUME

Controller adjustment - temperature in °C	Inhomogeneity in °C	Instability in °C	Radiation effect in °C
105	3,91	0,47	0,10
130	4,58	0,18	0,12

IV. CONCLUSIONS

The following important conclusions can be drawn from the research conducted and the results obtained:

- The use of a standardized calibration method [2] allows comparing calibration results obtained by different calibration laboratories, thereby ensuring the uniformity of measurements.
- We've considered the features of the standardized method [2] for calibrating CC and the requirements that test and laboratory equipment for reproducing and maintaining temperature and/or humidity must meet to be calibrated according to this method.
- Performing calibration and presenting the results according to the method discussed in this article provides the customer with the most complete information about the characteristics of their equipment's useful volume, such as instability, heterogeneity, load effect, etc.
- The possibility of applying this calibration method to equipment that formally meets its requirements but cannot be fully investigated due to design features requires further study. This is particularly relevant

when the UV of the equipment chamber is small, and the size of the thermometer's measuring sensors prevents their placement in the minimum required number according to the methodology.

ACKNOWLEDGMENT

The authors would like to thank the Calibration Laboratory PrJSC "MHP" for supporting the presented research.

REFERENCES

[1] ISO/IEC 17025:2017 General requirements for the competence of testing and calibration laboratories.

[2] DKD-R 5-7 Calibration of climatic chambers. Edition 07/2004. English translation 02/2009.

[3] EURAMET Calibration Guide No. 20 Guidelines on the Calibration of Temperature and/or Humidity Controlled Enclosures, version 5.0 (09/2017) – English version.

[4] IEC 60068-3-5:2018 Environmental testing - Part 3-5: Supporting documentation and guidance - Confirmation of the performance of temperature chambers.

SECTION XI
IONIZING RADIATION MEASUREMENTS

METROLOGYCAL ASSURANCE IN IONIZING RADIATION MEASUREMENTS AT KOZLODUY NPP EAD - ACCEPTANCE AND DEVELOPMENT

Temenuzhka Stoyanova
Metrological Assurance
Kozloduy NPP EAD
Kozloduy, Bulgaria
temenushka@abv.bg

Neli Ivanova
Metrological Assurance
Kozloduy NPP EAD
Kozloduy, Bulgaria
NSIvanova2@npp.bg

Alexander Mladenov
Metrological Assurance
Kozloduy NPP EAD
Kozloduy, Bulgaria
ADMladenov@npp.bg

Summary: The main objective of metrological assurance in measurement of ionizing radiation (IR) at Kozloduy NPP EAD is to ensure unity, accuracy and quality of measurements in accordance with the Bulgarian and international standards and traceability to internationally recognized primary standards.

Measurements in the field of radiation protection, control of radioactive discharges into the environment and technological control are extremely important.

The report is based on the years of experience gained by the Ionizing Radiation Measurement Laboratory at the Metrological Assurance Department of Kozloduy NPP EAD. It presents the main tasks of the Metrological assurance in measuring of ionizing radiation and the associated activities.

Key words: Metrological assurance, legal metrology, company metrology, calibration, verification

I. INTRODUCTION

Measurement of ionizing radiation (IR) is carried out in many areas of the production and monitoring activities performed at Kozloduy NPP EAD but the measurements are particularly important in the field of radiation protection, control of radioactive discharges into the environment and technological control.

Ensuring unity, accuracy and quality of the ionizing radiation measurement in accordance with the Bulgarian and international standards, and traceability to internationally recognized primary standards, is the main objective of the Metrological Assurance Department (MA) at the Quality Division of Kozloduy NPP EAD. It is an important prerequisite for compliance with:

- technical specifications;
- radiation protection regulations;
- dose exposure limits of personnel working in an ionising radiation environment;
- regulatory requirements for radioactive discharges to the environment;
- ALARA principle;
- Measurements Act.

II. TYPES OF IR MEASUREMENTS

IR measurements are carried out in many areas of production and monitoring activities at Kozloduy NPP EAD. The purpose is to provide for:

- radiation protection of personnel through individual dosimetry control, control of the radiation background in work premises, control of surface contamination;
- environmental protection through control of radionuclide composition and radionuclide content in waste water and air;
- control of technological measurements by monitoring the quantities of radioactive substances generated in the course of the electricity generation and minimizing the potential for spread of contamination.

The technological measurements of ionizing radiation are carried out in order to control the quantities of radioactive substances generated in the course of electricity generation and to limit the potential for their spread. Thus, there is a close connection amongst the three types of measurements for ionizing radiation measurement at NPP. Therefore, it is more convenient to classify the measurements according to the type of the radiation measured and the measurement method used:

- activity measurement - gamma spectrometry for measuring the total alfa-/beta- activity;
- dosimetry measurements - individual and operational dosimetry control

III. MA STRUCTURE IN MEASURING IR

Metrological assurance is divided in two main areas: Legal metrology and company (industry) metrology.

- Legal metrology - it`s task is to apply the legal requirements to measurements ensuring the accuracy and reliability of the measurements related to public safety, environmental protection, state and municipal takings and commercial payments, and carrying out metrological control (MC) of measuring instruments (MI) - Art. 5 of Measurements Act (MA). Metrological monitoring is carried out by the Bulgarian Institute of Metrology or individuals authorized by State Agency for Metrological and Technical Surveillance pursuant to the Measurements Act and the related regulations.
- Company metrology - it`s task is to ensure the quality of the measurements in a given production in accordance with the design documentation, specific technical requirements, safety requirements and other normative documents and standards related to the specific production process. It

is carried out by means of MA of the entire measuring process depending on the measurement specifics and is regulated by internal documents - quality procedures, methodologies, standards, etc.

Organisation and control of the metrological assurance of the ionizing radiation measuring instruments and systems at Kozloduy NPP EAD is conducted by the Ionizing Radiation Measurement Laboratory at the Metrological Assurance Department. The laboratory performs company metrological verifications and calibration of measuring instruments. In the cases under Art. 5 of the Measurements Act, the inspections are carried out by Directorate General Measures and Measuring Instruments (DG MMI) - Lovech, the Measurement of Ionizing Radiation Laboratory and Energotest Control Ltd.

IV. MA ACTIVITIES IN MEASURING IR

The main activity of the Ionizing Radiation Measurement Laboratory for the purposes of metrological assurance of ionizing radiation measuring instruments is:

- verification of the measuring instruments pursuant to Art.5 of the Measurements Act (only requesting and presenting measuring instruments for verification)
- company verification of measuring instruments (specialized receiving inspection, initial and periodic);
- calibration of measuring instruments;
- measurement quality control.

The technical procedures for caring out these activities are the same, but the objectives are different. When comparing the four types of activities, the following concussions can be drawn:

- The verification of the measuring instruments legally makes it possible, by relatively simple means, to achieve effective control of a large number of measuring instruments without requiring any special knowledge of the measurement from the user. Only the maximum permissible error in the operation of the measuring instrument is of interest;
- The verification ensures correct measurements with given measuring instruments for its intended use for a certain period of time. Therefore, verification can be considered a serious measure to ensure the necessary quality of the measurements in both legal and industrial metrology.
- The verification in the legal field is carried out according to methodologies approved by the Bulgarian Institute of Metrology, which are valid for the whole country. The company verifications are conducted under approved methodologies according to the specific application of the ionizing radiation measuring instruments at Kozloduy NPP EAD.
- The conclusion from the verification in the legal field is qualitative: the measuring instrument complies /does not comply with the approved type. This means that the measuring instruments do or do not comply with the regulatory requirements related to its purpose.

The company verification can also provide a quantitative assessment certifying whether a particulate measuring instrument fulfils its purpose, whether it is applicable for carrying out a given measurement.

Calibration is an important procedure in the industrial metrology measurement activities. Thorough knowledge about the specifics of the measurement, its implementation and results processing and evaluation is required to carry out the calibration. The measuring instruments to be calibrated are not typical in most cases, but are selected in a way they can be used for a specific purpose. Compared to the verification, the calibration provides for qualitative assessment showing to what extend a certain objective is achievable with a given measuring instruments when applying a specific measuring method.

Measurement quality control aims to control the entire measurement process. It is performed using the blind sampling method and has a particularly important role in metrological assurance of activity measurements.

V. ORGANISATION AND PERFORMANCE OF METROLOGICAL CONTROL OF MEASURING INSTRUMENTS

The Ionising Radiation Measurement Laboratory complies with the requirements of БДС EN ISO/IEC 17025:2018 - *General requirements for the competence, of testing and calibration laboratories* to evidence its competence and ability to obtain valid results.

In compliance with this document, the Laboratory plans and performs activities considering the risks and possibilities. This increases efficiency, improves the accuracy of results and prevents negative impact. The laboratory is responsible for defining the risks and possibilities to be considered.

The activities and documents meeting the requirements of БДС EN ISO/IEC 17025:2018 include:

- measurement processes
- measuring instruments and systems
- ensuring measurement traceability
- measurement methods
- measurement conditions

Metrological verification and calibration are carried out in compliance with approved methodologies.

The laboratory organises and carries out periodic metrological control and calibration of measuring instruments used for radiation monitoring to ensure the reliability and comparability of the measurement results and to enhance their reliability,

A specialized receiving inspection and initial check is carried out upon commissioning of the newly purchased equipment to ensure compliance with the technical and regulatory requirements.

VI. IONISING RADIATION MEASUREMENT LABORATORY STANDARD BASE

A. *Standard noble gas monitor*

The standard noble gas monitor, type RNG- 07 (Fig. 1) is used to calibrate radioactive discharge systems. The monitor measuring range for ^{133}Xe is $8{,}11.10^2$ up to $6{,}61.10^7$ Bq/m^3 and for ^{85}Kr is $1{,}69.10^3$ up to $1{,}38.10^8$ Bq/m^3, uncertainty 3 %. In 2023, traceability to an international standard in the Czech metrology institute (CMI) is provided.

Fig. 1 RNG - 07

B. *Dosimetry value standards*

The laboratory maintains three gamma irradiance standards reproducing values of air kerma and air kerma rate. Two of them, type IM6/M and IM1/P (Fig. 2), are located in the laboratory located at Units 5 and 6 and the third one, type CMS-NRD-WBM (Complex Measuring System - Neutron Radiation Dosimetry - Wide-Beam Modification) is located in the laboratory located at Units 1-4. Gamma irradiation lines are used to check and calibrate electronic personal dosimeters, thermoluminescent dosimeters, radiation monitoring system detector units and portable dosimeters for operational control.

Fig. 2 IM6/M and IM1/P

The calibration of these lines is performed with a dosimeter, type UNIDOS 1001 (Fig. 3), an air kerma unit power standard to ensure traceability of the results to a national standard. The dosimeter has an operating range from 0,2 μSv/h to 3,5 kSv/h in a set with 3 ionization chambers, type TW23361, 30 cm^3, TW23002, 1000 cm^3, TW23003, 10 000 cm^3.

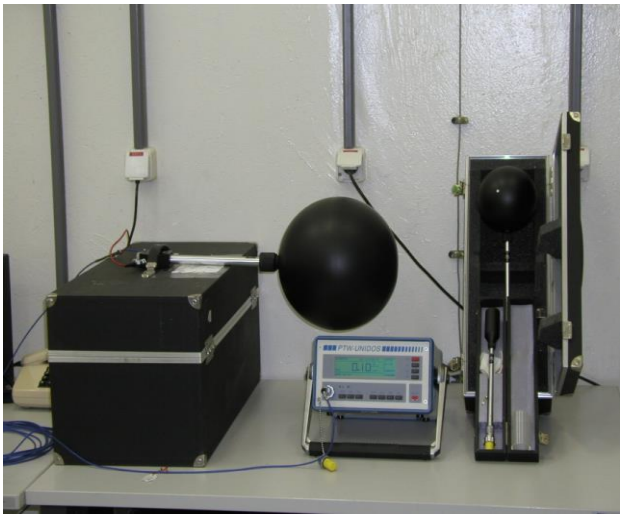

Fig. 3 UNIDOS 1001

C. *Certified reference materials*

Certified reference materials (CRMs) are standard samples whose geometry, activity and nuclide composition depend on their specific application, and, therefore, the variety among them is relatively large. The type and number of the necessary CRMs is stipulated in the calibration and verification methodologies and quality assurance procedures for measurements with radiometers for defining the total alpha/beta in samples.

Due to the decay properties of the radioactive substances, CRMs have a limited shelf-life, requires after the expiry date of the CRM specified in the certificate, the CRMs to be:

- scrapped and replaced with new ones;
- recertified by an institution entitled to carry out this activity and extend their shelf-life.

Selecting one of the two options depends on the design of the source, the radionuclide it contains and the accuracy to be achieved using it.

D. *Particle activity and surface emission rate standards*

Particle activity and surface emission rate standards are large-area alpha/beta-radioactive sources on a solid substrate of different sizes and nuclides. These sources are used for metrological control and calibration of portable and stationary radiometers for alpha/beta surface contamination, as well as radiometers for determining total alpha/beta in samples, along with CRM.

The storage and handling of standards is carried out in accordance with the requirements of the Regulation on radiation protection.

The traceability of the standards is achieved through continuous quality control and calibration.

The maintenance of activity and particle surface emission rate standards requires regular surface contamination and leak tests.

The Ionizing Radiation Measurement Laboratory has implemented a quality control system for the standards used. To verify the operability of the radioactive sources from the standard sets, they are periodically tested for surface contamination and leak in the laboratory. A radiometric alpha/beta counting system, type iSolo, is used for measurements (Fig. 4).

Fig. 4 iSolo

Table 1 presents the metrological characteristics of the iSolo radiometric alpha/beta counting system

TABLE 1 ISOLO METROLOGICAL CHARACTERISTICS

Attribute	Specified values	Dimension
Measuring range	1 ÷ 1000000	cts
Energy range	α: 3.0 ÷ 9.6 β: 0.125 ÷ 2,2	MeV
Background	α: ≤ 0.1 β: ≤ 16	cpm
Efficiency of registration	≥ 33 (^{241}Am) ≥ 25 (^{90}Sr/^{90}Y)	%

The laboratory has a gamma spectrometry system HPGe, manufacturer ORTEC, MCA - DSPec (Fig. 5), used to implement activities to evaluate the leak tightness of ionizing radiation sources and to carry out quality control through external laboratory control of Kozloduy NPP EAD organisational units.

Fig. 5 HPGe

Table 2 presents the metrological characteristics of the HPGe gamma spectrometer.

TABLE 2 METROLOGICAL CHARACTERISTICS OF HPGE

Attribute	Specified values	Dimension
Resolution at: 122 KeV	0,82	keV
1332.5 KeV	1,85	
Peak/Compton ratio ^{60}Co	56:1	-
Relative efficiency ^{60}Co	25%	%

The radioactive sources which fail the leak tests are not allowed for further use and are discarded. They are handed over in compliance with the Regulation on the Terms and Procedure for Handing Over Radioactive Waste to the State Enterprise Radioactive Waste for treatment as radioactive waste.

E. Standard wide-area windowless radiometer

An output standard is used (a radiometric system with a wide-area gas flow proportional detector, type LAPC-096 (Fig. 6)) for the inter-calibration checks of the radioactive sources and the calibration of the radioactive sources working standards.

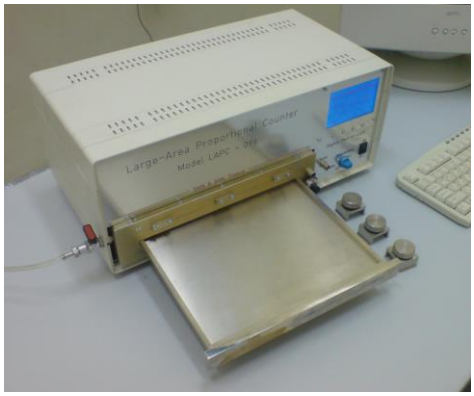

Fig. 6 LAPC-096

The LAPC-096 was declared a starting standard following verification of its characteristics and conducting calibration in the D.I. Mendeleev All-Russian Institute of Metrology (VNIIM), St. Petersburg in 2015. Due to the strained relations and military situation in Russia, no subsequent calibration was carried out to ensure traceability in VNIIM.

In 2023, in cooperation with the Scientific Research Centre at Sofia University St. Kliment Ohridski, and, in particular, K. Mitev, at the Department of Atomic Physics, Faculty of Physics, a study was carried out and a numerical Monte Carlo model was developed to evaluate the efficiency of a LAPC type flow proportional counter. This enabled the team of K. Mitev to continue the study of the characteristics and calibration of P9 alpha sources with the standard radiometer LAPC-096 the following year. Since 2024, following specialised training, the Ionising Radiation Measurement Laboratory reliably uses the LAPC-096 standard for the surface emission rate with traceability to an international standard of the National Metrology Institute of Germany (PTB) for the calibration of wide-area radioactive sources, types P9 and C0.

VII. DEVELOPMENT OF THE IONIZING RADIATION MEASUREMENT LABORATORY

In recent years, as part of the modernisation of radiation monitoring systems and equipment, many new measuring instruments have been delivered, mainly for operational radiation monitoring of the radiation situation in the controlled and supervised areas. These are new in terms of a model and manufacturer, as well as increasing the number of models available. This defines the activities and development of the Ionizing Radiation Measurement Laboratory in the following areas:

A. Ensuring and maintaining appropriate working conditions

In order to ensure the necessary conditions for obtaining reliable and accurate results during verification and calibration, a complete renovation of the laboratory's workspaces was carried out. An air conditioning system was installed providing for the temperature and humidity required for measurements.

A fully state-of-the-art video surveillance system was installed in the room housing the two gamma irradiation lines to ensure better conditions and radiation protection measures for personnel.

B. Development and maintenance of the standard base

The Laboratory maintains an extensive standard base and works on the improvement of the hierarchical schemes to ensure the quality execution of metrological control activities in accordance with the needs of the Kozloduy NPP organisational units. Delivery of a new high-precision UNIDOS-type dosimeter and installation of a new standard gamma irradiation line is expected to improve the quality of verifications and calibration of electronic personal dosimeters, thermoluminescent dosimeters, detector units from radiation monitoring systems, and portable dosimeters for operational monitoring.

For the purposes of metrological assurance of the newly purchased measuring instruments at Kozloduy NPP EAD, the Ionizing Radiation Measurement Laboratory continuously expands and updates the standard base with different in area, geometry, and nuclide composition. radioactive sources.

A traceability of all standard measuring instruments and standard radioactive sources used at Kozloduy NPP is provided to the primary standards in Germany, the Czech Republic, Russia, USA, etc., as well as to the national standards in Bulgaria, via certification and recertification, if needed.

The maintenance of the standard base is related to:

- Calibration of standards to ensure traceability to higher-level standards;
- Procurement of new standards;
- Participation in interlaboratory comparisons;
- Software support of measurements;
- Continuous control of standards' Characteristics.

The standards used by the Ionizing Radiation Measurement Laboratory have valid calibration certificates, approved registration records, and traceability schemes, in accordance with the quality procedures of the Metrological Assurance Department.

C. Implementation of new methods and methodologies for the calibration and verification of measuring instruments

The expansion of the range of verified and calibrated measuring instruments leads to the development of the standard base, as well as to the development and approval of new methodologies necessary for the activity, in accordance with the requirements of Bulgarian and international standards.

In 2023, under a contract concluded with the Scientific Research Centre at Sofia University St. Kliment Ohridski, Tatiana Boshkova carried out authorial maintenance and update of methodologies for the calibration and verification of gamma spectrometry systems with HPGe detectors.

In connection with the expansion of the Ionizing Radiation Measurement Laboratory's activities to include the calibration of standard gamma irradiation lines and standard wide-area alpha/beta sources, an update was carried out in accordance with the international standards and best practices in the methodologies thereto.

- Methodology for calibration of standard gamma irradiation lines;
- Methodology for calibration of standard wide-area alpha and beta sources of ionizing radiation;

Due to the wide variety of portable radiometer types, procedures for their calibration are to be jointly developed with K. Mitev. To facilitate the work of the laboratory specialists, training on the topic is also planned.

D. *Demonstration of the laboratory's competence*

The laboratory's specialists participate annually in international interlaboratory comparisons in various areas of ionizing radiation measurements, such as:

- International interlaboratory comparison 'Ringversuch Fortluft' for measuring the gamma-emitting nuclides when monitoring gaseous radioactive emissions in the environment, conducted by the German Federal Office for Radiation Protection (Round robin test for the determination of gamma emitters in water RV1)
- International interlaboratory comparison for defining the gamma emitters in water RV1, conducted by the German Federal Office for Radiation Protection (Round robin test for the determination of gamma emitters in water RV1)
- International interlaboratory comparison (proficiency test) for the measurement of anthropogenic radionuclides in water, soil, and surface contamination on a simulated filter, organized by the International Atomic Energy Agency (IAEA, Austria) – Proficiency Test (PT) on determination of anthropogenic and natural radionuclides in water, soil and simulated contaminated surface samples – provided by the IAEA Terrestrial Environmental Radiochemistry Laboratory (TERC)

Achieving good results is an important factor for demonstrating the laboratory's competence. Through its participations, the Laboratory confirms its competence in calibration and in providing for valid measurement results. The laboratory personnel possess the necessary competence to carry out the laboratory activities.

E. Personnel Training and Qualification

The Laboratory pays special attention to maintaining and enhancing the personnel qualifications in order to professionally implement the activities in view of the increasing requirements for the activities performed. This is achieved through:

- On-the-job training;
- Participation in specialised training courses, including English language courses;
- Participation in practical workshops, conferences and symposiums;
- Professional qualification in 'Metrology and Metrological Assurance' under a contract with Technical University of Sofia and Sofia University 'St. Kliment Ohridski'

VIII. CONCLUSION

The Ionizing Radiation Measurement Laboratory at Kozloduy NPP EAD is responsible for the metrological assurance of a large number of measurements and measuring instruments used in industrial and legal metrology. The metrological assurance principles and methods applied by the laboratory comply with the current international and national trends for metrological assurance development.

The metrology assurance of measuring instruments (MI) at the NPP is carried out in accordance with the following documentation regulated by the legal and regulatory framework:

- Measurements Act;
- Safe Use of Nuclear Energy Act;
- Regulation on measuring instruments subject to metrological control;
- Regulation on Radiation Protection;
- Regulation No.9 for the technical operation of power plants and grids

The Ionizing Radiation Measurement Laboratory at Kozloduy NPP EAD focuses its efforts on the metrological assurance of technological measurements: development of programmes to ensure the quality of individual measurements, calibration of measuring instruments, improvement and expansion of the standard base, enhancement of the quality of metrological verifications, preparation of measurement methodologies, receiving inspection, personnel qualification enhancement, etc.

TECHNICAL UNIVERSITY OF SOFIA

RESEARCH AND DEVELOPMENT SECTOR OF TECHNICAL UNIVERSITY OF SOFIA

The Technical University of Sofia is a modern educational and research institution, with highly qualified lecturers, researchers, engineers and technicians. The laboratory facilities with advanced equipment and qualified research staff provide high-quality scientific and experimental research.

The main goal of the Technical University of Sofia is its establishment as the leading European scientific and research center. Through its infrastructure, research potential and network of contacts, the University supports the solution of many scientific and engineering problems related to the needs of society.

Technical University of Sofia conducts a variety of applied research activities and provides opportunities for technology transfer at national and international level through the following units:

- Research and development sector
- "Technical University of Sofia – Technologies" Ltd.
- Small enterprises
- Educational-experimental enterprise
- The publishing house of the Technical University of Sofia

An important role for the establishment of TU-Sofia as a leading educational and research engineer center in the country and the region has the numerous annual scientific forums, united in the unique format "Science Days of TU-Sofia".

The strong international character, the high scientific level of the presented research findings and papers, included in proceedings, referenced and indexed in leading international science databases, and the significant support of the industrial partners make this forum an efficient environment for the transfer of knowledge, ideas and technologies from science to industry and business.

The introduced e-learning system E-SCIENCE provides the opportunity to obtain unified, complete and comprehensive information on scientific activities, projects and the scientists' career development. The system provides ways and methods for finding optimal management decisions and improves the effectiveness of research and applied work. Thanks to the publications module, updated daily, bibliographic data and summaries of scientific papers, publications, and posters are available on the web.

Training and Sport Wellness base "LAZUR" is the host of the annual international scientific conferences "Science Days of TU-Sofia" in the town of Sozopol, where the scientific elite of Bulgaria and the world is held.

The forums organized by the TU-Sofia are a meeting place for scientists from different research fields, challenged to transform innovative ideas into products and services that create sustainable partnerships between science and business, build high-skilled human potential, giving new skills that provides prepared researchers and specialists.

Technical University of Sofia
8 Blvd. Kl. Ohridski, 1797, Sofia, Bulgaria
Phone: (+359) 2 96 25 72, (+359) 2 868 51 83, Fax: (+359) 2 96 25 72
www. tu-sofia.bg


СЪЮЗ НА МЕТРОЛОЗИТЕ В БЪЛГАРИЯ
UNION OF THE METROLOGISTS IN BULGARIA